Minnesota U., Res. Rpt. 183

UNIVERSITY OF MINNESOTA

Institute of Technology

mfs

N64-15888 *

138 p.

CODE-1

CR-55718

ROSEMOUNT AERONAUTICAL LABORATORIES

[redacted]

OTS PRICE

XEROX $ 3.60 ph

MICROFILM $ 1.34 mf

ROSEMOUNT, MINNESOTA

RPT-183

Research Report No. 183

UNIVERSITY OF MINNESOTA
INSTITUTE OF TECHNOLOGY
ROSEMOUNT AERONAUTICAL LABORATORIES
ROSEMOUNT, MINNESOTA

U. Minneapolis 2. Rosemount 155 9251

TURBULENT BASE FLOW INVESTIGATIONS AT MACH NUMBER 3

by

R. E. Larson, C. J. Scott
D. R. Elgin, and R.E. Seiver

Jul. 1962 38p refs

cite only
(NASA CR-55718; Res. Rept. 183) OTS: $

Prepared for:

George C. Marshall Space Flight Center, Huntsville, Alabama
NASA Contract NAS8-1698, Request No. TP 81-120

and

U.S. Army Ordnance Missile Command
Redstone Arsenal, Alabama - Contract DA-11-022-ORD-3969,
Serial No. 0303970

Minneapolis 14, Minnesota
July 1962

ACKNOWLEDGEMENTS

The financial support of a two-year investigation on base flow phenomena recently completed at the Rosemount Aeronautical Laboratories and reported herein was provided jointly by three agencies. During the first year the work was supported by the Army Ballistic Missile Agency under Army Contract No. DA-11-022-ORD-3148 and monitored by Mr. Werner Dahm. The research effort of the second year was jointly supported by the Army Ballistic Missile Agency under Army Contract No. DA-11-022-ORD-3969 and the George C. Marshall Space Flight Center under NASA Contract No. NAS8-1698 with Mr. Gerhard Reisig and Mr. Werner Dahm as technical supervisors. After the Army Ballistic Missile and Rocket and Guided Missile Agencies were merged, Mr. Robert Moore provided technical direction for the Army Ordnance Missile Command.

The work was interrupted before completion because of the closing of the Laboratories on July 1, 1962. The results reported herein are not intended to be complete and are subject to further verification and amplification. At the time of the closing of the Laboratories, the research efforts were leading to a more complete understanding of the complicated flow process involved.

Administration of the contract at the University of Minnesota was provided by Professor John D. Akerman, Director of the Rosemount Aeronautical Laboratories and Mr. Karl H. Stefan, Administrative Scientist.

Included among those who cooperated in the study during the early phases were Mr. Nicholas Helm and Mr. Leon Zacho.

SUMMARY

over
15-888

This report presents results of an experimental investigation of supersonic base flow processes under turbulent wake flow conditions. The measurements were made in the near-wake region of a two-dimensional model at a free stream Mach number of 3.

Local heat fluxes and pressures were measured on the base of the model for various cooling rates over the transitional to fully turbulent flow regimes. It was observed that base temperature had a small, but measurable influence on heat transfer coefficient and mean base pressure. For turbulent flow with the base at recovery temperature, profiles of impact pressure, static pressure, and total temperature were obtained in the shear layers, and impact pressure and centerline static pressure data were measured in the recirculation zone.

Definite indications of reverse flow were found in the recirculation zone, and reverse-flow Mach numbers as large as 0.6 were observed. Although the overall nature of the flow was found to be steady, regions of fluctuating flow were found, and the total flow pattern proved to be more complicated than originally expected.

The existence of a thin "boundary layer - like film" on the base of the model was proven by temperature profiles measured normal to the base at base-to-tunnel, total-temperature ratios of 0.950, 0.716, 0.487, and 0.340 under turbulent shear layer conditions. Heat transfer data calculated using these profiles and the Fourier heat conduction equation agree with the directly measured wall values.

Noting the similarities between base flow and ordinary stagnation point flow, base heating rates were calculated using incompressible stagnation point theory. The velocity gradient was evaluated both from the vertical base pressure distribution and the centerline static pressure data. The heat fluxes so obtained were in good agreement with the measured values.

15884

Total temperature measurements made in the recirculation zone with wall cooling showed that although the region closest to the base senses the drop in temperature, the major portion tends to ignore it and remains near its recovery value, which is close to the free stream total temperature. These findings indicate that the largest barrier to heat flow into the base is the enveloping base boundary layer, with only small resistances encountered at the shear layer and in the recirculation zone. Although a large capacity exists for carrying heat into the base area, only a small portion can penetrate the base boundary layer. This explains the discrepancy between measured heat fluxes and those predicted by existing theories.

A survey of available base flow literature was completed and a critical study of Korst's mixing layer analysis was carried out. Korst's theory provides a reliable prediction of base pressure values and his heat transfer analysis is valid if the relation between base temperature and recirculation zone temperature is considered. Author

TABLE OF CONTENTS

TABLE OF CONTENTS (CONCL'D)

LIST OF FIGURES

LIST OF FIGURES (CONT'D)

APPENDIX FIGURES

NOMENCLATURE

Symbol	
A	area
a	speed of sound
C	Crocco number
c	chord
c_p	specified heat or pressure coefficient
erf	error function
H	base half height
h	heat transfer coefficient
h^+	heat transfer coefficient based on $(T_o - T_B)$
h/2	probe half height
i	enthalpy
k	thermal conductivity
L	mixing length
ℓ	disturbance length
M	Mach number
$\dot{m}$	mass flow per unit width
Nu	Nusselt number
Pe	Peclet number
Pr	Prandtl number
p	pressure
Q	dimensionless heat flow
Q*	heat flow per unit width
$\dot{q}$	heat flux
R	gas constant
Re	Reynolds number
St	Stanton number
T	temperature
t	thickness
U	velocity
u	velocity component in x direction
$\bar{u}$	time averaged velocity component in x direction

Symbol	
V	volume
v	velocity component in y direction
$\bar{v}$	time averaged velocity component in y direction
X	wake length
x	position coordinate
y	position coordinate
β	dummy variable
γ	ratio of specific heats
δ	viscous layer thickness
ε	eddy viscosity
η_p	position parameter, $1/2\sqrt{\xi}$
η	$\sigma\, y/x$
θ	time or streamline angle
λ	dimensionless energy flow rate/unit width
μ	absolute viscosity
ν	kinematic viscosity
ξ	transformed x - coordinate
ρ	density
σ	dimensionless spreading factor
τ	shearing stress
φ	dimensionless velocity $u/\bar{u}_{2a}$
ω	density of model base
H	dimensionless mass addition parameter
Λ	dimensionless temperature T_o'/T_{o2a}

Superscripts	
$'$	local value or fluctuating component
r	local value behind shockwave

Subscripts

B	base region, recirculation zone
b	base
f	forward
i	indicated value (not corrected for Re error)
ℓ	velocity difference indication
o	stagnation conditions or mixing layer origin
R	recovery conditions
r	rearward
s	wetted length
W	wall
X	wake length
x	station in shear layer
1	edge of forebody boundary layer at shoulder
2a	shear layer free stream
δ	outer edge of viscous layer

I. INTRODUCTION

The Rosemount Aeronautical Laboratories of the University of Minnesota have recently completed an experimental investigation of supersonic base flow processes under turbulent flow conditions. The primary purpose of the investigation was to obtain an understanding of the fundamental processes of convective base heat transfer in supersonic flow, leading to development of methods for predicting base heating under flight conditions.

Flow processes in the near-wake, or recirculation zone as it is sometimes called, dominate the thermal and fluid mechanical environment of the base. Considerable experimental and analytical effort has been expended to obtain a better understanding of the fluid mechanics of flow around bases. These early investigations were initiated because of the large drag created by underpressurization in the base regions of missiles and aircraft. Base heating of ballistic missiles has been responsible for the recent interest shown in this type of flow. During the high Mach number portion of missile trajectories, base aerodynamic heating can become serious, and at lower altitudes, the recirculation of hot exhaust gases in the base region creates a severe heating problem. Since no method exists for reliable prediction of these heating effects, the tendency has been to overprotect, with resulting increases in vehicle weight and corresponding decreases in range and performance.

It is hoped that these findings will contribute to a better understanding of the base flow process and will help those who are trying to overcome the base heating problem.

2. THEORETICAL BACKGROUND

2.1 Formulation of Flow Model

Flow in the base region of a missle with an exhausting jet presents a formidable problem, both to the theoretician, who wants to derive a set of equations describing the flow processes involved, and to the experimentalist, who wants to simulate those conditions in the wind tunnel. At the present time, a flow model and accompanying theory which accurately describe the flow picture and reliably predict both base pressures and heating rates have not been obtained.

Using a philosophy of starting simply and advancing later to complex configurations more closely related to flight conditions, it was felt that a simple, two-dimensional model, with a flush base would provide a good vehicle to establish a base flow environment amenable to theoretical analysis and experiment. As turbulent flow is usually encountered during portions of the vehicle trajectory of interest, similar conditions were desired in our experiments. A Mach number of 3 was chosen because even at hypersonic speeds, blunt vehicles of moderate length have shoulder Mach numbers near this value.

Due to the complexity of the problem, it may be helpful to divide the assumed flow model into smaller sub-regions. The reader is referred to Figure 1 which displays the zones of interest. We shall consider only a two-dimensional, compressible, near-wake, region behind a slender body immersed in a moderately supersonic flow ($1 \leq M \leq 3$). The following zones of interest are presented:

1. The initial free stream extends from the outer edge of the leading boundary layer outwards, presumably terminating at a shock wave.

2. The initial upstream boundary layer. The local Reynolds number is taken large enough such that only turbulent boundary layers need be considered. Extremely low density and intermediate laminar range boundary layers are omitted.

3. The expansion zone. The sub-region wherein the turbulent boundary layer interacts with the irrotational Prandtl-Meyer flow.

4. The near-wake free stream. This region lies downstream of the inviscid portions of Regions 1 and 3.

5. Region 5a includes the expanded boundary layer above the lip shock. Experiments indicate that this region is formed of the outer portions of the upstream boundary layer and the velocity gradients are greatly diminished as the expansion zone is bridged. A nearly uniform flow results.

5b. Region 5b involves the expanded lower portions of the upstream boundary layer. The upper boundary of Region 5b is the lip shock which is generally accepted to result from the expansion process.

6. Region 6 includes the portion of the mixing layer which falls above the dividing streamline. The boundary between Regions 5b and 6 defies exact specification due to the turbulence present and to the asymptotic nature of the mixing layer. The lower boundary, the dividing streamline, falls close to the inflection point of the mixing layer velocity profile.

7a. Region 7a involves the lower portion of the mixing layer below the dividing streamline, and, for convenience, above the zero velocity line. The flow in this region is recirculated when the wake is closed.

7b. This region is often referred to as the "dead-zone", despite experimental evidences reported herein and recurrent experimental reportings of the existence of large reverse flow velocities of the order of 0-0.6 in Mach number. Regions 7a-7b, when lumped together, will be called the "recirculation zone".

8a. Region 8a may be a boundary or a zone. The experimental evidence of this report supports the existence of a thin "boundary layer" like film flowing over the rearward vertical surface of the body.

8b. Region 8b involves the stagnation region of the wall boundary layer mentioned above. It also includes any "roller-bearing" vortices which may occur in the corner region.

9. Region 9 includes either a. the horizontal solid surface (in the case of a rearward facing step), or b. a plane of symmetry. In the first case the velocity is zero on the wall while the velocity gradient is finite. In the second case the centerline recirculation velocity is finite while the velocity gradient is zero.

10. Region 10 is loosely classified as the recompression region. Its boundaries are incapable of description since the region encompasses the aft portions of Regions 5a-9 and the trailing shock.

11. Region 11 is another mixed flow region, not to be considered here, which is called "far-wake".

The brief description of the zones of interest demonstrates that we are not dealing with a single, basic, fluid mechanics problem. Each zone involves complicated processes, not in themselves fully understood, much less their interactions. The philosophy of this discussion is to present a few of the available theoretical analyses and experimental results which hopefully apply to the individual zones and to suggest methods whereby these techniques may be synthesized to provide the "total-picture". Of course, such a "building block concept" necessarily requires a host of simplifying assumptions. This condition typifies the present state of the knowledge of near-wake flow - the simple, relatively inaccurate solution prevailing over the cumbersome, numerical step-by-step computation.

The near-wake problem is not a separation process in the accepted terminology. The separation process depends upon the interaction of the pressure distribution with the low speed portions of the upstream boundary layer and is relatively independent of the free stream conditions.

Bloom (1)* describes the class of separated flows describable in terms of the boundary layer approximations as moderately separated viscous flows - with negligible pressure variations normal to the surface. For shock or step-induced turbulent separation with small pressure gradients, such methods are satisfactory for engineering relations but the formulation fails for the more difficult case of large pressure differences because of the inadequacy of the turbulent mixing hypothesis under these conditions.

2.2 The Production of the Heat Flux Into the Base Region of a Supersonic Vehicle

2.2.1 General

Preceding and concurrent with the experiments, a survey of the unclassified literature pertaining to separated flows was carried out. The study of this type of flow is growing at an increasing rate because of the widespread interest shown by those encountering this phenomenon in investigations of base heating, hypersonic control and stability, aerodynamic noise generation, and such longstanding problems as airfoil performance and internal aerodynamics of channels and ducts.

Rosenhead (2) has presented a critical summary of knowledge and ignorance, both theoretical and experimental, of the classical phenomena of vortex systems in wakes. Krzywoblocki (3) has given an extensive review of the literature on jets which deals with the fundamentals and mathematical theory of free boundary flow in jets; with the distribution of velocity, density, pressure and temperature in laminar jets and the transport of mass momentum and energy in turbulent jets.

Subsonic Versus Supersonic Wakes

At low subsonic Reynolds numbers a vortex is formed in the wakes behind obstacles. The primary Karman vortex streets are not stable (4).

*Numbers in parentheses indicate references.

They become deformed as the distance behind the obstacle increases and finally break down. Thereafter the wake rearranges itself into a secondary vortex street much larger that the primary one and the process continues. A model commonly used for the determination of incompressible viscous flow in large Reynolds numbers about a bluff body placed in a uniform stream is the Helmholtz-Kirchhoff free streamline model or the modified Kirchhoff model of Roshko. The essential features are that the fluid velocity be zero everywhere inside the wake bubble (5).

Ryan (6) measured quite low recovery factors behind blunt bodies - a phenomenon which has been described by Ackeret's non-steady potential vortex theory (7). Thomann (8) also found that the recovery factor was greatly influenced by the vortex sheet in subsonic flow. The suppression of the vortex sheet has been accomplished by a splitter plate which increases the recovery factor from 0.1-0.2 to 0.8-0.9. At transonic and supersonic speeds where the vortex sheet disappears, the measured recovery factors are again 0.8-0.9. Shadowgraph observations of the supersonic case indicate that there is no evidence of large scale vortex formation. The expansion-shock process seems to stabilize the flow pattern, according to the laws of forbidden signals.

Since subsonic and supersonic near-wake flows appear to possess quite different flow characteristics, extreme caution must be observed in extrapolating subsonic experimental data into the supersonic range.

The Near-Wake Region Versus Gaps and Steps

The step-gap process is a combination of separation and mixing. Frequently there are high normal gradients near the face of step and a vortex of considerable strength in this region. Gaps are notorious sound generators (9-12). In (13) cavity resonance was accompanied by a large decrease in transition Reynolds number at the lower test Mach numbers. If the gap is of sufficient length transitions for which the flow changes from the type of one to the type of two dead air regions complicates the process (14). Also the critical cavity depth comes into

play, i.e., the depth beyond which the depth increases has no effect on pressure distribution in the cavity.

The type of flow reattachment is a dominant factor in the flow patterns. Gaps and steps permit flow reattachment to occur on the body. The recompression process is sensitive to body geometry in the recompression region. Therefore, it is difficult to compare experimental results taken on bodies of varying geometries.

In (15) Chung and Viegas present a boundary layer type of heat transfer analysis which considers laminar separation heat transfer at reattachment. This is another example of the formulation of a boundary layer under vortical motion bearing a certain resemblance to the base boundary layer found in the present experiments but differing due to the relatively large recompression pressure gradients.

In the near-wake case, recompression does not occur on the body. A flow reattaches to its image flow downstream of the body. Since the body is not in close proximity to the recompression region and its associated high pressure and heat fluxes, the influence of the recompression process on the body heat transfer characteristics is not direct, but secondary through the mean base pressure.

2.2.2 Discussion of Zones of Interest

The Initial Free Stream and Body

In the absence of upstream protuberances such as wings and fins, the initial free stream condition will be a nearly-constant-pressure, constant-velocity, flow. Ferri (16) has made calculations on the inviscid effects of the entropy layer caused by body bluntness on base pressure and heat transfer. He concluded that at high Mach numbers the pressure on the rear part of the blunt body is higher than free stream and the heat transfer on the afterbody can be important. He found that heat transfer data obtained at low Mach numbers cannot be extrapolated directly to high Mach numbers since relative levels of heat flux on the front part and rear portions of the body change rapidly with Mach number. Bogdonoff (17) has observed these phenomena

which differ with the low-Mach number, flow picture of Figure 1. He cautions that at high Mach numbers,once the wake is closed or has a minimum section, the assumption that downstream disturbances have no effect, cannot be used. The sensitivity of the wake disturbance casts doubt on the comparisons of base pressure measurements taken at hypersonic speeds.

The Initial Boundary Layer

When the boundary layer on the body surface is turbulent the free shear layer is also turbulent; however, if the boundary layer is laminar the laminar free-shear-layer shows an increased stability at supersonic speeds. The upstream boundary layer can influence the near-wake flow model. The low base pressure presumably propagates upstream in a manner which is the inverse of a boundary-layer-shock-interaction. The boundary layer profiles (laminar or turbulent) must be included, as initial conditions in a complete analysis of the near-wake problem. For example, in the Crocco-Lees analysis (19), the initial boundary layer thickness is a fundamental variable since it is a boundary condition for the integration of their differential equation which governs the base pressure.

Clauser (20) suggested a possible relation of the known laminar boundary layer solutions to the outer region of turbulent boundary layers. Sandborn (21) presented a general empirical relation for the mean velocity distribution of both the laminar and turbulent boundary layers. Coles (22) suggested that the development of the attached turbulent boundary layer is ultimately interpreted in terms of an equivalent wake profile which is modified by the presence of a wall, i.e., the streamwise mean velocity distribution in a turbulent boundary layer can be expressed as a linear combination of wall and wake components. There is similarity between this philosophy and that of Crocco and Lees who attempted a qualitative analysis of turbulent shear flows in which they visualize a continuous spectrum of mixing processes having both the wake-like and boundary-layer-like properties.

The laminar-like characteristics of both the upstream turbulent boundary layer and the following turbulent shear layer suggest that

a generalized treatment of the coupling of these two flows may be possible.

Holder and Gadd (18) presented a physical argument that the initial boundary layer thickness is not an important factor in setting the base pressure. Their argument, which is based on an inviscid fluid analysis, yields the result that the velocity gradient normal to the stream direction is reduced upon passing through a sudden expansion in the ratio of downstream pressure to the upstream pressure. The expansion accelerates the boundary layer so that just downstream of the corner the large shear portions of the mixing layer are considerably thinner than the original boundary layer.

The experimental information concerning the effects of the initial boundary layer on the wake flow process covers a spectrum. In the upper limit the boundary layer dominates the wake flows in the experiments of (23) and (24). In the other class (67), the initial boundary layer is sufficiently small such that the shear layer dominates the near-wake processes. Most experiments fall somewhere in between, i.e., the initial boundary layer measurably affects experimental findings and must be included in any realistic analysis of results.

The Expansion Zone

The supersonic expansion causes the flow to accelerate, resulting in a lower static pressure. In the absence of the upstream boundary layer, the final flow field is that resulting from a Prantl-Meyer expansion.

The exact calculation of the expansion phenomenon is difficult to handle because the pressure distribution assumes a constant static pressure normal to the surface while a Prandtl-Meyer expansion experiences pressures which are constant along rays from the apex. The two analytical models are not compatible. It is undoubtedly necessary to include the next higher order terms in the Navier-Stokes

equations. The unknowns in the expansion region are the radial and tangential components of velocity and pressure. The three available equations are the conservation of both radial and tangential momentum and the continuity equation.

Pai (26) applied first-order corrections to the irrotational Prandtl-Meyer flow for small vorticity of the initial stream. It was shown that in passing the corner a parallel shearing flow is turned into a non-parallel flow. Roy (27) presented an integral analysis which predicts a dimunition of the boundary layer thickness following an expansion. Korst (28) has suggested an approximate treatment by the stream tube method.

Studying expansions over solid surfaces, Murphy and Hamitt (25) found that for expansion angles of the order of 25°, a new, thin, boundary layer seems to start at the corner. Downstream of the corner the original boundary layer tends to merge with the free stream. This model agrees with the expansion process in the near-wake region revealed by schlieren photographs taken during the present investigation. Ferri has treated the solid wall expansion problem and deals with an inviscid expansion around the corner and treats the boundary layer downstream of the corner as two layers. Zakkay and Tani (29) performed the analysis and found agreement with pressure and heat transfer experiments. The flow downstream of the discontinuity is obtained by expanding both the supersonic and subsonic flow field inviscidly around the corner. Downstream of the discontinuity the flow is represented by a viscous shear layer which starts at the discontinuity and a viscous outer layer which has the inviscid profiles immediately downstream of the discontinuity as an initial condition. The velocity and stagnation enthalpy profiles are divided into strips, each strip expanded isentropically around the corner. This is justified on the ground that the region near the wall expands very rapidly and the distances along the streamline direction are very small and therefore the viscous effects on pressure and velocity are negligible. In this way an extended velocity

profile is obtained having a non-zero value at its lower edge. This flow model is adaptable to the near-wake problem.

The Near-Wake Free Stream

Since the flow region 4 (Figure 1) results from an inviscid expansion of a uniform flow to a higher Mach number, its properties should be regular and of no further concern. The flow reflects the initial geometry. Eventually this flow enters into the outer layers of the far-wake.

The Expanded Boundary Layer Above the Lip Shock

This flow is treated as having small vorticity resulting from the boundary layer-expansion process. Napolitano (30) has investigated the turbulent mixing of a non-uniform free stream of constant vorticity with a fluid at rest. The solutions are given in terms of the vorticity number first suggested by Li. It was found that the effects of external vorticity are sizable for turbulent mixing.

The lower boundary of this region occurs at the lip shock. The generally accepted explanation for it is as follows (31). During the rotational expansion process a system of waves of both families is generated. When the Mach number is greater than 2, an expansion is reflected as an expansion into the lower layer and a compression wave is emitted into the upper one. These shocklets coalesce to form the lip shock. This explanation does not seem to be consistent with the present experimental data where the lip shock occurs at a Mach number of approximately 3.6. The effect of the lip shock on the shear layer development has not as yet been included in the analyses. Examples of the lip shock are available in the published photographs of (23) (30), and in Figure 1 of this report. The existence of the lip shock tends to make the interpretation of experimental probing data, which are already compromised by experimental imperfections, more difficult to analyze.

The Expanded Lower Portions of the Upstream Boundary Layer

Below the lip shock there is a continued dimunition of the local velocities. This makes the determination of the outer edge of the shear layer difficult to determine experimentally. Since there is a slight variation of the "main stream velocity" at the lower edge of Region 5b, this boundary is truly artificial.

The Mixing Layer Above the Dividing Streamline

Ignoring the previously described zones, the theoreticians have been quite active in describing this case. The pressure, in the first approximation, can be assumed constant. Experience indicates that the width of the mixing zone increases linearly with x, if x is the distance from the point where mixing starts. Liepmann (32) presented a dimensional argument confirming this feature.

Momentum transfer theory requires similarity between momentum and heat transfer. Experiments show that heat spreads faster than momentum and that this is in qualitative agreement with the vorticity transfer theory. Since the theories of free turbulence link momentum and thermal exchange with the gradients of velocity and temperature, comparison should preferably be made with the measured gradients. The measured velocity and temperature distributions in wakes and jets all resemble an error-curve in form, but the results are too scattered to permit the slopes of experimental curves to be determined with confidence. The spreading factor σ is commonly used in such correlations.

Tripp (39) and Vasiliu (40) present different correlations on the variation of σ with temperature ratio and with Mach number. An increase is noted. The larger values of σ, the spreading factor, correspond to a smaller rate of divergence of the mixing zone. All listed values of σ are based on data for jets discharging into a medium at rest and may not be applicable to the present situation.

It is beyond the scope of the present discussion to describe the various assumptions of the several theoretical analyses. Three general modes of attack are available:

1. Crocco-Lees analyses
2. Pohlhausen integral techniques
3. Mixing layer analyses

The Crocco-Lees analyses (19) is not fundamentally different from the Pohlhausen method (33). The results of the Crocco-Lees method, although in general qualitative agreement with experiments, are probably no better than those obtained much more readily by a Pohlhausen type of calculation.

The mixing lengths deduced by comparison with experiment are greater than 10% of the width of the wake. This is an indication that in turbulent free layers the eddy viscosity depends on overall conditions and not on such local conditions as local velocity gradients. Eddy viscosity values do fall to zero not far from the edge of the mixing region so the assumption of constant exchange coefficient leads to velocity distributions which are incorrect near the edges. However, the use of a constant exchange coefficient in turbulent flow permits a unified treatment of the equations for laminar and turbulent mixing. Gortler (34) reduced the turbulent incompressible mixing equations to the Blasius problem, which is typical of incompressible laminar dissipative flow fields which exhibit similarity. Crane (35) and Napolitano (36) showed that, to a good approximation, the turbulent, compressible, two-dimensional mixing profiles can be obtained by taking velocity profiles as originated by an equivalent incompressible laminar mixing. The turbulent mixing layer analysis of (37) is of significance. In his analysis, two-dimensional boundary layer equations for free jet mixing with an initial boundary layer were reduced to the heat conduction equation by means of Pai's small perturbation method (38). The equations are solved in an intrinsic coordinate system with the same initial boundary conditions as for a reference system based on a corresponding jet. The method requires a determination of two empirical quantities for the kinematic viscosity formulation. Chapman and Korst present low speed experiments on this problem. One quantity, the exchange coefficient, is nearly constant; the other is a function of the

initial boundary layer. Bailey and Kuethe (23) demonstrated that these linearized theories for jet mixing (42) do not correlate supersonic turbulent mixing experimental results. The second mixing coefficient shows radically different behavior for supersonic rather than subsonic flows.

In the two-dimensional case the compressibility effect on laminar and turbulent flow is to decrease and increase the width of the mixing region respectively (41). For axially symmetric jets, the same holds true for the laminar case whereas for turbulent flow the tendency is reversed. Crane (35) showed that with turbulent mixing the influence of compressibility on the form of the non-dimensional velocity profiles is almost negligible. The effect of temperature differences are shown to be rather unimportant. The latter calculations support the use of the error-function-velocity-profile, independent of Mach number and temperature ratio, as used by Korst (28).

Knowledge of the turbulent Prandtl number is necessary before a complete calculation of the temperature and velocity profiles may be carried out. The common procedure is to assume a turbulent Prandtl number equaling one. Forstall and Shapiro (43) have found that the turbulent Prandtl number and Schmidt number are both equal to 0.7 within 10%-independent of the experiment. Thus they find that the turbulent Prandtl number and Schmidt numbers are approximately equal, and that mass and temperature diffuse at equal rates, a rate greater than the diffusion of momentum. Corrsin (44) found that the average of an effective turbulent Prandtl number in a round jet is equal to the laminar value within the probable accuracy of his experiment. Bailey and Kuethe (23) inferred the existence of a turbulent Prandtl number which is less than unity from supersonic mixing of jets in turbulent boundary layers. That the effective turbulent Prandtl number might possibly be the same as the laminar Prandtl number was apparently first suggested by Dryden (45), though not with any particular physical justification.

The thermal solution of the incompressible laminar near-wake problem has been given by Chapman (46) for several Prandtl numbers. In view of Gortler's reduction, the discussion above suggests a Prandtl number correction based on the laminar incompressible results may be applied to the turbulent case. Another possible alternative is the work of Spence (47), which is an extension of Mager's formulation (48) as applied to free mixing problems (49), which may be used to generalize the problem when the turbulent Prandtl number is not equal to one.

The lower boundary of this region occurs at the main dividing streamline by which the reverse flow region is isolated from the main flow. The concept of the dividing streamline has been used extensively theoretically and has received verification by Tani (50), whose experiments show that the dividing streamline followsclosely to the points of inflection of the velocity profiles even through the recompression region.

The Mixing Layer Below the Dividing Streamline

Nothing new of a theoretical nature appears in the treatment of this region, as distinguished from Region 6b. The region is difficult to study experimentally because of the diminished streamwise component of velocity and the increase in the transverse component as one penetrates further into the mixing layer. As a result probing errors are admittedly large in this region and techniques such as the interferometric studies of Reference (51) are to be preferred.

The Reverse-Flow Region

A fundamental question concerning the flow in this region concerns the stability of the flow and its temperature distribution.

As mentioned previously, the Mach numbers in this region can reach as high as 0.6 in a direction opposite that of the main flow. Forthmann (52) measured the characteristics of the reverse flow profile in a partially expanding subsonic jet which have the same general characteristics as the present case.

Carlson's analysis (53) of the wake flow problem is unique in that the integral method is carried out across both the "dead-air region" and the mixing layer, and takes into account the reverse flow in the recirculation zone. His solution, however, does not apply to the near-wake problem.

Lin (54) has presented an elegant analysis concerned with the effect of viscous forces upon the vortex streets in the wake of blunt bodies using an improved Oseen approximation. He introduces additional linearization valid for vortices not too close to the generating body which enables him to solve for the steady wake velocity distributions.

The ratio of the Strouhal and Reynolds numbers is the basic parameter governing the structure of wakes with periodic vortices.

Using Batchelor's concepts on free convection, Squire (55) suggests treating this vortical motion as a "core" with constant vorticity surrounded by a boundary layer. The cavity motion is maintained by shear stresses along the dividing streamline. In the core viscous effects are small, although viscosity is responsible for the development of the motion. The vorticity is taken to be constant along streamlines and viscous effects are absent. The total pressure is constant along streamlines within the core. He argues that the vorticity will tend to be constant in the core due to the residual action of viscosity. Since viscosity tends to destroy vorticity gradients, the constant core viscosity assumption may not be true in the physical case since the mixing region is turbulent. The core streamlines may cross into the turbulent mixing zone. Each streamline may have constant vorticity in the core but the vorticity is not uniform throughout the core.

Lam (56) has shown that the pertinent parameter for closed streamline problems is the Peclet number,

$$Pe = Pr\ Re.$$

For $Pe = 0$ the problem is one of pure heat conduction Q_o. For $Pe > 0$, in steady flow, the heat transfer through the region without dissipation is always higher than Q_o. At large Peclet numbers, Lam infers that a boundary layer type of solution develops outside of the core. Based on conditions along this dividing streamline, typical values of the Peclet number for the present experiments are 10^6.

There are certain laminar boundary layer solutions called "lower-branch" solutions which resemble the profiles of the recirculation zone as they have a region of reverse flow near the wall. Stewartson (57) first drew attention to the possible use of these solutions as representative of flow in a separated region.

Abramovich (58) presented an inviscid compressible flow model which contains many features which are similar to those of viscous flow, in particular, a region where the flow is reversed. The "reentrant Jet"

model has been widely proplsed for explaining the cavity behind the flat plate or other obstacles in the infinite stream. The back of the cavity is supposed to end in a reentrant jet which disappears on another sheet of the "Riemann surface" representing the physical plane. This approach is discussed at great length in Reference (59). Wall-jet analysis, as exemplified by References (60) and (61) also may be applied.

The Base Region

There is still some uncertainty as to the existence of secondary "roller-bearing vortices" in the region of the wall. It is difficult to sketch the flow pattern in this region without including them when the walls and planes of symmetry have sharp corners. The exact shape of the wall has only been accounted for by Carlson (53) for the laminar case. Reference (62) presents heat transfer data revealing higher heat transfer measured in the center of a base as compared with the rim of an axisymmetric body. In the rear stagnation region the heat transfer coefficients are much lower than the maximum values on the front of a blunt body (63). In general, laminar separated heat transfer values are only about 2/3 of the equivalent solid surface values, where the turbulent fraction varies from 1/4 to 2/3.

Richardson (64) has presented a heat transfer prediction of the subsonic problem based on physical arguments and analogies. He relates the flow behind a transverse cylinder to some paradoxical flows in free and forced convection. At low Rayleigh and Reynolds numbers the development of these flows is associated with critical values of these numbers. At high Rayleigh and Reynolds numbers these flows exhibit mutually similar heat transfer characteristics. He advances the hypothesis that the local Nusselt number may be found by the same method as that for the horizontal flat plate and rotating cylinder using the local critical Reynolds number. The hypothesis predicts that, for the case of a bluff flat plate, the highest local heat transfer coefficient occurs at the rear stagnation point and falls slightly toward the edges. One free

constant is left for experimental evaluation. The form of this heat transfer prediction is

$$Nu = \text{constant } Re^{2/3}$$

The two means of experimental verification of the Richardson relation involve the leading constant and the exponent of the Reynolds number. Subsonic experiments (65) confirm the power. The supersonic data of Larson (66), although influenced by geometrical recompression effects, also support the 2/3 exponent.

The collected trends indicate that the heat transfer is higher along the center portions of the base, falling off very slowly as one progresses outward. This agrees qualitatively with the laminar stagnation point region heat transfer variations. It seems reasonable to conclude that the heat transfer process is governed by the recirculation zone processes. Where time-averaged, these may be comparable in the subsonic and supersonic cases, thus rendering the Richardson analogy more palatable to the supersonic experimentalist.

The Wall or Plane of Symmetry Boundary

The type of boundary conditions along the horizontal surface is importance for the mixing layer analyses although the existence of the recirculation zone violates the asymptotic nature of the mixing layer theories. On the average, symmetry prevails if this boundary is a free surface. This condition illustrates the basic difference in the flow pattern between the near-wake problem and a gap or rearward facing step. No analysis illustrating the results of the differences in these boundary conditions is available.

The Recompression Region

The examination of the available base pressure data is frustrating due to factors such as sting effects, the presence of wings and fins, boat-tailing, mass addition, etc. Unifying principles have been advanced by Chapman (67) and Korst (28).

The wake pressure is found from a mass balance which takes into account the pumping action due to the mixing process. Love (70) has offered a simple, semi-empirical method for estimating base pressure which stems from an analogy established between the base pressure phenomenon and the peak-pressure-rise associated with the separation of the boundary layer. These estimates give fair predictions of experimental results. Charwat (68) has offered a hypothesis for the observed base pressure increase with increased Reynolds number. Continual compression, idealized to multiple compression cells, conforms conceptually with experimental evidence. The base pressure variations with Reynolds number also agree qualitatively with the theoretical predictions of Crocco and Lees throughout wake transition (69).

Both Korst and Chapman assume that the total pressure on the dividing streamline approaching reattachment is equal to the static pressure downstream (in the far-wake). Chapman (laminar mixing) assumed isentropic recompression for both the viscous region and the free stream. Korst (turbulent mixing) used an oblique shock to specify the recompression pressure. Each assumption seems appropriate to its case of application.

The compression is approximately isentropic along the dividing streamline through the recompression zone. If one includes the case where the boundary layer thickness is sizable, the calculation of the velocity along the dividing streamline is complex since similarity is not present. Since the correlations of Korst and Chapman compare favorably with the experimental data for base pressure, the expected variations of the dividing streamline velocity are not large.

In our opinion, the Korst turbulent base pressure theory, which is based on more than the usual number of first-order approximations and other assumptions typical of turbulent boundary layer theory, is more accurate than originally expected.

Far Wake

The rear stagnation point occurs one or two diameters from the base. The diameter of the neck is approximately the body radius. References

(71), (72), and (73) have described the flow processes in the far-wake, which begin at the neck below the trailing shock. Only the fluid elements above the dividing streamline pass into the far-wake. The typical velocity exceeds 60% of the main flow velocity outside of the free shear layer. The enthalpy in this region is about 90% of the total enthalpy outside the wake if the body surface is insulated. Thus a hot core of fluid is generated in the inner wake which cools off downstream of the neck, requiring an inner and outer, two fluid, system similar to that proposed above.

2.2.3 Discussion of Korst Analysis

The Korst analysis was studied to determine its applicability in predicting base pressures and heating rates for the conditions of the present experiments. The concept of the theoretical model employed by Korst, Chow, and Zumwalt (28) includes the interaction between nearly isentropic flow regimes and dissipative regions (see Figure 2). Their analysis is restricted to two-dimensional, constant-pressure mixing and is attacked by an integral technique.

In contrast to the important influence of a wall in turbulent boundary layer flows, free turbulent flows (not confined by solid walls) are more amenable to analysis. Here turbulent friction everywhere dominates laminar friction to such an extent that the latter (and its associated mathematical complications) is omitted completely.

As in the case of laminar wake flows, free turbulent flow possesses qualities of a boundary layer nature and are studied with the aid of the boundary layer equations. For constant-pressure, steady, two-dimensional mixing, these are:

$$\rho\left(\bar{u}\,\frac{\partial \bar{u}}{\partial x} + v\,\frac{\partial \bar{u}}{\partial y}\right) = \frac{\partial}{\partial y}\left(\tau_t\right) \qquad (1)$$

$$\frac{\partial(\rho\bar{u})}{\partial x} + \frac{\partial(\rho\bar{v})}{\partial y} = 0 \qquad (2)$$

where τ_t denotes the turbulent shearing stress. To solve the system, it

is necessary to express the turbulent shearing stress in terms of the main flow. This has been done empirically by Prandtl who stated that for free turbulent layers

$$\tau_{xy} = \tau_t = -\overline{\rho u' v'} = \rho \varepsilon \frac{d\bar{u}}{dy} = \rho C \delta \left(\bar{u}_{max} - \bar{u}_{min} \right) \frac{d\bar{u}}{dy} \qquad (3)$$

Here C denotes a dimensionless number to be determined experimentally and δ is the height of the mixing layer. Implicit in this equation is the assumption that the scale of the lumps of fluid which move in a transverse direction during turbulent mixing is of the same order of magnitude as the height of the mixing zone.

The application of the boundary layer equations is not restricted to regions near a solid wall. They can be applied to any layer in which the influence of friction dominates, such as in the wake behind a body or when a fluid is discharged through an orifice. Considering the wake case, Pai made the assumption that the velocity difference in the wake

$$\bar{u}_\ell (x,y) = U_{2a} - \bar{u} (x,y) \qquad (4)$$

is small compared to U_{2a} so that quadratic and higher terms in u_ℓ may be neglected. For constant pressure mixing, the momentum equation is then linearized by use of the small perturbation method proposed by Pai (38) to yield

$$\frac{\partial \bar{u}_\ell}{\partial x} = C_1 x \frac{\partial^2 \bar{u}_\ell}{\partial y^2} \qquad (5)$$

where the quadratic terms in $\bar{u}_\ell$ and $\bar{v}_\ell$ have been omitted.

At $x = 0$, the velocity is zero for negative y's, is equal to the free-stream velocity u_{2a} for $y > \delta_2$.

Taking $\xi = x/\delta_2$, $\eta_p = 1/2\sqrt{\xi}$, the general solution of this linear problem is

$$\varphi = \frac{\bar{u}}{u_{2a}} = \frac{1}{2} \left[1 + \text{erf} \left(\eta - \eta_{\delta 2} \right) \right] + \frac{1}{\sqrt{\pi}} \int_{\eta - \eta_{\delta 2}}^{\eta} f \left(\frac{\eta - \beta}{\eta_{\delta 2}} \right) e^{-\beta^2} \, d\beta \qquad (6)$$

The inclusion of the upstream boundary layer does not permit general results to be expressed. A more expanded treatment has been given by Korst in Reference (37). Restricting the present discussion to no initial boundary layers, $\eta = \sigma\, y/x$, and we obtain Gortler's first approximation solution (34).

$$\varphi = \frac{\bar{u}}{u_{2a}} = \frac{1}{2}\left(1 + \operatorname{erf}\eta\right) \tag{7}$$

where σ is the empirical spreading factor.

For a turbulent Prandtl number of one, the velocity profile can be related to the temperature profile by utilizing Crocco's integral of the energy equation such that the total temperature profile is given by

$$\Lambda = \frac{T_o'}{T_{o2a}} = \frac{T_B}{T_{o2a}} + \left(1 - \frac{T_B}{T_{o2a}}\right)\varphi \tag{8}$$

Thus $T = T(\bar{u})$, curves of constant velocity are identical with the isotherms. For constant pressure mixing of a perfect gas, the Crocco number ($C = \bar{u}/u_{max}$) is convenient to use since the analysis and results all become independent of specific heat ratio γ. The density ratio is given by (with $\varphi = \frac{\bar{u}}{u_{2a}}$),

$$\frac{\rho_{2a}}{\rho} = \frac{T}{T_{2a}} = \frac{\Lambda - C_{2a}^2\varphi^2}{1 - C_{2a}^2} \tag{9}$$

Energy Balance

Korst's turbulent energy balance, with no upstream boundary layer, is as follows: (refer to Figure 2)

$$\text{energy added at } x_o = \int_o^R \rho_{2a} u_{2a} c_p T_{o2a}\, dy \tag{10}$$

$$-\text{energy leaving at } x = \int_{y_j}^R \rho \bar{u} c_p T_o'\, dy$$

$$-\text{energy added by added mass} = \int_{y_j}^{y_d} \rho \bar{u} c_p T_B\, dy$$

= energy added to dead zone from the shear layer, Q_B,

$$Q_B^* + \int_{y_j}^{y_d} \rho\bar{u}c_p T_B dy = \int_{y_d}^{R} puc_p(T_{oa} - T_o^*)dy + \int_{y_j}^{y_d} \rho\bar{u}c_p T_o^* dy \qquad (11)$$

where the integral limits are shown on Figure 2 and R represents an arbitrary value of y in the inviscid flow.

It is here that Korst justifies the concept of a "dead air" region in dealing with the dynamic aspects of the two-dimensional base pressure and base temperature problem. He states that for studying the mechanism of the wake flow itself, as Carlson (53) did, such assumptions must be discarded as trivial.

Since $\int_0^R \rho_{2a}u_{2a}dy = \int_{y_d}^R \rho\bar{u}dy$, assuming x-momentum conservation,

$$Q_B^* + \dot{m}i_B = \Omega_B \qquad (12)$$

using the Korst notation. Since

$$\lambda_B = \frac{\Omega_B}{H\sqrt{T_{o2a}}P_{o2a}} \sqrt{\frac{1}{2R}} \left(\frac{\gamma-1}{\gamma}\right)^{3/2} \qquad (13)$$

$$\mathcal{H}_B = \frac{\dot{m}\sqrt{T_{o2a}}}{HP_{o2a}} \sqrt{\frac{\gamma-1}{2\gamma}R} \qquad (14)$$

Then:

$$Q_B = \frac{Q_B^*}{P_{o2a}H\sqrt{T_{o2a}}} \sqrt{\frac{1}{2R}} \left(\frac{\gamma-1}{\gamma}\right)^{3/2} = \lambda_B - \mathcal{H}\frac{T_B}{T_{oa}} \qquad (15)$$

is the energy added to the mixing layer from sources other than the added mass m, where H is the reference length taken here to be the half base height. H is related to the wake slant length X by the relation

$$H = X \sin\theta_{2a} \qquad (16)$$

Korst has demonstrated the generalized presentation λ_B vs. H_B for an approach Mach number of 2.0 and a simple rearward-facing step. The calculation has been repeated for an approach Mach number of 3.0, paralleling the present experiment (Figure 3). Equation 15 was used to

subtract the energy rate of the added mass from the total rate of energy added to the wake from the outside flow (all energy rates are per unit wake width). This was done in order to obtain an energy rate analogous to the heat transferred by conduction at the wall in an attached boundary layer case. The resulting presentation is shown as Figure 4. It is seen that when the base temperature is equal to the freestream stagnation temperature, no energy flows from the shear layer into the dead zone ($Q_B = 0$), irrespective of mass addition. The unexpected result is that for a fixed base temperature ratio, T_B/T_o, Q_B increases with $\dot{m}$, instead of decreasing. The latter situation occurs in boundary layer flow with mass addition at the surface (but at constant pressure). However, mass addition produces an increase in base pressure ratio P_B/P_1 as shown in Figure 5. If the base pressure is held constant at its zero-mass-addition-value, i.e., by decreasing the tunnel total pressure in an experimental study, the dimensionless heat flux increases shown in Figure 6 are shown to decrease (see Figure 7). The dominant effect of mass addition is to increase the base heat flux by increasing the base pressure despite the presence of the thicker thermal layers normally generated by mass addition.

On Figures 3 - 7, adiabatic flow conditions were assumed from the tunnel stagnation chamber to the outer edge of the shear layer. Therefore, $T_{oa} = T_{o2a} = T_o$ = tunnel stagnation temperature.

3. EXPERIMENTAL EQUIPMENT AND TECHNIQUES

3.1 Discussion of Test Facilities

The early experiments were conducted in channel 4 of the main continuous flow facility. To obtain the best possible experimental environment for continuation of the base flow program, the final tests were made in the supersonic channel of the propulsion research laboratory. Because of its remoteness from the main continuous flow facility, the propulsion research building is free of all vibrations emanating from the compressors and vacuum pumps and lends itself nicely to measurements requiring considerable precision.

The basic facility consists of a 6-in. x 9-in. supersonic channel and variable diffuser with an isolated control room and laboratory space. This channel utilizes the compressors, exhausters, and heaters of the continuous wind tunnel facility and was designed to handle stagnation pressures up to 110 psig.

The compressor installation consists of five parallel-connected, electrically-driven, reciprocating two-stage air compressors. Four are Ingersoll-Rand 700 hp compressors and the fifth is a Chicago pneumatic 1000 hp unit. The compressors pump into five buffer tanks from which the air for the tunnel operation is drawn. The air can be delivered at a maximum continuous rate of 23.2 pounds per second at a 110 psig which is equivalent to 17000 cfm of free air.

The exhauster system consists of seven Allis-Chalmers rotary vane pumps driven by four 250 hp motors. Two pumps are rated at 2270 cfm each, four at 2680 cfm each and one at 3390 cfm. Three electric motors drive two pumps each and the fourth motor drives the 3390 cfm pump. The pumps may be operated in various combinations to provide the necessary air flow and pressure level.

Figure 8a is an overall view of the test set-up in the wind tunnel room and Figure 8b shows the control room.

3.2 Model Design

3.2.1 General

The final model shape and size chosen for these experiments was the result of several compromises. The initial requirement was a two-dimensional, channel-spanning model of adequate height to house internal cooling lines and instrumentation leads, and provide the larges possible test region for ease of probing in the recirculation zone. In addition, the model had to be sufficiently long to allow the necessary wetted length required for natural transition to turbulent flow before separation without the necessity of using excessive stagnation pressures. Opposing these requirements were the possibility of tunnel choking because of the blockage area of the model and impingement of reflected shock waves from the model nose with the base region.

It was felt that a sharp leading edge with a gradual taper to the rear of the model would enhance the possibilities of natural transition and move the shockwave intersection with the nozzle blocks downstream as far as possible. The shape chosen for the model contour was a 3.8/1 caliber tangent-ogive with a straight extension. The base height was 1.5 inches and the model was 8.19-in. long. Figure 9a is a design drawing of the model forebody and Figure 9b shows the forebody attached to the steel mounting window.

Separate bases and afterbody components were used for the heat transfer and probing runs. Greater precautions were taken in minimizing conduction errors with the heat transfer base. The base used during most of the probing run had additional pressure taps.

3.2.2 Heat Transfer Base

The heat transfer base was made of pure nickel 0.0185 inch thick. Copper-constantan thermocouples and pressure taps were imbedded in the base at selected locations. Figure 10 illustrates the location of the complete instrumentation on the base and forebody.

The base and coolant passages were housed in a micarta afterbody to thermally isolate the base from the model and increase the reliability of the heat transfer data.

A steel cover plate was installed on the bottom to provide access into the model. After the plate was screwed into position, the cover plate and the forebody were ground into a smooth contour to prevent any disturbances to the flow. The disassembled model is shown as Figure 11.

Although the micarta afterbody effectively isolated the base from the forebody, the possibility of conduction effects on the base itself had to be considered. Bench tests of a small test sample showed that slots 14 miles wide, filled with Armstrong cement, formed an effective barrier to conduction heat transfer. Based on these experiments, the thermocouples on the base plate were insulated by means of the cement-filled slots shown in Figure 12. The slots had not yet been filled with cement at the time the photograph was taken. The thermocouples appear as small light colored dots in the photograph. The vertical slots were added to minimize horizontal transfer of heat across the base plate because of conduction through the brass pressure-tap extensions.

3.2.3 Pressure and Probing Base

In the early experiments difficulty was encountered in preventing small amounts of air leakage from inside the base plate into the recirculation zone. It was found during the present experiments that small amounts of air bleed can appreciably affect the base pressures. This problem was solved with the heat transfer base but it was felt that a more positive seal between the interior of the model and the recirculation zone was required. A new base plate was built which eliminated the possibility of air leakage. This base plate was also of pure nickel 0.0185 inch thick and had additional static pressure taps in the vertical direction as well as at some of the previous positions (refer to Figure 13). Thermocouples on the plate and provisions for internal cooling were retained. Figure 14a shows a rear view of the base plate and Figure 14b shows two views of the cooling chamber.

3.3 Heat Transfer Measurement Technique

The transient technique was used to obtain base heat transfer values. In this method the model is initially at a temperature below the equilib-

rium wall temperature. The flow is started and the connective heat transfer process tends to bring the wall temperature up to an equilibrium value.

The use of the transient technique to measure heat transfer applicable to steady state conditions requires assumption of a quasi-stationary process. At each instant in time the heat transfer rate is assumed to be equal to that which would exist for steady state conditions identical to those which exist at that instant. This assumption has been studied by Sparrow and Gregg (76), who analyzed the case of a semi-infinite flat plate with arbitrary variation of surface temperature with time. Using their results it can be shown for the present case that the error introduced by the quasi-steady assumption is negligible.

Initially neglecting heat conduction through the model skin and radiation effects, the rate at which heat is transferred from the boundary layer at any point on the model surface may be equated to the heat stored at the same location, or

$$\dot{q}\, dA = -\omega c_p dV dT_b/d\theta \tag{17}$$

Using the Newtonian heat flow equation

$$\dot{q} = h(T_b - T_R) \tag{18}$$

and combining with equation (17), we obtain

$$h = \frac{-\omega c_p dV/dA dT_b/d\theta}{T_b - T_R} \tag{19}$$

The heat transfer coefficient can then be obtained by measuring the instantaneous wall temperature and rate of wall temperature change. A constant density can usually be used which is evaluated at the wall temperature. The wall recovery temperature can either be calculated or measured as a function of the tunnel total temperature.

Simulation of the proper direction of heat transfer requires that the model be at a temperature below recovery temperature. This can be accomplished by precooling the model and using ambient temperature tunnel

air. For these tests internal cooling lines were installed inside the model to bring the base down to -320°F at the start of the run. A shield was placed behind the model to retard aerodynamic heating until proper flow had been established in the tunnel.

For the transient technique of heat transfer measurements, the skin thickness is a major governing factor. For a given heating rate, if the skin is too thin the time rate of change of the element temperature may be beyond the response limitations of the temperature recorders. On the other hand, if the skin is too thick, the assumptions made in using the transient heat transfer technique are not valid, as equation (17) assumes a zero temperature gradient normal to the skin.

Past experience has shown that the maximum permissible rate of temperature change would be 100°F/sec based on recorder response and data reduction procedures. From data of Naysmith (77), who measured heat transfer on and around a rearward facing step, a preliminary value of the heat transfer coefficient was obtained. His flow field was not exactly the same, but, as his data were in the same Mach number and Reynolds number range, his values were close enough for design purposes. Solving equation (19) for dV/dA and realizing that $dV/DA = t_b dA/dA = t_b$ and inserting the proper values, a wall thickness lower limit of 0.006 inch was obtained. As this was too small for structural integrity, a thickness of 0.0185 inch was chosen. Previous calculations have shown that this thickness is below the minimum required so as not to violate the assumption of constant temperature through the skin. The calculated and measured temperature response rates for this thickness were of the order of 30°F/sec.

4. SUMMARY OF EXPERIMENTS PERFORMED

4.1 The Establishment of Undisturbed Turbulent Base Flow

4.1.1 General

The establishment of a proper flow situation and definition of a suitable control region which defined the boundaries of the recirculation zone were the most important aims of the early experiments. A "clean" flow, undisturbed by interactions between the near wake and reflected nose shockwave, were essential. Consideration was given to the existence of any three-dimensional flow perturbations which would detract from the desired two-dimensional situation. The model had to be sufficiently thick to allow a reasonable test region for probing purposes, and long enough to allow transition on the model with resulting turbulent flow in the base region. It was feared that the latter two requirements could cause flow blockage and serious shock wave-wake interactions. Details of the wake starting process and knowledge of the Reynolds number required to give turbulent flow were desired.

The above problems were studied using several optical techniques and pressure measurements. The following is a discussion of the preliminary experiments carried out to add validity to the assumed flow model.

4.1 The Establishment of Undisturbed Turbulent Base Flow

4.1.2 Blockage Runs

Several preliminary tests were carried out to insure that the wind tunnel selected for these tests would run properly over the desired range of Reynolds numbers and to provide visual assurance that the correct flow field was established. These tests were very informative and the results were used as a basis for the heat transfer and probing runs.

For these runs a model 10-inches long with a 1.5-inch base height was sting mounted in the position where the final heat transfer model would be installed (Figure 15). Theoretical calculations showed that this size

should be well below the blocking area for Mach number 3. This was verified as the tunnel ran nicely with the model installed and no blocking tendencies occurred. Schlieren and shadowgraph viewing of this model provided such information as location of reflected nose shock wave with respect to wake, transition location, and model flow blocking characteristics.

Schlieren observation of the flow around the base region showed that the 3/4-in. diameter sting was very influential in determining the wake flow geometry, as were the reflections of the nose shock off the tunnel wall. Figure 16a is a schlieren photograph showing improper wake flow as a result of these combined effects. The schlieren photographs showed that it would be of interest to be able to examine the entire flow field about the model. Plexiglas windows of large enough diameter to allow visualization of the entire model and adjacent wake flow field were installed in the tunnel. Subsequent tests using this technique resulted in shadowgraph flow pictures such as Figure 16b.

In an attempt to improve flow conditions in the wake, one inch was cut off the rear of the model and it was cantilever mounted to one of the Plexiglas windows to allow removal of the sting. A view of this installation is shown as Figure 17. These efforts resulted in proper wake flow over the entire Reynolds number range (see Figure 18).

4.1.3 The Development of Proper Wake Flow

In the starting process described by Chapman (78), the final equilibrium conditions are obtained when a balance is reached between the scavenged mass flow and the reversed mass flow. According to the theory of Crocco and Lees (19), disturbances inserted into the flow downstream of the wake throat would not influence the wake flow. They state that any disturbances upstream of the wake throat would influence the flow and would create higher base pressures. A measure of this phenomenon is the minimum disturbance length. Van Hise (69) found disturbance length by two methods. One was the insertion of a probe downstream and gradual movement forward until disturbances were noted. The other was by extending the straight portion of the trailing shock

waves on schlieren photographs and measuring the distance from their intersection to the base. This latter method was used for the present data.

All measurements made during the first phase were for the case of a smooth model surface. It was found that to get fully turbulent flow in the wake a Reynolds number of the order of 4.0×10^6 was required. For further assurance, the majority of the data were taken at a Reynolds number of 6.7×10^6. When the experiments were resumed in the new installation it was discovered that sand blasting had roughened the surface to such an extent that conditions of the early experiments could be duplicated at a lower Reynolds number (2.75×10^6). Disturbance length data for the model in a roughened condition are presented as Figure 19 and shown for comparison are the data of Van Hise taken over the transitional regime. It can be seen that it fairs nicely into the rough surface data which are mostly turbulent and only partially transitional.

The criteria of the starting process are more severe than when flow is fully established. During the initial phases of the starting process the wake throat is located downstream past its equilibrium position. Because of the scavenging effect of the shear layers on the air contained in the circulation zone, portions of this dead air are transported downstream. This causes a drop in base pressure which effectively creates a larger Prandtl-Meyer expansion angle. The larger angle of turning increases the velocities in the shear layers, which in turn increases the scavenging action and lowers the base pressure even further. The final base pressure obtained is a function of the balances between the mass flow scavenged from the recirculation zone and the mass flow reversed because of the adverse downstream pressure gradient. As the throat moves closer to the base, the angle of the trailing shock wave increases. This increase in back pressure makes it more difficult for the scavenged air to proceed downstream. Equilibrium is reached when the scavenging action is exactly balanced by the reversing action (Figure 20). Disturbances created by the presence of a probe or shock wave are sometimes strong enough to prevent passage of this excess mass out of the "dead air" region and the base pressure does not reach its proper equilibrium value.

The wake starting process is in some ways analogous to the starting process of a supersonic wind tunnel. To swallow the normal shock wave it is necessary to open the downstream throat to some value depending on the test section Mach number and size. After the additional mass created by the movement of the shock wave has passed downstream of the throat it is possible to close the throat down to a size which approaches the first throat size. An analogous situation exists in the base flow starting process. In order to lower the base pressure, the excess mass in the dead air region has to be scavenged and passed downstream. Once the wake has closed, the effects of various disturbances are not as readily sensed.

With the early probe holder configuration it was found that the presence of the probe anywhere in the wake region during the starting process had such a strong influence on the flow field that proper wake flow could not be established. Figure 21a is a schlieren photograph showing base flow not established because of the presence of the probe. It was usually necessary to move the probe holder above an imaginary horizontal line extending from the upper surface of the model into the wake region. At a certain critical position the wake flow would establish and it was then possible to move the probe down into the recirculation region. The probe could then be moved into practially any position in the shear layers or recirculation zone without disturbing the flow to any large extent. This was proven by schlieren observations and the base pressure data. With the improved probe holder configuration (see Appendix), disturbances near the wake throat were reduced and shockwaves from the probe were minimized to such an extent that flow could be established and maintained with the probe in any desired position. Figure 21b is a schlieren photograph showing undisturbed base flow with the improved probing configuration.

4.1.4 Flow Visualization

4.1.4.1 Spark Schlieren Photography

A series of runs were made in which the tunnel unit Reynolds number was changed by varying the stagnation pressure from 30 in. Hga to 130 in. Hga. Base pressure measurements were made and schlieren photographs

(Figure 22) of one power magnification were taken over this range for increments in stagnation pressure of 10 in. Hga.

4.1.4.2 Fastax Schlieren Photography

High speed Fastax pictures were taken at a film speed of 3500 frames per second to determine the existence of any possible flow fluctuations and to view the starting process in more detail. In addition, black and white and color schlieren movies were taken at a slower film speed of 32 frames per second using a Bolex motor driven camera.

The wake starting process is shown clearly on 9 frames taken from the Fastax movies over a 40 millisecond time period (Figure 23). These frames show that wake flow is fully established approximately 15-20 milliseconds after supersonic flow exists at the forebody shoulder. Viewing of the complete movie shows no indication of flow fluctuation. No evidence of wake "breathing" as reported for cavities in Reference 12 can be seen and it is felt that once wake flow is established, the flow boundaries remain unchanged with time.

4.1.4.3 Microschlieren Photography

An 8-power magnifying schlieren system was installed to obtain additional information regarding localized portions of the flow field. Figure 24a shows the microschlieren equipment installed for the magnified flow visualization and Figure 24b shows the locations at which the microschlieren photographs were taken. Several photographs were taken at various locations in the boundary layer and shear layers. Figure 24c shows a microschlieren photograph of the flow separating from the model, Figure 24d is a photograph of the wake throat region, and Figure 24e shows an enlarged view of the boundary layer on the model.

4.1.4.4 Oil Streakline Photography

Normally the runs were made by passing the tunnel air through an upstream filter in the air supply system. This was done to filter out oil and dust particles contained in the flow. On one of the preliminary runs the air filters were not used. After running for about 1/2 hour, the oil accumulations started coming down the tunnel, and finally reached

the windows of the test section. The oil lines then traced paths on the windows representative of the actual flow streamlines. The effects of the Prandtl-Meyer expansion over the base can be seen and observation of the flow in the wake shows several of the streamlines reversing into the recirculation zone. Figure 25 shows the oil streaklines in the base region. An interesting phenomenon can be seen occurring slightly upstream of the downstream shock waves. Regions of double reversals in the flow direction can be seen in the flow between the lip shock wave and the shear layers. No explanation can be presented for these reversals. It must be realized, however, that flow patterns on the windows can be influenced by disturbances which are not felt in the two-dimensional portion of the flow.

4.1.4.5 Color Schlieren Photography

During one of the runs the usual knife edge assembly was replaced by a series of colored filters and the mercury light source was replaced by a zircon white-light source. Examination of the color schlieren photographs showed details not visible using oridinary black and white techniques. It is felt that much useful information can be obtained using color schlieren although the exposures have to be of much longer duration (approximately 1/25 sec. as compared to 10 μ sec), which can reduce the sharpness.

4.1.5 Boundary Layer Measurements

Simultaneous probings of total temperature and impact pressure were made on the upper surface of the model to determine the condition of the separating boundary layer and to perfect the probing techniques. These probings were made adjacent to the lateral ray of static pressure taps using the probe shown in Figures A5 and A6 of the Appendix and the traversing mechanism described in Section 4.3.2. This information, combined with the static pressure readings obtained from the surface taps, was sufficient to obtain enthalpy and velocity profiles through the boundary layer.

Figure 26a shows the uncorrected total temperature variation through the boundary layer and Figure 26b presents data corrected for Reynolds number effect (see Appendix). The plot shows the familiar "ethalpy bump" which is characteristic of boundary layer flows with the wall at recovery temperature.

The determination of local values of Mach number through the boundary layer was made using the Rayleigh pitot tube equation along with measurements of impact pressure (Figure 27a) and surface static pressure. Figure 27b shows the Mach number variation through the boundary layer. The Mach number at the edge of the boundary layer (2.95) agrees with the value calculated by taking into account the total pressure loss across the model nose shock wave with a free stream Mach number of 3. Normalized velocity data calculated from the Mach number distribution followed a 1/7 power law, which is characteristic of a turbulent boundary layer. See also Section 4.3.3.3 where it is shown that the rate of spreading of the shear layer is linear, which is consistent with turbulent mixing layer theory.

4.1.6 Two-Dimensional Flow Considerations

The static pressure taps placed along the upper surface and base of the model (see Figure 10) were used to aid in the determination of the extent of two-dimensional flow over the rear of the model. Plots of these static pressure distributions were examined to detect any disturbances that would detract from the two-dimensional character of the flow.

Chapman, Kuehn and Larson (67) used static pressure measurements to show that for two-dimensional channel-spanning models at Mach numbers above 2.3 the flow was essentially two-dimensional over the middle portion of the model. They also found that with or without end plates the static pressure distributions did not change. Oil film methods were also used to aid in determination of the two-dimensional flow region.

On rearward-facing step models Ginou (79) found evidence of three-dimensional flow. He made these three-dimensional flow perturbations visible by use of an azobenzene technique. The perturbations were noticed

particularly in the transitional flow regime and in earlier work he also observed evidence of three-dimensional flow perturbations in turbulent flow using an oil film on the surface downstream of the step.

Czarnecki and Schueller (80) investigated interaction effects arising from side wall boundary layers in supersonic wind tunnel tests on airfoils. They found that these disturbances would spread to a considerable distance from the tunnel wall, particularly on surfaces where the Mach number approaches unity. These disturbances propogated from the juncture between the model and tunnel wall along a wave inclined at an angle slightly greater than the Mach angle for the local stream. They found also that the magnitude of the pressure disturbances depends to a large extent on the ratio of maximum model thickness to tunnel wall boundary layer thickness. When the model is large compared to the boundary layer thickness the magnitude of the disturbances may be relatively small.

From data of Dorrance (81) it was calculated that the disturbance lines arising from the edges of the nose of the model would divide the model surface area such that approximately 60% of the model surface could be considered as under two-dimensional flow conditions. This predicts that a 1-inch section of the model base would be two-dimensional. Czarnecki's criterion indicates that only the middle one-half inch would be under two-dimensional flow conditions. According to our measurements both of these estimates would appear to be quite conservative. The static pressure data showed that at least the middle one-third of the model was in two-dimensional flow. It is felt that in the region where the heat transfer data were taken the flow was definitely two-dimensional (Figure 9). The heat transfer data tend to confirm this observation.

4.2 Base Pressure Measurements

4.2.1 General

The base pressure measurements were taken not only to obtain their variation over the Reynolds number range but also to detect the Reynolds

number at which fully turbulent flow was occurring in the base region. In addition, these readings were continuously monitored during the probing runs to determine whether the probes were disturbing the recirculation zone flow process.

During the early runs the base pressures were measured on a mercury manometer board but, to obtain greater accuracy, all final runs were made using a 9-foot silicone oil board (Figure 28). This increased the reading accuracy by an order of magnitude and resulted in a considerable improvement in the reproducibility of the measurements.

All base pressure data are presented in the form of ratio of base pressure to model surface static pressure as a function of Reynolds number, which is evaluated at conditions existing at the outer edge of the boundary layer at the rear of the model. At this location the Mach number is 2.95 and the wetted distance, s, is 8.19 inches. The tunnel unit Reynolds number was varied by changing the stagnation pressure.

4.2.2 Variation of Base Pressure With Reynolds Number

The data obtained during the present investigation are compared with other available data for comparable shapes and nearly equal Mach numbers in Figure 29. Immediately evident is the wide divergence that can exist in base pressures for similar model configurations in the transitional flow regime while in the fully turbulent flow regime they tend to agree more closely. This tends to confirm that shear layer transition location exerts a strong influence on the flow field. When transition finally moves forward on the model surface, the base flow appears to "forget" what has happened previously, and transition location does not dominate the flow process.

The data of Van Hise (69) agree quite closely with the present measurements while the data of Holder and Gadd (18) and Charwat and Yakura (31) are considerably lower. The closed symbols represent data obtained during the first phase of the program with a smooth model surface roughened by sandblasting and correspond to the disturbance length data of Figure 19.

Presented also for comparison is the theory of Korst (28). Most of the experimental data fall below theoretical predictions. Assuming truly undisturbed wake flow for all the experiments, and as any disturbances tend to increase the base pressure ratio, it can be concluded that Korst's theory predicts a base pressure which is slightly high.

One major conclusion that can be reached from the foregoing discussion is that it is extremely difficult, if not impossible, to compare transitional data for various experimental conditions and models with different surface roughnesses. However, good success can be obtained when comparing fully turbulent data.

4.2.3 Variation of Base Pressure in Vertical Direction

Base pressures at various vertical stations were measured over the Reynolds number range covered by the centerline base pressure data of Figure 29. These data are presented in Figure 30 with the pressure normalized by dividing by p_{b5} (the centerline pressure). The data for all Reynolds numbers show a maximum at the centerline with a slight decrease in the vertical direction. A minimum is reached at a vertical position represented by $\frac{y}{H} = 0.620$. The pressure then starts to increase toward the corner. The figure also shows that the base pressure gradient increases with increasing Reynolds number. As the maximum variation in base pressure measured is of the order of 5%, one might question the assumption that the base pressure is sensibly constant over a two-dimensional base.

Charwat and Yakura (31) found no significant variations in base pressure in the vertical direction along the base either in the turbulent or in the laminar regime. They found this also to be true for pressure along the centerline in the recirculation zone except near the recompression region. They thus concluded that the two-dimensional wake is isobaric. Centerline static pressure data presented herein show a gradient in the axial distribution (Section 4.3.4).

Fuller and Reid (82) performed base pressure measurements on two-dimensional bodies at Mach number 2.4, both with and without exhausting jets. At a Reynolds number of 3.24×10^6 per foot with a ratio of momentum thickness to step height of 0.008 they found that the base pressure ratio reached a maximum at about 0.64 inch from the inside corner. The pressure ratio near both edges of the step was about 0.355 while at the maximum it was 0.370 which is an increase of approximately 4 percent.

The experimental points in Figure 30 at $\frac{y}{H} = 0.207$ for Reynolds numbers of 6.43×10^6 and 7.02×10^6 were slightly in doubt and for that reason the connecting lines to the two adjacent stations are dashed. As the pressure gradient can be directly related to the velocity gradient by use of the momentum equation, it can be seen that the velocity gradient at the centerline also shows a variation with Reynolds number. These data were used to calculate base heat transfer using stagnation point theory (see Section 4.4.3.2).

4.3 Recirculation Zone Probing Runs

4.3.1 General

A series of probing measurements were carried out to compliment the heat transfer and base pressure measurements and to provide detailed information pertaining to various portions of the total flow field. Figure 31 shows the 20-power binocular microscope which was used for positioning the probes in the boundary layer and base region.

4.3.2 Probe Positioning Device

To allow probings in the various regions of interest, a special probe positioning device was designed and constructed. With this device the angle of attack and the vertical and longitudinal positions of the probe could be accurately adjusted during operation of the tunnel. The internal drives of the traversing mechanisms are composed of micrometer components inserted in low-drag housings. The gears for the angle of attack components are enclosed in a special chamber not exposed to the flow. The probe positioning device and the first shear layer probe installed in the tunnel are shown in Figure 32a and the details of the

probe actuating mechanism are shown as Figure 32b. When these photographs were taken, the positioning mechanism did not have the axial traversing component. The micrometer drive assembly for this component is actuated by a flexible shaft. This mechanism with a probe installed is shown in Figure 32c.

4.3.3 Shear Layer Measurements

4.3.3.1 Temperature Data

Simultaneous measurements of total temperature, impact pressure, and static pressure were made through the shear layer at two locations using the probe shown in Figure A6 of the Appendix. This probe installed in the tunnel is shown in Figure 32a. These profiles were made at a Reynolds number of 6.7×10^6. The zero ordinate locations for the two probing stations are shown on Figure A10 of the Appendix. The probe positioning mechanism was used to align the probes with the flow and visual guidance was provided by schlieren observation. Only the temperature data are presented for these runs.

Figure 33 shows uncorrected and corrected variations of total temperature through the shear layer at the two stations. The shapes of these curves are somewhat similar to data obtained by Charwat and Yakura (31). Parts b) and d) of the figure show the total temperature data corrected for Mach number and Reynolds number error. The plots show an enthalpy defect near the inner portion but do not display an enthalpy excess at the outer edge as is common for attached boundary layers. The measurements indicate a mean recirculation zone recovery factor of 0.955 (Section 4.3.5).

4.3.3.2 Pressure Data

Additional measurements of impact pressure and static pressure were made through the shear layer using a new probe and the modified probe positioning mechanism. These runs were made at a Reynolds number of 4.30×10^6 with a roughened forebody. The modified probe shown in Figure A6 of the Appendix had impact pressure tubes facing both forward

and rearward with a static tap located at the center. With this probe simultaneous rearward and forward readings of impact pressure as well as static pressure could be obtained. It is felt that only limited reliance can be placed on the static pressure data as the tap placement and probe are not optimum for this type of measurement. Eight profiles of impact pressure and static pressure were obtained using this modified probe. The profile data were machine reduced on an LGP-30 computer. Presented in this report are data for three profiles obtained by traverses perpendicular to the shear layer flow direction with the probe aligned with the flow direction. The locations of the probings are shown in Figure 34 which indicates both the starting and ending points of the traverses. As the probe measures both forward and rearward impact pressures, two simultaneous profiles were obtained with each traverse. For each run, the notation "f" designates the forward facing probe, and "r" designates the rearward probe, with a distance of 0.32 inch between the probe ends. For all runs the probing station, x, is measured from the base upper corner to the line of traverse, parallel to the probe (shear layer) angle and perpendicular to the traverse.

The probing data are presented in groupings of three for each run (Figure 35). The first figure for each run presents the forward impact pressure and static pressure variation through the shear layer. Included also for reference is the base pressure corresponding to each probe position. The second figure shows the Mach number distribution and the third indicates the velocity distribution. Included also are data obtained from the rearward facing probe for Run 199.

For these runs it was assumed that the streamwise variation in static pressure was negligible and meaningful Mach number data could be obtained either from the base pressure or the measured local static pressure. No calibration was made for the static probe and, as the readings are probably in error, the data obtained with this probe can only be considered qualitatively. However, the probe does indicate changes in pressure level and can be used to evaluate the gross characteristics of the flow field. The second figure in each grouping

compares the measured static pressure with the base pressure, with the Mach number evaluated from both pressures.

During Run 198 a sudden change occurred in base pressure. This in turn caused the shear layers to assume a steeper angle and the flow impinging on the probe was from a higher velocity region of the shear layer. This discontinuity in the profile is shown by the closed points (Figure 35a, b, c). For some reason the shear layer angle again changed to its original position and the profile was completed. This event points out one of the difficulties encountered in making probing measurements of this type. The interruption was not caused by a change in tunnel stagnation pressure and at the present time the cause is unknown.

Most of the data obtained with the rearward-facing probes present definite proof of reverse flow. Indications of reverse flow of Mach number and velocity are shown for Run 199, obtained from the rearward-facing probe. In the portion of the shear layer above the zero velocity line the rearward probe senses a "base" pressure and gives an erroneous indication of Mach number. Below this line the forward probe gives a wrong indication. Missing points for Run 199 for which impact pressure data are presented can be explained because of this.

4.3.3.3 Comparison of Velocity Profile Data with Incompressible Mixing Layer Theory

The velocity data presented in Figure 35 are plotted against the turbulent similarity parameter $\sigma y/x$ in Figure 36. Shown for comparison is Tollmien's prediction for an incompressible jet (83). The y coordinate was chosen so as to make $u/u_{2a} = 0.50$ at $\sigma\ y/x = 0$. The x distance for each profile station was measured along the shear layer and the y values were measured perpendicular to x. Curves faired through the data are also presented for spreading factors (σ) of 10 and 15. A σ of 12 fits the data best. For subsonic jets a σ of 12 is usually best. The correlation of Tripp (39) exhibits a value of 24 for an approach Mach number of 3.0. The Vasiliu (40) correlation

predicts a value of 40. With this large a discrepancy, further experiments on this problem are in order.

According to incompressible mixing layer theory, it has been assumed that the value of the "mixing length" is constant across the mixing zone and the mixing length L is proportional to the distance from the nozzle,

$$L = cx$$

where the constant is $\sqrt{1/2\ \sigma^3}$. Liepmann and Laufer (32), using a hot wire method, showed that for supersonic flows the mixing length is not constant across the mixing layer.

Charwat and Yakura (31) found that a σ of 20 fit their supersonic data. As σ is a measure of the amount of turbulence, they felt either that this discrepancy was related to the increased stability of supersonic jets or that their flow was not yet fully turbulent. Considering the present data, the latter reason seems likely, as their data were taken at approximately the same Mach number (2 and 3).

Crane (35) showed that the effect of compressibility on the non-dimensional velocity profile can be divided into two parts. The first is what he called "change of scale" which is related to differences in temperature. The second is the effect of increasing Mach number. They found that these two effects practically cancelled out, leaving the profile relatively unchanged from the incompressible case although a different σ may be required.

The spreading factor σ is a primary unknown in calculating turbulent near-wake heat fluxes. Available estimates range from 12 to 40 for the present situation. A σ of 12-15 seems to fit the present data. This range is supported by comparisons of the present heat transfer data with the analytical predictions of Korst (see Figure 42). We have concluded that a proper analytical model should include only the low speed value of σ and that the diminished wake thicknesses (as the Mach number increases) must result from improved turbulent shear stress assumptions.

4.3.4 Recirculation Zone Total Pressure Measurements

Traverses were made through the recirculation zone using the double-facing probe shown in Figure A6 of the Appendix. Figure A7 shows a schlieren photograph of this probe in the flow field. No attempt was made to align the probe with flow direction and all traverses were made with the probe face in a horizontal plane. Figure 37 shows data obtained from these traverses. In some cases the readings are less than the static pressure, designating flow in the opposite direction.

4.3.5 Centerline Pressure Measurements

Measurements of static pressure and total pressure were made along the centerline of the recirculation zone using the recombination total pressure and static pressure probe described in the Appendix. Figure A8 of the Appendix shows this probe installed on the model. This probe was traversed downstream from the base through the recirculation zone throat, and in so doing, profiles of static pressure and impact pressure were obtained.

Reverse flow locations are identified by the relationship between the probe impact pressure and the local static pressure. Figure 38 shows a plot of these pressures as a function of axial location. These measurements show reverse flow to a distance of approximately one and one-half inches downstream of the base. When the flow is moving downstream, the rearward-facing impact probe senses a "base" pressure and the values so measured are lower than the static pressure. The model base pressure is indicated by the cross on the ordinate.

Assuming no mechanism for dissipation of total pressure, the second stagnation point exists where the two pressures are equal. Badrinarayanan (24) found similar results for both axisymmetric and two-dimensional models.

4.3.6 Temperature Measurements

Recirculation zone temperatures were measured at three vertical positions and five longitudinal stations using the rake described in the

Appendix. These measurements were made over a base to stagnation temperature ratio range of 0.365 to 0.965 at a Reynolds number of 4.5 x 10^6 (Figure 39).

Temperature data obtained using the recirculation zone rake showed that some influence of wall cooling was exerted on portions of the recirculation zone downstream toward the second stagnation point, although this influence diminished quite rapidly. The data presented in Figure 39 show that the recirculation zone temperature remains at approximately 95 percent of free stream total temperature, independent of wall cooling, until a location approximately 1 inch from the base is reached. This is close to the downstream stagnation point, as evidenced by other measurements in this report. Because of the reverse flow, the recirculation zone then starts to sense the wall cooling and the temperature drops to approximately 90 percent of free stream value and remains at this ratio until a position approximately 40 to 60 mils from the base plate is reached, where the temperature starts dropping to the wall value. A description of temperature measurements in this region is presented in the following section.

For these runs a base temperature recovery factor of 0.965 was obtained which agrees closely to earlier measurements of 0.973. The recirculation zone recovery factor was approximately 0.95, which also was measured with the shear layer total temperature probe. Charwat and Yakura (31) found a recirculation zone recovery factory of 0.945.

As the recirculation zone temperature measurements were made with small diameter thermocouple wires (3 mils), temperature readings obtained are influenced by Reynolds number effects (a Reynolds number of the order of ten based on half wire diameter exists in the recirculation zone) as well as conduction influences and radiation. Performing calculations suggested by Bradfield (84), it was found that the radiation and conduction influences can be neglected but the error introduced by the Reynolds number effect has to be considered. The best available experimental information as presented in References 84, 85, and 86 indicates that the data are about 2 percent too low. Interpreting those data

it must be realized that the interference created by the presence of the rake disrupted the flow field but the gross condition remained relatively unchanged (Section 4 of Appendix).

4.3.7 Base Boundary Layer Measurements

Because of the strong indications of a base thermal boundary layer presented by the recirculation zone total temperature measurements, a special thermocouple probe was designed. It was similar to those used in the shear layer measurements (Section 3.1 of Appendix). Temperature profiles were obtained for wall temperatures of recovery, $-78^{\circ}F$, $-200^{\circ}F$, and $-278^{\circ}F$ (Figure 40). The probes were positioned to within 0.001 inch using the binocular microscope. The profiles were measured at base thermocouple T_{B4} (refer to Figure 13). The probe body was inclined at an angle of approximately 15° with the base and faced the base horizontal centerline (Figure A7g).

As the probe was traversed inward, indications of a temperature gradient were obtained at approximately 40-60 mils from the base.

The temperature drops at a linear rate until a point 4 to 6 mils from the base plate is reached. Because of the probe size used it was not possible to bring the center of the thermoucouple wire closer than 4 mils from the base, and a detailed picture of the variation inward was not obtained. The temperature drops rapidly to the wall value from this point.

At the present time the exact character of this thermal layer is uncertain. Impact pressure data were not obtained, so the shape of the velocity profile could not be used as a criterion to determine whether the flow is laminar or turbulent.

The separated zone behind a body immersed in subsonic flow is characterized by unsteadiness and fluctuation of the flow boundaries. In supersonic flow this is not the case since the present measurements indicate that the flow boundaries do not fluctuate with time. The question of whether small scale turbulence exists in the recirculation zone has yet to be answered. Although the separating shear layers are

turbulent, it cannot be stated with certainty that the small scale fluctuating motion is carried into the recirculation zone. However, the wind vane measurements described in the next section indicate considerable variation in the flow patterns. If flow in the recirculation zone is characterized by turbulent fluctuations, it is quite certain that these fluctuations would be impressed on the base boundary layer.

Very little data exist for the variation of total temperature through either a laminar or a turbulent subsonic stagnation point boundary layer. However, Livingood and Donoughe (89) present a summary of solutions of theoretical calculations for laminar wedge type flow. The solutions were obtained for small Mach numbers with a Prandtl number of 0.7 and for various conditions of wall cooling and mass injection.

The thermal boundary layer data were transformed to a non-dimensional form to allow comparison with the stagnation flow data of Livingood and Donoughe (89). Comparison of the data showed only slight correlation in the inner portion of the profile with a large deviation in the outer portion. It thus appears that the present experimental temperature profiles may be composed of a laminar sublayer with a form of turbulent outer region probably impressed by the recirculation zone flow. This assumption is partially substantiated by the concept of a turbulent eddy process, which increases the apparent thermal conductivity in the outer portion where the temperature gradient is fairly small. In the inner portion, the turbulent motion decreases while the gradient increases and the conductivity approaches its molecular value.

True stagnation point flow is usually laminar, and early transition occurs only for conditions of extreme surface roughness. However, for the model of the reported investigation, it is quite possible that no laminar portion exists because the recirculation flow fluctuations may be strong enough to overcome any stable tendencies of the boundary layer.

4.3.8 Wind Vane Measurements

Runs were made with a small wind vane inserted at different locations in the recirculation zone. The vane oscillated quite severely at most locations and in some areas was rotating too fast to be seen. However, several regions were located in which the vane assumed a stable attitude. One such area was close to the second stagnation point indicated by the centerline static pressure data. Spark schlieren photographs were taken by positioning the vane against a background of 0.1 grid line superimposed on the tunnel window (See Figure A7h). This method shows promise although a means of applying a variable friction to the vane would have to be devised to damp out the oscillations.

4.4 Heat Transfer Measurements

4.4.1 Heat Transfer Measurements Using Transient Technique

The heat transfer data were taken with the model forebody at the local recovery temperature. It has been shown (Reference 87) that if heat transfer has occurred before the point of separation, conditions in the base region would be affected. Chapman, Kuehn, and Larson (67) have observed that heating of a boundary layer prior to separation has a stabilizing effect rather than the destablizing effect exhibited by attached boundary layers. The heat transfer chamber at the rear of the model was thermally isolated from the model forebody to prevent a transfer of heat during the cooling process. As the cooling process was accomplished with the tunnel running, the model forebody wall temperature approached its equilibrium value before the data were taken. Temperatures were measured at three different locations on the model forebody during the heat transfer runs.

Model temperatures and the wind tunnel stagnation temperature were recorded on Brown Electronik recorders. As the number of recorders available was limited, it was necessary to record more than one thermocouple on each recorder. This was done by stepping switches which allowed alternate one-second traces for each of two thermocouples on each switching unit.

Past experience with these recorders has shown that the calibration tends to drift occasionally. A check was made on recorder calibration before and after each run by measuring two fixed temperatures. As the heat transfer recorders had a temperature range of -350°F to +100°F, a liquid nitrogen bath of -320°F was used for the low end reference point and for the high end a bath of carbon dioxide and alcohol with a temperature of -110°F was chosen.

Before each run the base was pre-cooled by flowing cooled, gaseous nitrogen or helium over the inside surface. The coolant gas (from pressurized cylinders) was led through a liquid nitrogen and carbon dioxide-alcohol 2-stage heat exchanger which lowered the temperature to -320°F. The coolant line was then led through a special fitting in the mounting window and followed a path internally through the model to a chamber in the micarta after-section. Four laterally spaced holes then directed the gas over the nickel heat transfer surface. The coolant was exhausted through another internal line which led again through the steel window and finally to a vacuum pump. A vacuum pump was used to assist in the flow of the coolant gas through the model.

During this cooling procedure the base heat shield was in the extended position (Figure 41a). The shield was then pulled (Figure 41b) and the rate of temperature change of the model base was recorded. During this time simultaneous readings of base pressure and model surface pressure were also obtained.

During a ten minute tunnel running period approximately eight separate heat transfer runs were accomplished. Immediately after the conclusion of a run, which usually lasted about 20 seconds, the shield was extended and the cooling process again was repeated. The length of time needed to bring the model base back to -320°F was approximately 15 seconds. This method allows heat transfer data to be taken before the temperature gradients, which tend to develop in the base due to unequal heating rates, have time to develop. Thus, extensive corrections for conduction through the model skin need not be made.

Additional heat transfer measurements were made with the base pressure model. For these runs, the cooled exhaust line was vented to the tunnel section to maintain a minimum pressure differential across the model base and prevent leakage of the coolant into the base region. Helium was used as the cooling medium to prevent liquefaction and accumulation of liquid in the cooling chamber. It was found that the cooling system had sufficient capacity to bring the base down to -280°F during operation of the tunnel. For these runs, the heat shield mechanism was not required and visual observations of the flow field was possible. This base was not thermally isolated as well as the heat transfer model but it was found that if the data were taken during the early part of the run the conduction errors were minimized.

The heat transfer data were reduced using the procedures presented in Section 3.3. The data in the form of heat transfer coefficient are presented in Figure 42a as a function of Reynolds number. The data on this figure were evaluated at instantaneous wall temperatures of -100°F, -200°F and -250°F. The early data are shown as closed symbols while data taken using the second base are represented by open symbols. The average of these data correlated on the basis of transition Reynolds number are shown in Figure 42b.

4.4.2 Other Calculations of Heat Transfer

4.4.2.1 Stagnation Point Analysis

The intuitive picture of the heat transfer process on the rear-wake region is that of a two-dimensional stagnation point type flow. It is of interest to make a qualitative numerical comparison of this type of analysis with the present experimental results. Assuming laminar flow, the correlations of Reshotko and Cohen (88) for this case are summarized below:

Table I Heat Transfer Summary of Reshotko and Cohen

Tw/To	$Nu/\sqrt{Re}$	
	Pr = 1.0	Pr = 0.7
0.5	0.541	0.471
1.0	0.571	0.498

For stagnation point flow, the heat transfer coefficient is written as:

$$h = \left(\frac{Nu}{\sqrt{Re}}\right)\left(\frac{c_p}{Pr}\sqrt{\mu}\sqrt{\rho}\right)\sqrt{\left(\frac{dv_\delta}{dy}\right)_o} \qquad (20)$$

The first bracketed term decreases with decreasing wall temperature ratio. The second bracketed term involves only molecular transport properties which, for simplicity, will be evaluated at the freestream total temperature. The third term involves the density which is to be evaluated from the mean base pressure and the freestream total temperature. The fourth term involves the velocity gradient at the stagnation point which must be obtained from experiment. For locally isentropic flow just outside of the assumed boundary layer

$$\frac{dv_\delta}{dy} = \frac{a_\delta \frac{dM}{dy}}{1 + \frac{\gamma-1}{2}M_\delta^2} \qquad (21)$$

Near the stagnation point the Mach numbers are quite small so that Equation 21 may be written

$$\frac{dv_\delta}{dy} \approx a_\delta \frac{dM_\delta}{dy} \qquad (22)$$

The Mach number distribution is found from the static pressure distribution using one-dimensional isentropic flow relations, assuming that the pressure measured at the apparent stagnation point is the total pressure.

Using Equations (20) and (22) and Table I, the following results were obtained:

Sample Results

a.) Low Reynolds number value ($Re_s = 4 \times 10^6$)

Wall static pressure survey

$$\sqrt{\left(\frac{dv_\delta}{dy}\right)_o} = 97 \text{ sec}^{-1/2}; \quad h = 4.7 \frac{\text{BTU}}{\text{ft}^2\text{-hr}^\circ\text{R}}$$

b.) High Reynolds Number Comparison ($Re_s = 6.7 \times 10^6$)

Centerline pressure survey

$$\sqrt{\left(\frac{dv_\delta}{dy}\right)_o} = 164 \text{ sec}^{-1/2}; \; h = 10.9 \quad \frac{\text{BTU}}{\text{ft}^2 - \text{hr}^\circ\text{R}}$$

Wall static pressure survey

$$\sqrt{\left(\frac{dv_\delta}{dy}\right)_o} = 113 \text{ sec}^{-1/2}; \; h = 7.5 \quad \frac{\text{BTU}}{\text{ft}^2 - \text{hr}^\circ\text{R}}$$

Results over the whole Reynolds number range calculated from the wall static pressure data are shown on Figure 42b. The laminar stagnation point theory exhibits an S-shaped Reynolds number dependence rather than the conventional square root dependence. It is the velocity gradient change which gives an S-shape to the laminar curve which closely matches the experimental results. If the stagnation point theory applies to laminar separation also, then the velocity gradient must greatly diminish, since the mean base density is known to be about twice the turbulent case. The Reynolds number dependence of the measured data indicates that this is true. In addition, a film exists close to the wall independent of the nature of the covering shear layers. This analysis can be modified after the exact nature of the base boundary layer is determined.

4.4.2.2 Heat Transfer From Measured Thermal Boundary Layer Data

At the wall the slopes of the total temperature and static temperature profiles are equal. Using the Fourier heat conduction equation and evaluating k at the wall temperature, close agreement was obtained between heat flux obtained using this method and those measured using the transient technique (Table II). These measurements were made only at one Reynolds number and appear as the vertical bar on Figure 42b at $Re_s = 4.07 \times 10^6$.

TABLE II

Calculation of Heat Transfer Coefficient From Probing Data

T_b/T_o	Δx (ft)	ΔT (^oF)	T_b (^oR)	k (BTU/fthr^oR)	T_o (^oR)	T_R (^oR)	$\dot{q}$ (BTU/ft^{2}hr)	h (BTU/ft^{2}hr^oR)
0.716	.000333	32.6	384	0.0111	536	509	1085	8.68
0.487	.000333	75.6	261	0.0077	537	510	1745	7.05
0.340	.000333	117.7	182	0.0054	536	509	1960	6.01

4.4.2.3 Sample Calculations Using the Korst Analysis

For conditions representative of the present experiments,

$M_{1a} = 3.0$, $p_B/p_1 = .121$, $M_{2a} = 4.57$, $U_{2a} = 2239$ fps.,

$P_{2a} = 0.0001760$ slugs/ft^3, $\theta_{2a} = 228^0$, X = wake length = 2.22 in., and

$C_{2a}^2 = 0.80$, the product σ St ($T_B = .5\ T_o$) = .58. The heat transfer coefficients can be evaluated by choosing a value for σ. Using the incompressible value of 12,

St = 0.00483, and h = 66.9 BTU/ft^{2}hr^{o}R.

Using the value predicted by Tripp (39) of 24.6,

St = 0.00236, and h = 32.7 BTU/ft^{2}hr^{o}R.

The curve in the upper left hand corner of Figure 42b represents the Korst prediction for a spreading factor of 24.6 and for $T_B = T_b$. Since Korst gives no indication of which values of the base temperature to select, this assumption is the most natural one, since the wall temperature is most easily measured. However, the assumption is physically unrealistic as shown by the experimental data.

All of the Korst predictions are linear in Re_s since the heat transfer coefficient is directly proportional to pressure and in the Korst model the base pressure has a unique value at this Mach number.

The turbulent theory of Chapman (46) applies only for the case of M = 0, $T_B = T_b$. His results for this case are in complete agreement with the Korst calculations. Therefore it is necessary to make comparisons only with the Korst predictions.

To modify the Korst calculation such that the heat transfer coefficient is based on the more easily measured wall temperature instead of the recirculation zone temperature, the Korst value should be multiplied by the appropriate temperature difference $(T_o - T_b)$ instead of $(T_o - T_B)$. The relation

$$q = h^+ (T_o - T_B) = h (T_o - T_b) \tag{23}$$

defines h such that

$$h = h^+ \left[\frac{T_o - T_B}{T_o - T_b}\right] \tag{24}$$

The correction term in the brackets must, at present, be found experimentally. Since the present heat transfer data were obtained under cooled-wall conditions ($T_b \approx 0.5\ T_o$), $T_b < T_B$, and $h < h^+$. Two choices are available.

1. The recirculation zone total temperature measurements ($.010 \leq x \leq 1.000$ inches)
   From Figure 39, for x = 0.75 in., when $T_b/T_o = 0.5$, $T_B/T_o = 0.9$ and the correction term assumes the value $0.1/0.5 = 0.2$ and
   $h\ (\sigma = 24.6) = 6.5$
   $h\ (\sigma = 12) = 13.3$
   BTU/ft^2hr^oR

2. The base boundary layer total temperature profiles ($.004 \leq x \leq 0.024$ inch). From Figure 40, when $T_b/T_o = 0.5$, then by interpolation $T_B/T_o = 0.76$ and the correction term assumes the value $0.24/0.50 = 0.48$ and the modified heat transfer coefficients become
   $h\ (\sigma = 24.6) = 15.7$
   $h\ (\sigma = 12) = 32.1$
   BTU/ft^2hr^oR

Since the first set of measurements encompasses the complete recirculation zone while the second involves the base boundary layer region only, the first set was adopted for theoretical comparisons since it agrees more closely with Korst's physical picture. These data are presented in Figure 42b.

The laminar mixing layer theory of Chapman was also included for reference. The close proximity of the laminar and turbulent predictions is due primarily to the higher laminar base pressures. The laminar curve follows a square root variation with Reynolds number. The Chapman laminar theory also includes the assumption that $T_B = T_b$. The effect of the assumption is to increase the predicted heat transfer coefficients as indicated by the Korst comparisons.

5. SUMMARY AND CONCLUSIONS

The flow models proposed by Chapman (46) and Korst (28) assume that the major mechanism for heat transfer to a wall in a separated flow region is governed primarily by the behavior of the mixing layers. In Chapman's study it was assumed that the wall temperature was equal to the separated zone temperature, which implies zero resistance to heat transfer between the wall and the separated zone. Heat transfer predictions by Chapman for pure laminar separation were experimentally substantiated by Larson (66), who showed that for gap-induced separation on a flat plate the heat transfer was approximately 60 percent of the equivalent attached case. The turbulent theories of Chapman and Korst (assuming $T_B = T_b$), predicted heating rates approximately six times those for equivalent attached cases. Larson's work (66) and the results reported herein for heat transfer measurements under turbulent separated flow conditions showed a considerable reduction in heat transfer. The primary reason for this discrepancy, as reported in both investigations, is that the recirculation zone temperature deviates considerably from the wall temperature. Both investigations showed that the total temperature of the recirculation zone is approximately 90-95 percent of the free stream total temperature. The current measurements made in the recirculation zone with wall cooling showed that, although the region closest to the base sensed the drop in temperature, the major portion tended to ignore it and remained at recovery value, which is close to the free stream total temperature.

The presence of a thermal boundary layer was proven by measurements of several profiles of total temperature. These findings indicate

that the largest barrier to heat flow into the base is the boundary layer, with only small resistance encountered at the shear layer and in the recirculation zone.

In the light of the present experimental data, it appears that the recirculation zone flow field is a combination of pure boundary layer type flow (temperature influences are not felt outside of the thermal boundary layer) and the flow field postulated by Chapman (46) and Korst (28) (perfect heat transfer between separated zone and wall). The flow field appears, however, to follow the first model more closely.

Further theoretical study should consider the behavior of the base boundary layer, and how it is influenced by the shear layers and external flow field. It now appears that the base flow heat transfer process is controlled by a complicated series of factors such as 1) influence of forebody boundary layer and external flow field on shear layer development, 2) control of recirculatory flow process by shear layer transition, and 3) recirculation zone influences on the base boundary layer. If the flow region near the base is really of a boundary layer nature, variations of wall cooling, pressure gradient, surface roughness, and intensity of turbulence in the recirculation zone could all affect the heat transfer process.

The velocity profiles in the shear layer exhibited normal turbulent tendencies and the average value of the spreading factor was found to be in the range of 12 to 15.

The Korst theory, in heat transfer coefficient form, depends upon proper evaluation of spreading factor and temperature potential. The fully turbulent shear layer results ($Re_s > 4 \times 10^6$) are in closest agreement with the Korst predictions when a spreading factor of 12 and measured recirculation zone temperatureare used. Thus, the Korst model, which considers only the profiles outside of the dividing streamline, undoubtedly is conceptually correct. The agreement of

the heat transfer data again leads one to believe that spreading factor data obtained on jets does not apply to the near wake case.

The directly-measured wall heating rates agree with the heat fluxes as determined by the total temperature profiles and the values obtained using the stagnation point analysis.

REFERENCES

1. Bloom, M.H., "On Mederately Separated Viscous Flows", J. Aerospace Sci. Vol 28, No. 4, (1961).

2. Rosenhead, L., "Vortex Systems in Wakes", Advances in Applied Mechanics, III, 185-1953, Academic Press, Inc., New York, (1953).

3. Krzywoblocki, M.Z.V.,"Jets-Review of Literature", Jet Propulsion, Vol. 26, No. 9, (1956).

4. Taneda, S., "Downstream Development of the Wakes Behind Cylinders", J. Phys. Soc. Japan, Vol. 14, No. 6, (1959).

5. Batchelor, G.K., "A Proposal Concerning Laminar Wakes Behind Bluff Bodies at Large Reynolds Number", J. of Fluid Mech., Vol. 1, No. 4, (1956).

6. Ryan, L.F., "Experiments on Aerodynamic Cooling", Mitt. No. 18, Inst. für Aerodynamics, Tech. Hochschule (Zurich), C. (1951).

7. Ackeret, J., "On the Temperature Distribution Behind Cylinders in a Flow", NASA Technical Translation F-2, (1959).

8. Thomann, H., "Measurements of the Recovery Temperature in the Wake of a Cylinder and of a Wedge at Mach Numbers Between 0.5 and 3", Flygtekn. Forsoksanst. Medd 84, (1959).

9. Donaldson, J.C., and Bell, D.R., "Sound and Pressure Measurements in Cavities on a Body of Revolution at Supersonic Speeds", AEDC-TN-60-233, (1961).

10. Krishnamurty, K., "Accoustic Radiation from Two-Dimensional Rectangular Cutouts in Aerodynamic Surfaces", NACA TN 3487, (1955).

11. Roshko, A.,"Some Measurements of Flow in a Rectangular Cutout", NACA TN 3488, (1955).

12. Charwat, A.F., Roas, J.N., Dewey, F.C., and Hitz, J.A., "An Investigation of Separated Flows, Part I, The Pressure Field", J. of Aerospace Sci., Vol. 28, No. 6, Part II, "Flow in the Cavity and Heat Transfer", J. Aerospace Sci., Vol. 28, No. 7, (1961).

13. Larson, H. K., and Keating, S.J., "Transition Reynolds Numbers of Separated Flows at Supersonic Speeds", NASA TN D-349, (1960).

14. McDearmon, R.W., "Investigation of the Flow in a Rectangular Cavity in a Flat Plate at a Mach Number of 3.55", NASA TN D-523, (1960).

15. Chung, P.M., and Viegas, J.R., "Heat Transfer at the Reattachment Zone of Separated Laminar Boundary Layers", NASA TN D-1072, (1961).

16. Ferri, A. and Pallone, A., "Note on the Flow Fields on the Rear Part of Blunt Bodies in Hypersonic Flow", WADC TN 56-294, (1956).

17. Bogdonoff, S.M., "Exploratory Studies of Hypersonic Fluid Mechanics", NATO Report 142, (1957).

REFERENCES (CONT'D)

18. Holder, D.W. and Gadd, G.E., "Interactions Between Shock Waves and Boundary Layers and Wakes", Symposium on Boundary Layer Effects in Aerodynamics, NPL, Teddington, England, Philosophical Library, Inc. New York, New York, (1955).

19. Crocco, L. and Lees, L., "A Mixing Theory for the Interaction Between Dissipative Flows and Nearly - Isentropic Streams", Princeton University, Aeronautical Engineering Laboratory Report No. 187, (1952).

20. Clauser, F.H., "The Turbulent Boundary Layer", Advances in Applied Mechanics, Vol. 4, Academic Press, Inc., (1956).

21. Sandborn, V.A., "An Equation for the Mean Velocity Distribution of Boundary Layers", NASA Memo 2-5-59 E, (1959).

22. Coles, D., "The Law of the Wake in the Turbulent Boundary Layer", J. of Fluid Mech., Vol. 1, Part 2, (1956).

23. Bailey, H.E., and Kuethe, A.M., "Supersonic Mixing of Jets and Turbulent Boundary Layers", WADC TR 57-402, (1957).

24. Badrinarayanan, M.A., "An Experimental Investigation of Base Flows at Supersonic Speeds", J. of the Royal Aeronautical Society, Vol. 65, No. 607, (1961).

25. Murphy, K.R.A., and Hammitt, A.G., "Investigation of the Interaction of a Turbulent Boundary Layer with Prandtl-Meyer Expansion Fans at M = 1.88", James Forrestal Research Center Rept. No. 434, (1958).

26. Pai, S.I., "Two-Dimensional Supersonic Shear Flow Around a Corner", Proc. Second U.S. National Congress of Applied Mechanics, June 1954, ASME (1955).

27. Roy, A.J., "Supersonic Viscous Flow Past a Convex Corner", Department of Aeronautical Engineering, Indian Institute of Science Proceedings, (1959).

28. Korst, H.H., Chow, W.L., and Zumwalt, G.W., "Research on Transonic and Supersonic Flow of a Real Fluid at Abrupt Increases in Cross Section" (Final Report), University of Illinois Engineering Experiment Station Technical Report NE 392-5, (1959).

29. Zakkay, V. and Tani, T., "Theoretical and Experimental Investigation of the Laminar Heat Transfer Downstream of a Sharp Corner", Polytechnic Institute of Brooklyn, PIBAL Report No. 708, (1961).

30. Napolitano, L.G., "Incompressible Mixing of a Shear Flow with Fluid at Rest", Polytechnic Institute of Brooklyn, PIBAL Report No. 318, (1957).

31. Charwat, A.F., and Yakura, J.K., "An Investigation of Two-Dimensional Supersonic Base Pressures", J. of Aeronautical Sci., Vol. 25, No. 2, (1958).

REFERENCES (CONT'D)

32. Liepmann, H.W. and Laufer, J., "Investigations of Free Turbulent Mixing", NACA TN 1257, (1947).

33. Bray, K.N.C., Radd, G.E., and Woodger, M., "Some Calculations by the Crocco-Lees and other Methods of the Interactions Between Shock Waves and Laminar Boundary Layers", British A.R.C. 21, 834, F.M. 2937, (1960).

34. Gortler, H., "Berechnung von Aufgaben der Freien Turbulenz auf Grund eines neuen Naherung Sansatzes", ZAMM Bd. 22, Nt. 5, (1942).

35. Crane, L.J., "The Laminar and Turbulent Mixing of Jets of Compressible Fluid. Part II The Mixing of Two Semi-Infinite Streams", J. of Fluid Mech., Vol. 3, Part 1, (1957).

36. Napolitano, L.G., "Two-Dimensional Plane Mixing of Homogeneous and Non-Homogeneous Streams", Polytechnic Institute of Brooklyn, PIBAL Report No. 400, (1957).

37. Chapman, A.J., and Korst, H.H., "Free Jet Boundary with Consideration of Initial Boundary Layer", Proc. of Second U.S. Congress of Applied Mechanics, 1954, ASME (1955).

38. Pai, S.I., "Two-Dimensional Jet Mixing of a Compressible Fluid", J. Aeronautical Sci., Vol. 16, No. 8, (1949).

39. Tripp, W., "Analytical and Experimental Investigation of the Base Pressure Behind a Blunt Trailing Edge for Supersonic Flow", Ph.D. Thesis, University of Illinois, (1956).

40. Vasiliu, J., "Turbulent Jet Mixing of Gases of Different Kinds Including Chemical Reactions", Convair (Astronautics) Division of General Dynamics, Report ERR-AN-005, (1960).

41. Crane, L.J. and Pack, D.C., "The Laminar and Turbulent Mixing of Jets of Compressible Fluid. I: Flow Far from the Orifice", J. Fluid Mech., Vol. 2, No. 5, (1957).

42. Reichardt, H., "New Theory of Free Turbulence", Zeit. Ang. Math. u. Mech. 21, 257 (1941). Royal Aeronautical Society Journal 47, 167, (1943).

43. Forstall, W., and Shapiro, A.H., "Momentum and Mass Transfer in Coaxial Gas Jets", J. of Applied Mech., Paper No. APM-13, (1950).

44. Corrsin, S. and Uberai, M.S., "Further Experiments on the Flow at Heat Transfer in a Heated Turbulent Air Jet", NACA TN 1857, (1949).

45. Dryden, H.L., "Aerodynamics of Cooling", Vol. VI of Aerodynamic Theory, Div. T, W.T. Durand, ed., Julius Springer-Verlag, Berlin, (1934).

46. Chapman, D.R., "A Theoretical Analysis of Heat Transfer in Regions of Separated Flow", NACA TN 3792, (1956).

REFERENCES (CONT'D)

47. Spence, D.A., "Some Applications of Crocco's Integral for the Turbulent Boundary Layer", Proc. Heat Transfer and Fluid Mechanics Institute, Stanford, Calif., (1960).

48. Mager, A., "Transformation of the Compressible Turbulent Boundary Layer", Proc. Heat Transfer and Fluid Mechanics Institute, Pasadena, Calif., (1957).

49. Ting, L., and Libby, P.A., "Remarks on the Eddy Viscosity in Compressible Mixing Flows", J. of the Aerospace Sci., Vol. 27, No. 10, (1960).

50. Tani, I., "Experimental Investigation of Flow Separation over a Step", International Union of Theoretical and Applied Mechanics Symposium on Boundary Layer Research, H. Gortler, ed., Springer-Verlag, Berlin, (1958).

51. Gooderum, P.B., Wood, G.P., and Brevoort, M.J., "Investigation with an Interferometer of the Turbulent Mixing of a Free Supersonic Jet", NACA TR 963, (1950).

52. Forthmann, E., "Turbulent Jet Expansion", NACA TM 789, (1936).

53. Carlson, W.O., "Heat Transfer in Laminar, Separated, and Wake Flow Regions", Heat Transfer and Fluid Mechanics Institute, (Proc. of), University of Calif. at Los Angeles, (1959).

54. Lin, C.C., "On Periodically Oscillating Wakes in the Oseen Approximation", Studies in Mathematics and Mechanics, Academic Press, New York, (1954).

55. Squire, H.B., "Note on the Motion Inside a Region of Recirculation (Cavity Flow)", J. of the Royal Aeronautical Society, Vol. 60, No. 543, (1956).

56. Lam, S.H., "Heat Transfer Through a Region of Closed Streamline", Princeton University Report 469, AFOSR TN 59-727, (1959).

57. Stewartson, K., "Further Solutions of the Falkner-Skan Equation", Proceedings of the Cambridge Phil. Society, Vol. 50, (1954).

58. Abramovich, G.N., "A Flow of Air with a Region of Reverse Flow", Royal Aircraft Establishment, Translation 740, (1958).

59. Birkhoff, G. and Zarantonello, E.H., Jets, Wakes, and Cavities, New York, Academic Press, (1957).

60. Bloom, M.H., and Steiger, M.H., "Some Compressibility and Heat Transfer Characteristics of the Wall Jet", Third U.S. National Congress of Applied Mechanics, Brown University, (1958).

61. Glauert, M.B., "The Wall Jet", J. of Fluid Mechanics, Vol. 1, Part 6, (1956).

62. Rabinowicz, J., "Measurement of Turbulent Heat Transfer Rates on the Aft Portion and Blunt Base of a Hemisphere-Cylinder in the Shock Tube", California Institute of Technology, Guggenheim Aeronautical Laboratory Memorandum 41, (1957).

REFERENCES (CONT'D)

63. Bechwith, I.E., and Gallagher, J.J., "Heat Transfer and Recovery Temperatures on a Sphere with Laminar, Transitional, and Turbulent Boundary Layers at Mach Numbers of 2.00 and 4.15" , NACA TN 4125, (1957).

64. Richardson, R.D., "Estimation of the Heat Transfer from the Rear of an Immersed Body to the Region of Separated Flow", Brown University, WADD TN-59-1, (1960).

65. Sogin, H.H., Buckkhard, K., and Richardson, P.D., "Heat Transfer in Separated Flows, Part I and II", Brown University, ARL-4, (1961).

66. Larson, H.K., "Heat Transfer in Separated Flows", Institute of Aeronautical Sciences, Preprint 59-37, (1959).

67. Chapman, D.R., Kuehn, D.M., and Larson, H.K., "Investigation of Separated Flows in Supersonic and Subsonic Streams with Emphasis on the Effect of Transition", NACA TN 3869, (1957).

68. Charwat, A.F., "A Modified Model of the Supersonic Laminar Wake", J. of the Aeronautical Sci., Vol. 25, No. 12, (1958).

69. Van Hise, V., "Investigation of Variation in Base Pressure Over the Reynolds Number Range in which Wake Transition Occurs for Two-Dimensional Bodies at Mach Numbers from 1.95 to 2.92", NASA TN D-167, (1959).

70. Love, E.S., "Base Pressure at Supersonic Speeds on Two-Dimensional Airfoils and on Bodies of Revolution With and Without Fins Having Turbulent Boundary Layers", NACA TN 3819, (1957).

71. Vaglio-Laurin, R., and Bloom, M., "Chemical Effects in External Hypersonic Flows", Polytechnic Institute of Brooklyn, PIBAL Report No. 640, (1961).

72. Feldman, S., "On Trails of the Axisymmetric Hypersonic Blunt Bodies Flying Through the Atmosphere", J. of the Aerospace Sci., Vol. 28, No. 6, (1961).

73. Lees, L. and Hromas, L., "Turbulent Diffusion in the Wake of a Blunt-Nosed Body at Hypersonic Speeds", IAS Paper No. 62-71, (1962).

74. Schlichting, H., Boundary Layer Theory, Pergamon Press, New York, (1955).

75. Hartnett, J.P., Eckert, E.R.G., Birkebak, R., and Sampson, R.L., "Simplified Procedures for the Calculation of Heat Transfer to Surfaces with Non-Uniform Temperatures", University of Minnesota Heat Transfer Laboratory, WADC TR 56-373, (1956).

76. Sparrow, E.M., and Gregg, J.L., "Nonsteady Surface Temperature Effects on Forced Convection Heat Transfer", Readers' Forum, J. of Aeronautical Sci., Vol. 24, No. 10, (1957).

REFERENCES (CONCL'D)

77. Naysmith, A., "Heat Transfer and Boundary Layer Measurement in a Region of Supersonic Flow Separation and Reattachment", T.N. No. Aero 2558, Royal Aircraft Establishment, (1958).

78. Chapman, D.R., "An Analysis of Base Pressure at Supersonic Velocities and Comparison with Experiment", NACA Report No. 1051, (1951).

79. Ginoux, Jean, "Experimental Evidence of Three-Dimensional Perturbations in the Reattachment of a Two-Dimensional Laminar Boundary Layer at M = 2.05", TCEA TN 1, (1958).

80. Czarnecki, K.R. and Schueller, C.F., "Investigation of Interaction Effects Arising from Side-Wall Boundary Layers in Supersonic Wind Tunnel Tests of Airfoils", NACA RM L8G27, (1948).

81. Dorrance, William A., "Two-Dimensional Airfoils at Moderate Hypersonic Velocities", Convair Report ZA-7-005, (1952).

82. Fuller, L. and Reid, J., "Measurements on Two-Dimensional Base Flow at M = 2.4", Reports and Memorandum No. 3062, (1956), R.A.E. Rep. Aero. 2569, (1956).

83. Tollmien, W., "Calculation of Turbulent Expansion Processes", NACA TM 1085, (1945).

84. Bradfield, W.S., "Research on Laminar and Turbulent Boundary Layers at Supersonic Speeds", University of Minnesota Rosemount Aero. Labs. Research Report No. 131, (1957).

85. Laufer, J. and McClellan, R., "Measurement of Heat Transfer from Fine Wires in Supersonic Flows", J. of Fluid Mech., Vol. 1, Part 3, (1956).

86. Kovasznay, L.S.G., "The Hot-Wire Anemometer in Supersonic Flow", J. of Aeronautical Sci., Vol. 17, No. 9, (1950).

87. Kurzweg, H.H., "Interrelationship Between Boundary Layer and Base Pressure", J. of Aeronautical Sci., Vol. 18, No. 11, (1951).

88. Reshotko, E., and Cohen, C.B., "Heat Transfer at the Forward Stagnation Point of Blunt Bodies", NACA TN 3513, (1955).

89. Livingood, J.N.B., and Donoughe, P.L., "Summary of Laminar-Boundary Layer Solutions for Wedge-Type Flow Over Convection and Transpiration Cooled Surfaces", NACA TN 3588, (1955).

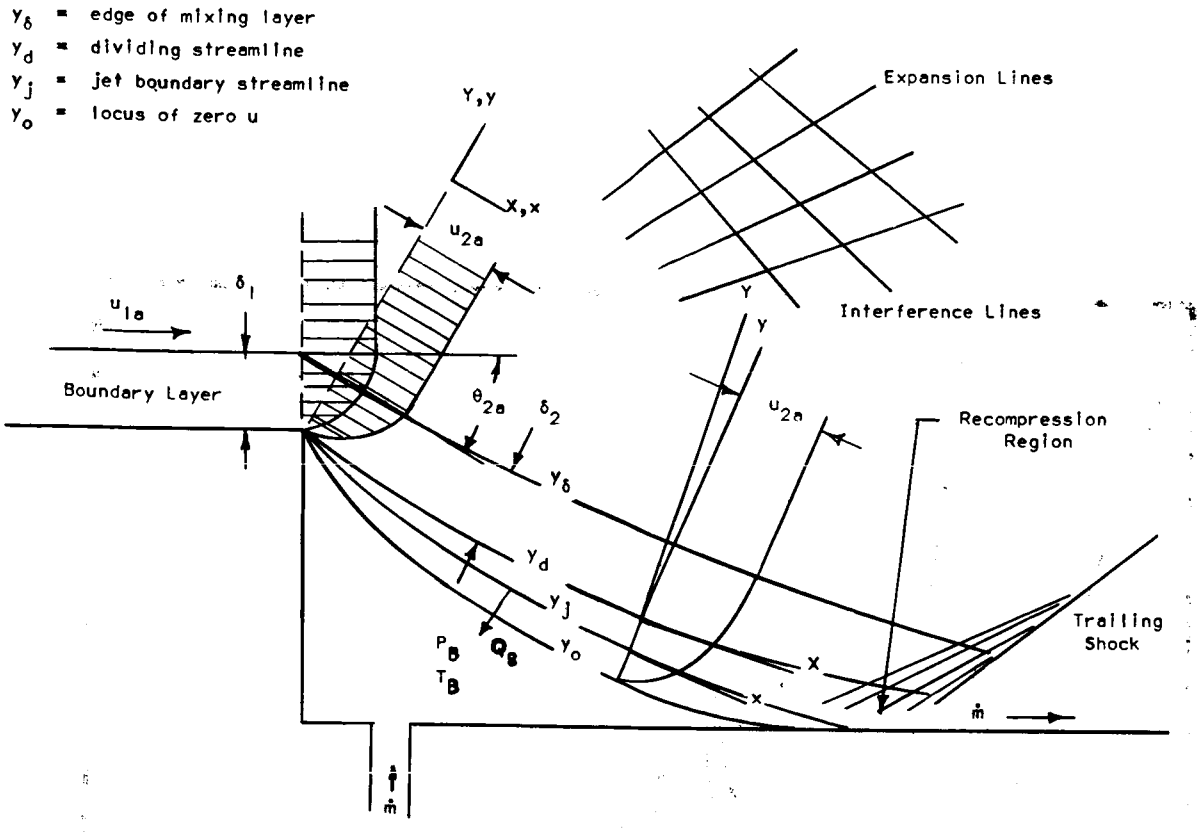

FIGURE 2. MODEL FOR KORST'S ANALYSIS

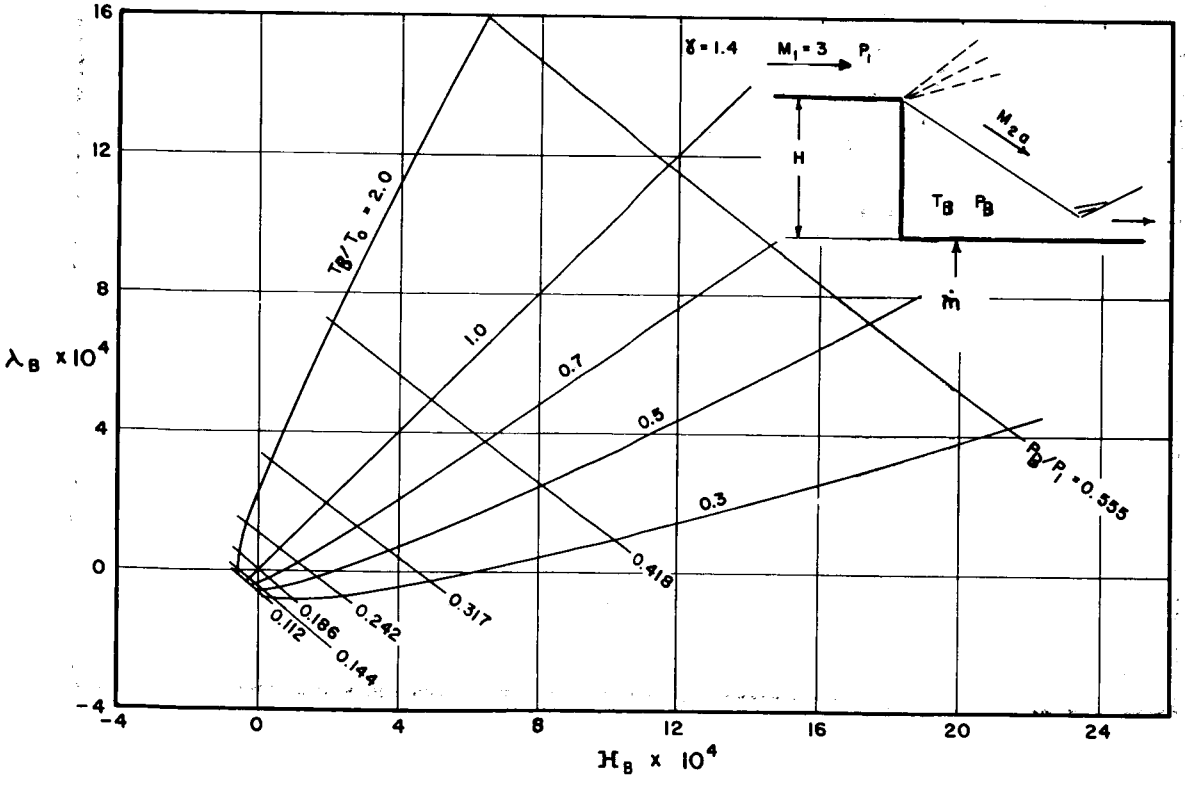

FIGURE 3. GENERALIZED PRESENTATION OF THE EFFECTS OF HEAT AND MASS ADDITION INTO THE WAKE REGION, M_1 = 3.0

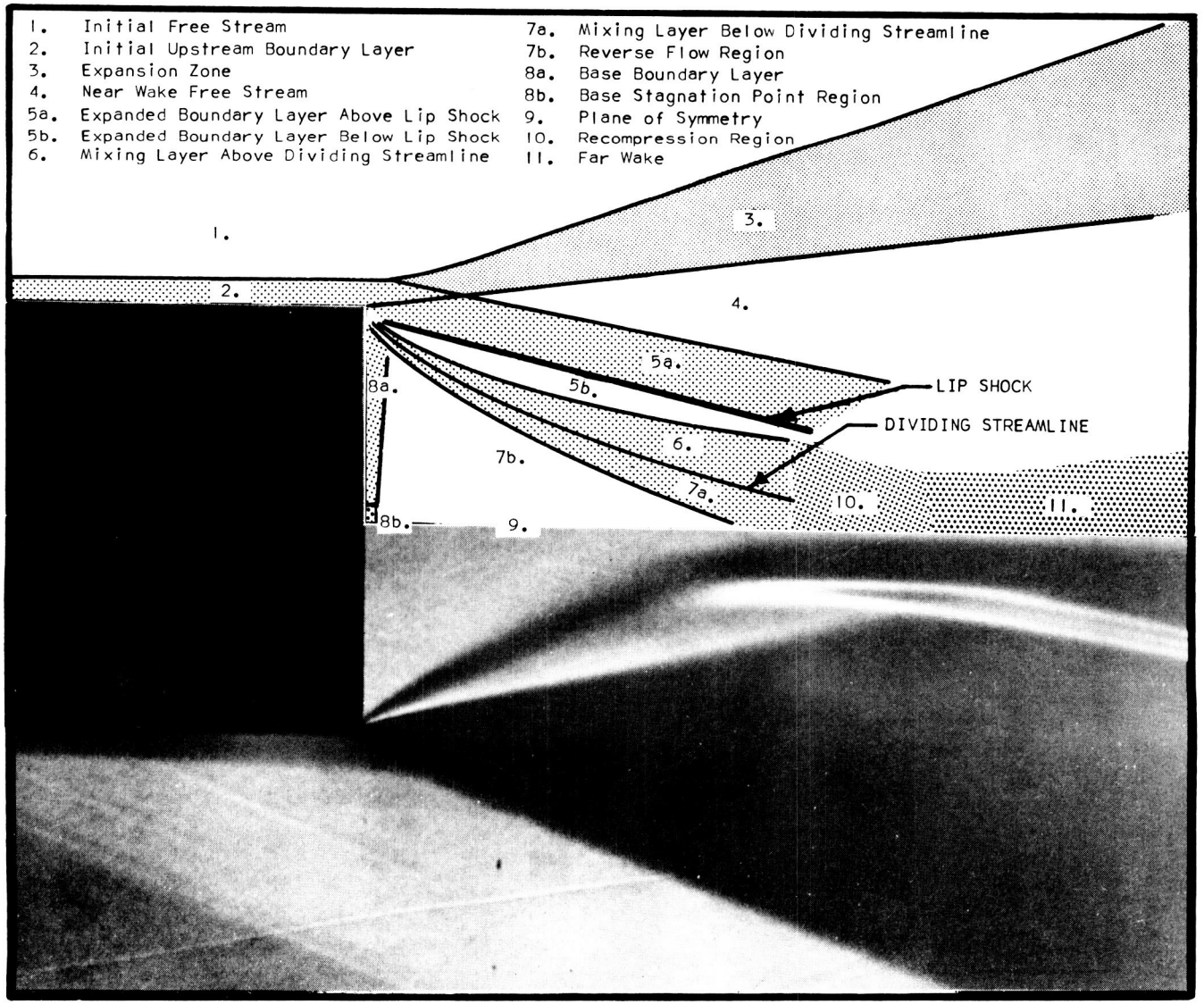

FIGURE 1. FLOW FIELD MODEL

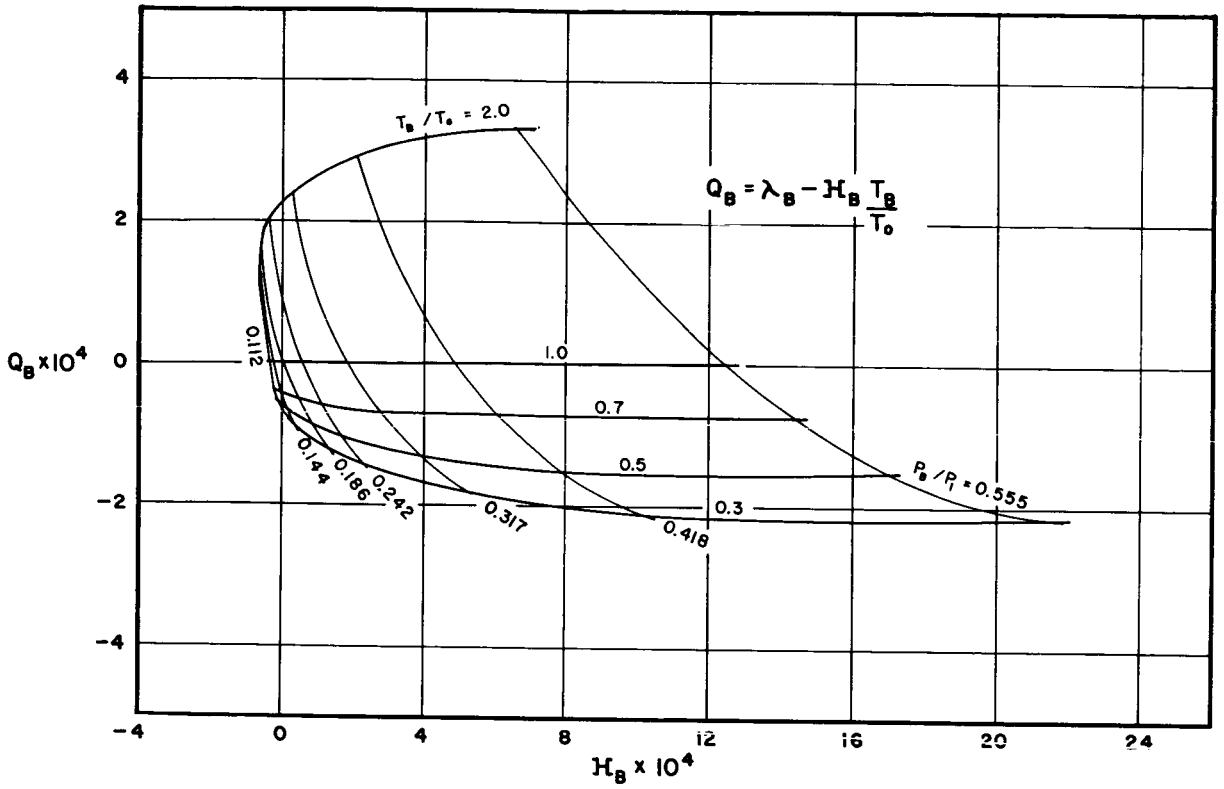

FIGURE 4. BASE HEAT FLUX, $M_1 = 3.0$

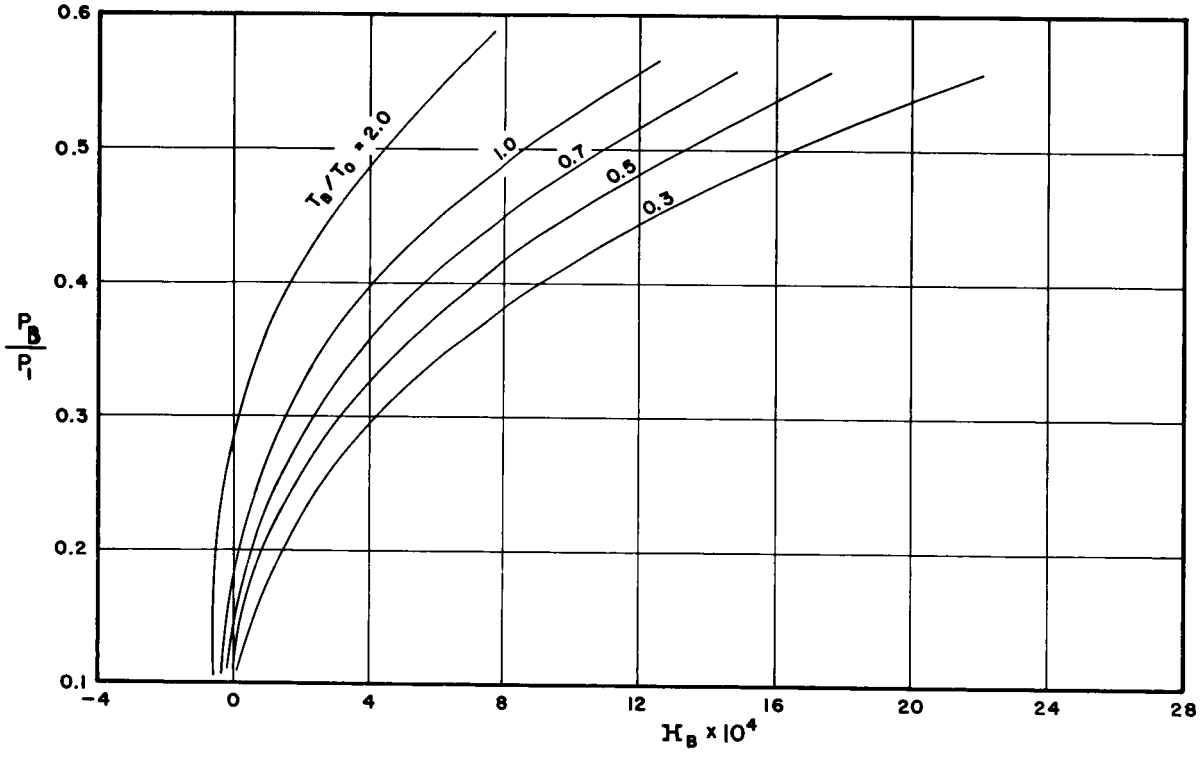

FIGURE 5. VARIATION OF BASE PRESSURE RATIO WITH BASE TEMPERATURE - INCLUDING THE EFFECTS OF MASS ADDITION, $M_1 = 3.0$

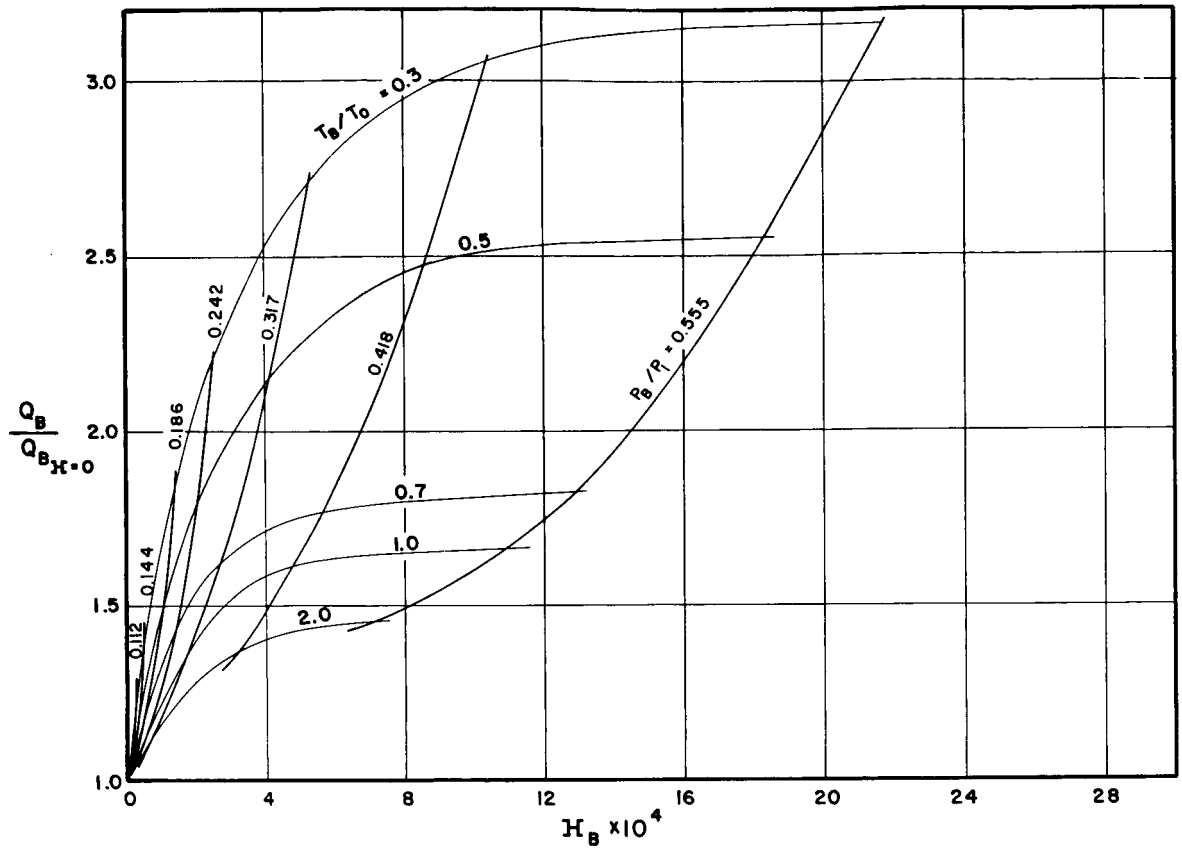

FIGURE 6. THE INCREASE IN BASE HEAT FLUX WITH MASS ADDITION - VARIABLE BASE PRESSURE, $M_1 = 3$

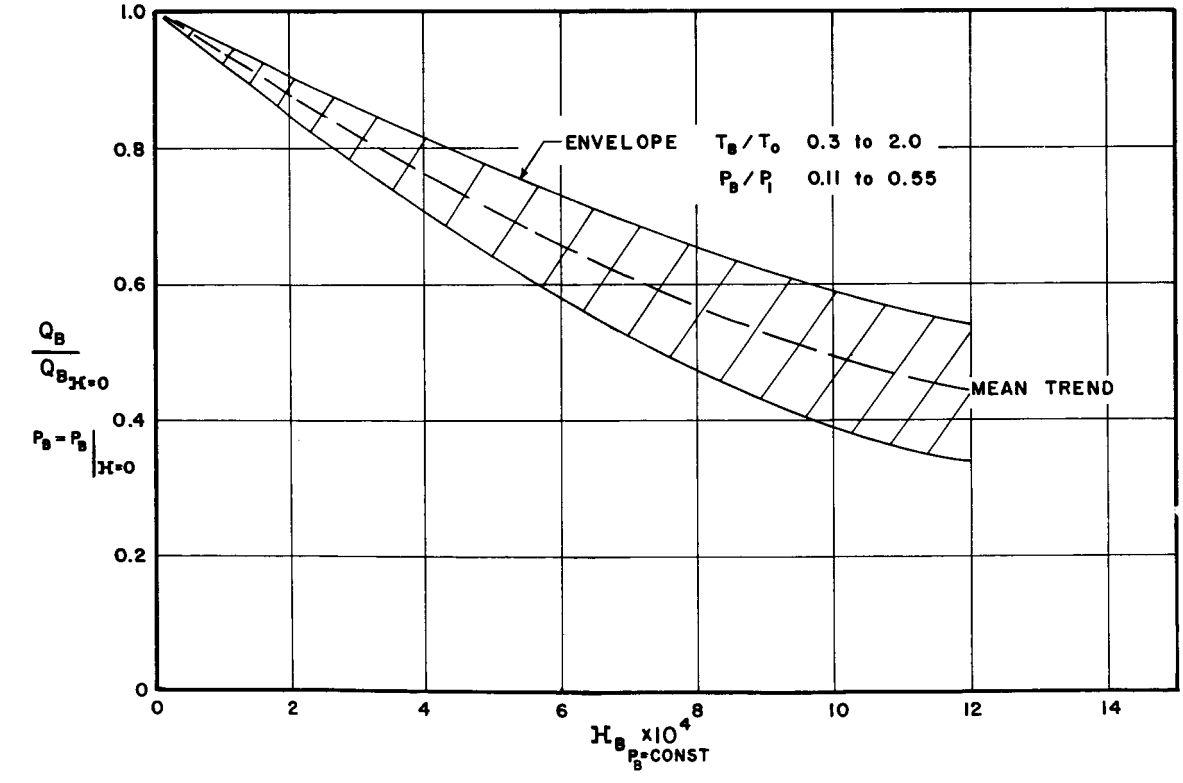

FIGURE 7. THE DECREASE IN BASE HEAT FLUX WITH MASS ADDITION - CONSTANT BASE PRESSURE, $M_1 = 3.0$

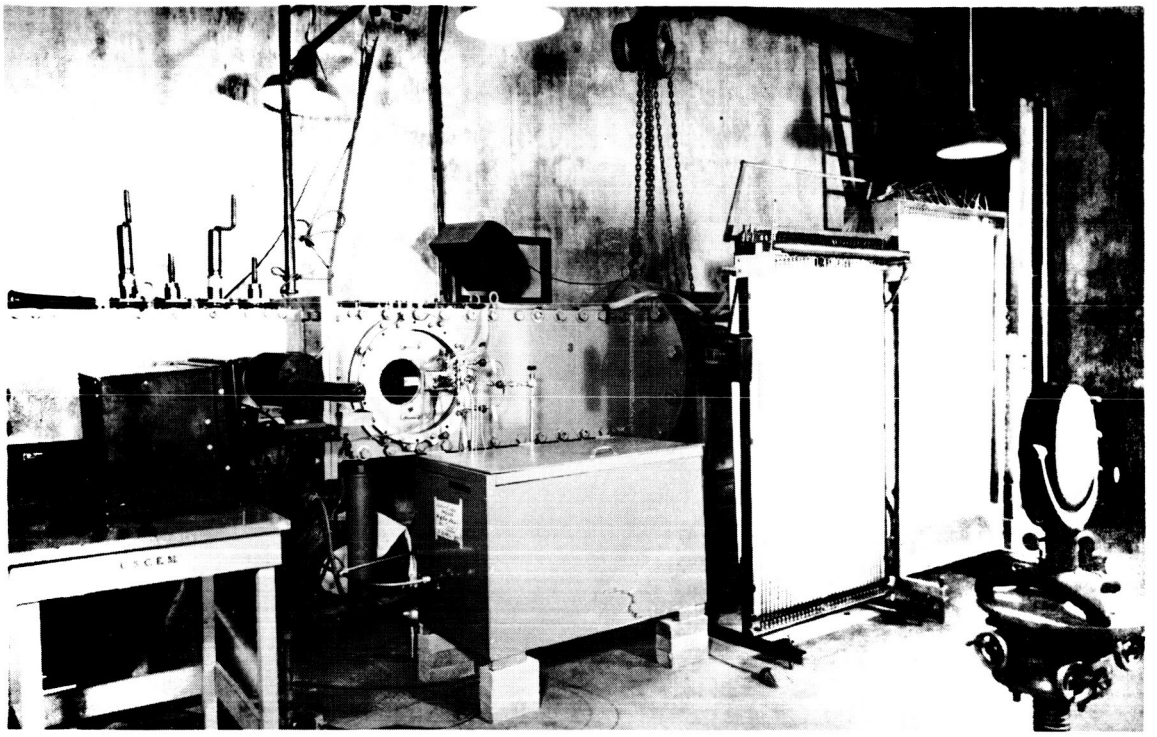

a) Test Setup in Wind Tunnel Room

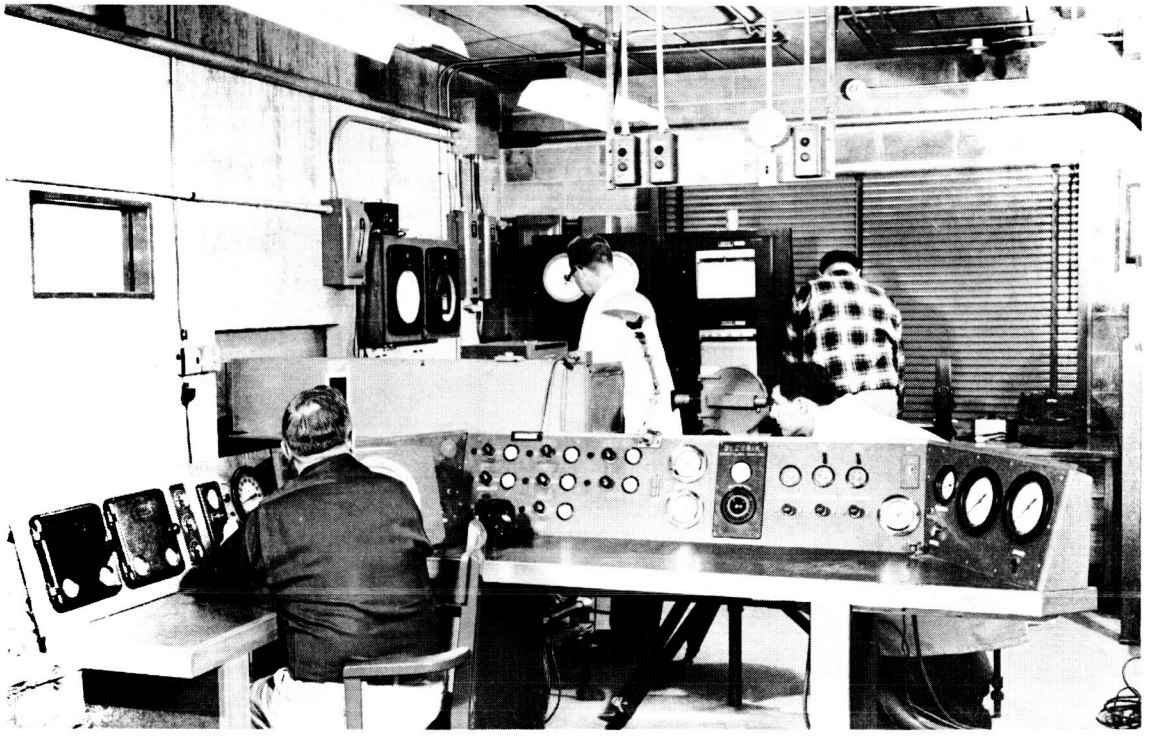

b) Control Room

FIGURE 8. TEST FACILITY AND CONTROL ROOM

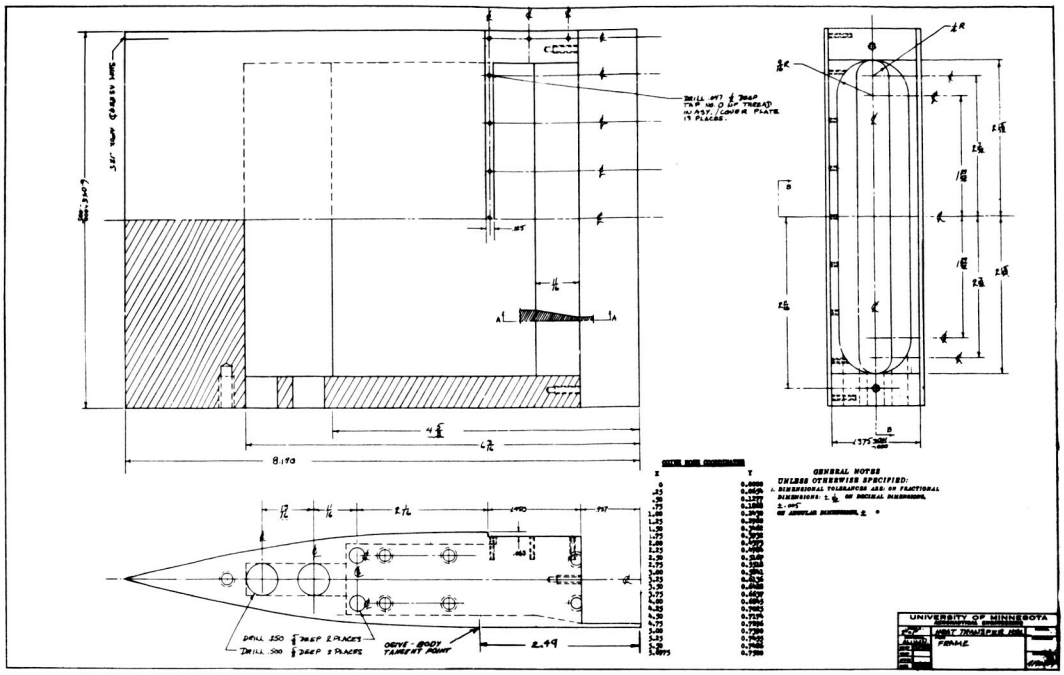

a) Design Drawing

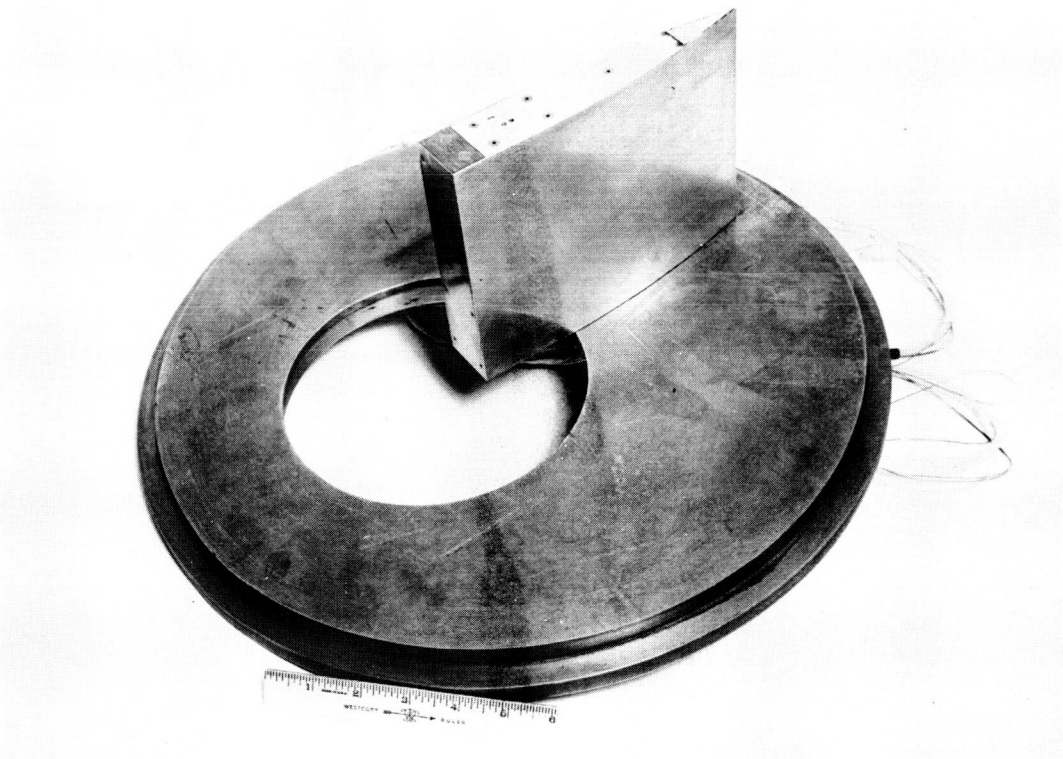

b) Installation

FIGURE 9. MODEL FOREBODY

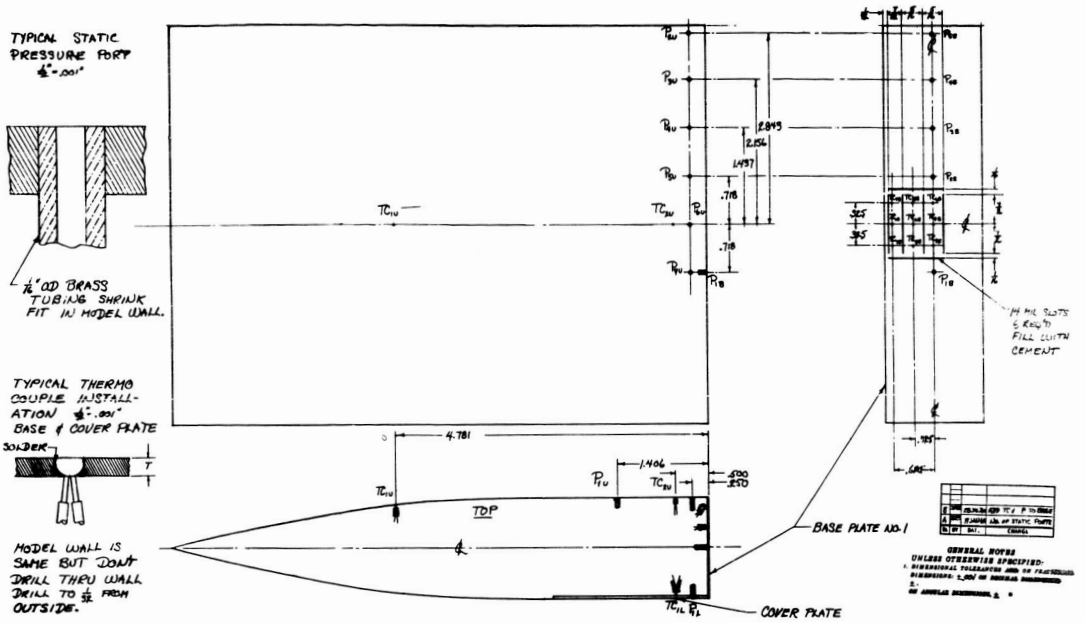

FIGURE 10. FOREBODY AND HEAT TRANSFER BASE INSTRUMENTATION

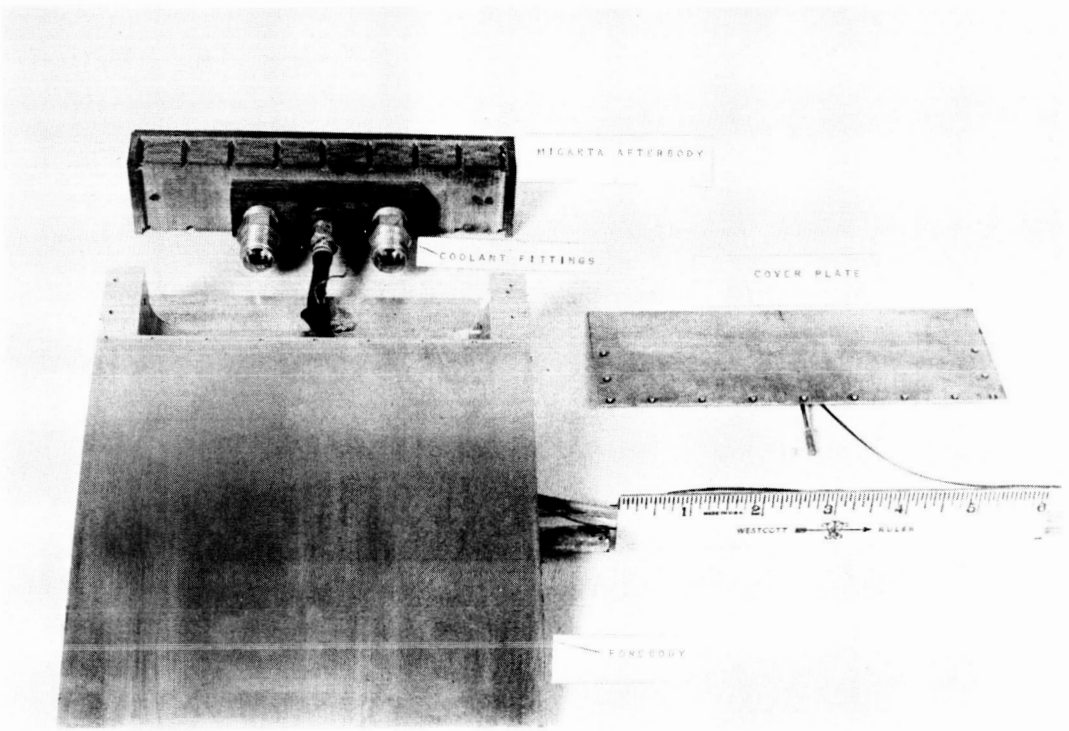

FIGURE 11. HEAT TRANSFER MODEL DISASSEMBLED

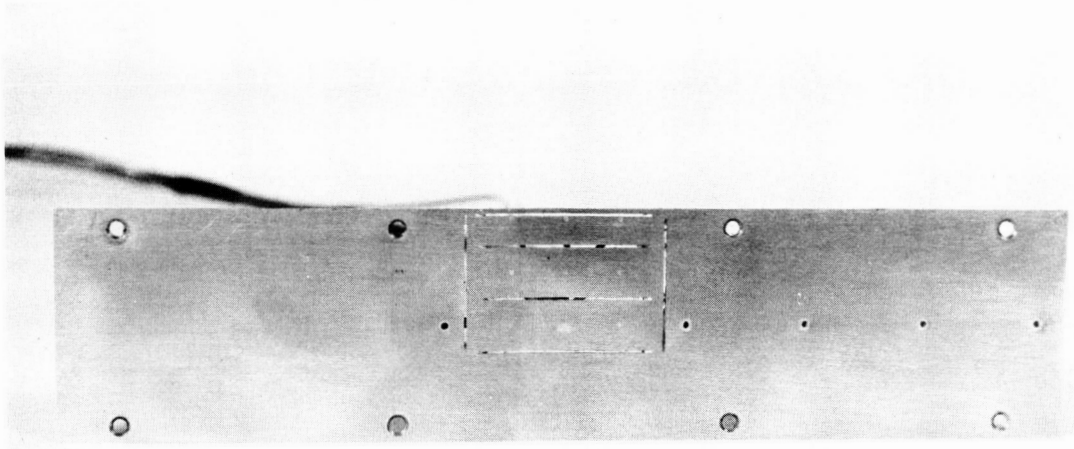

FIGURE 12. HEAT TRANSFER BASE

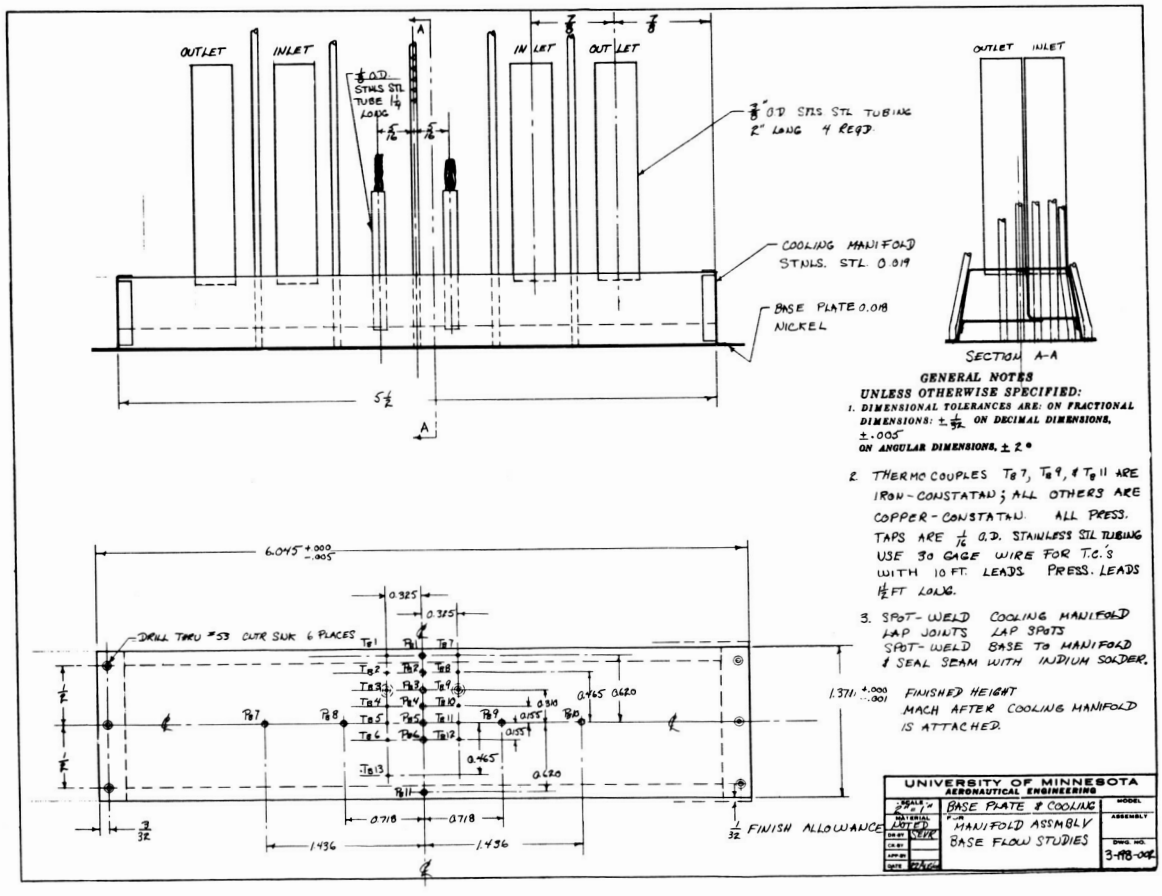

FIGURE 13. PRESSURE AND PROBING BASE INSTRUMENTATION

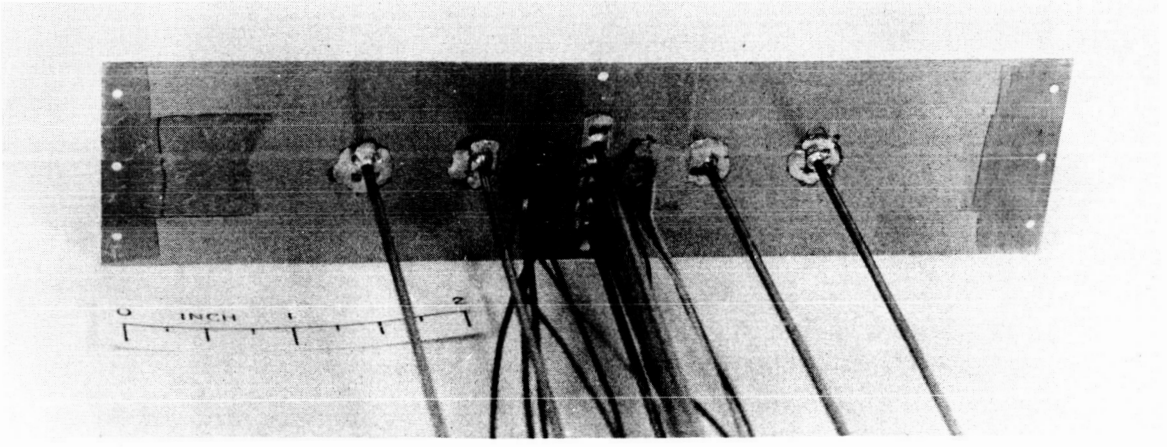

a) Rear View of Base Plate

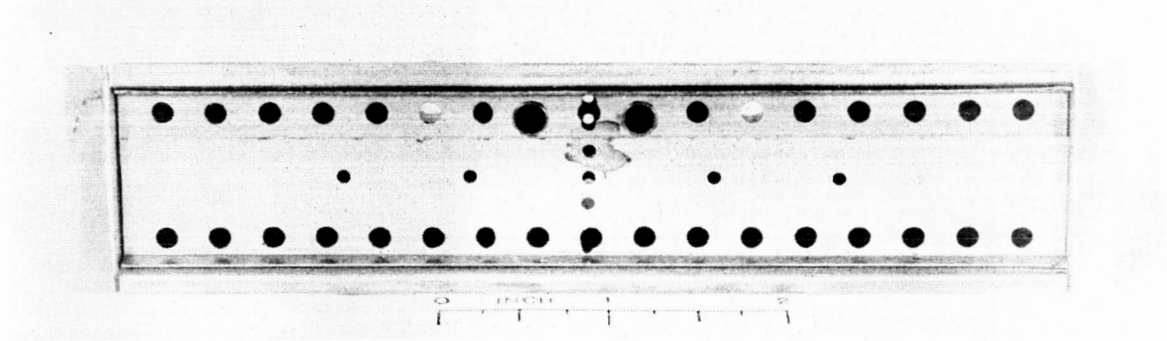

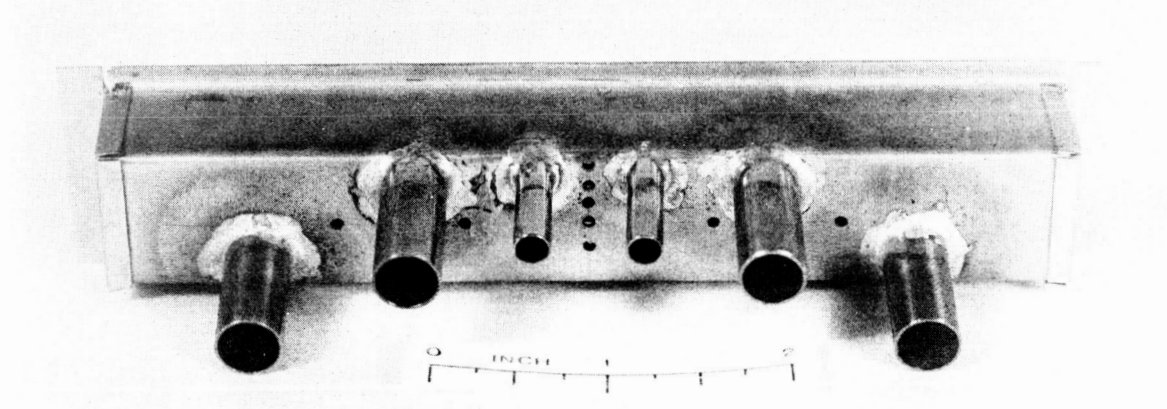

b) Two Views of Cooling Chamber

FIGURE 14. BASE PLATE AND COOLING CHAMBER

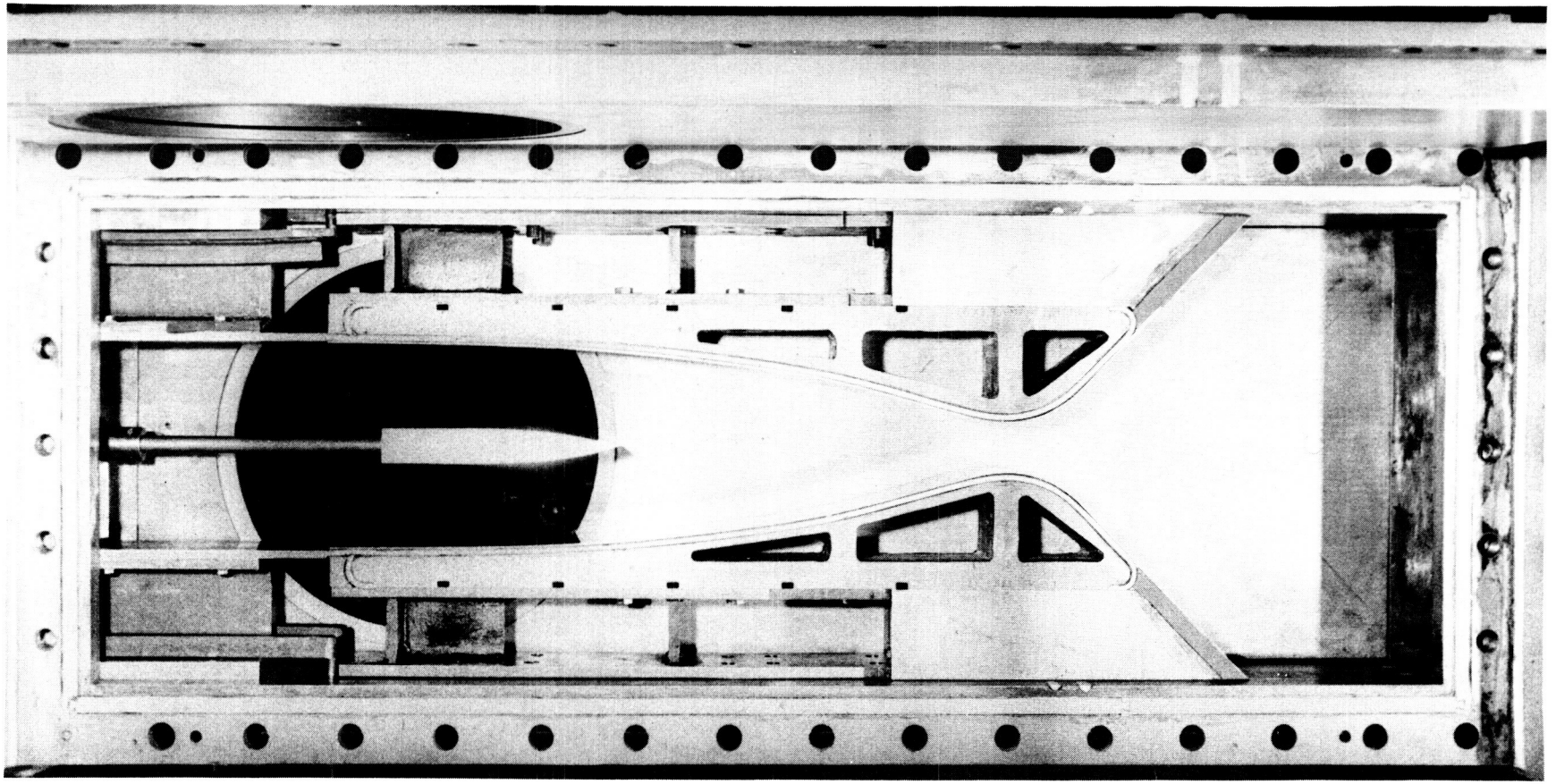

FIGURE 15. STING INSTALLATION OF BLOCKAGE MODEL

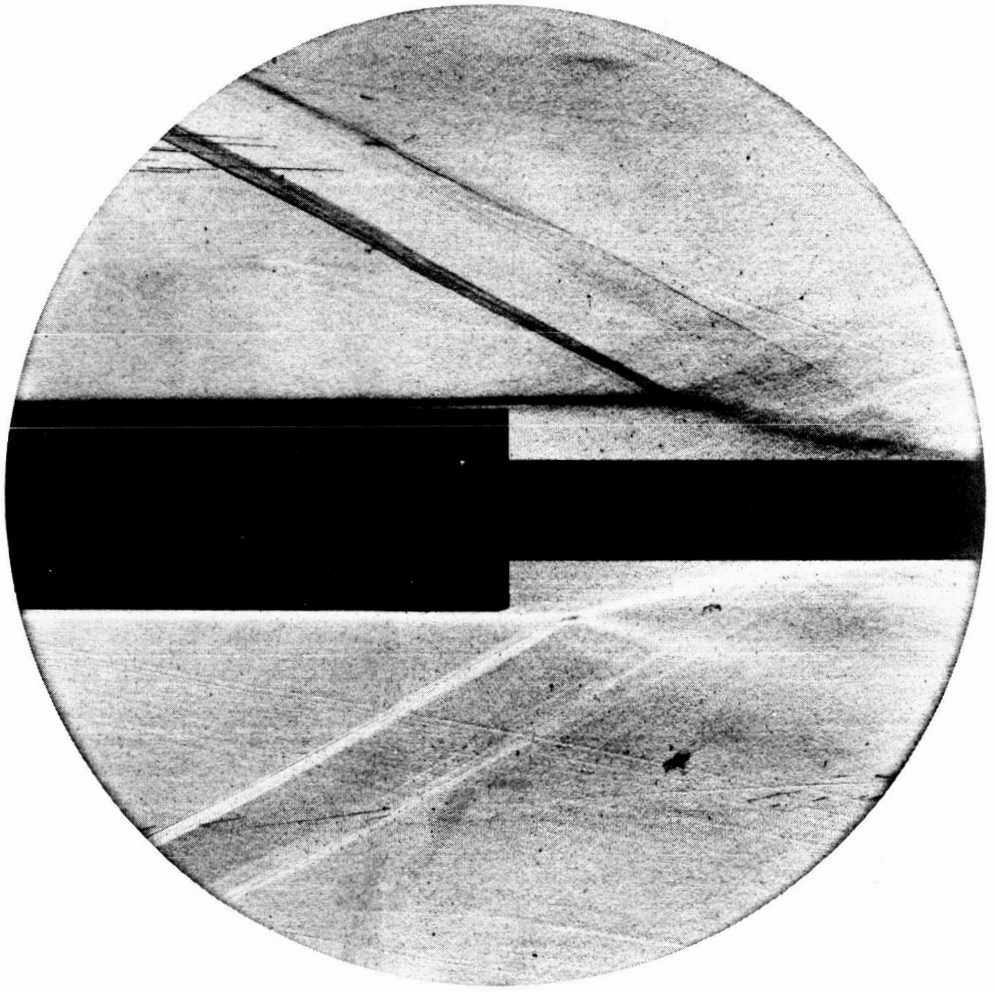

a) Schlieren Photograph

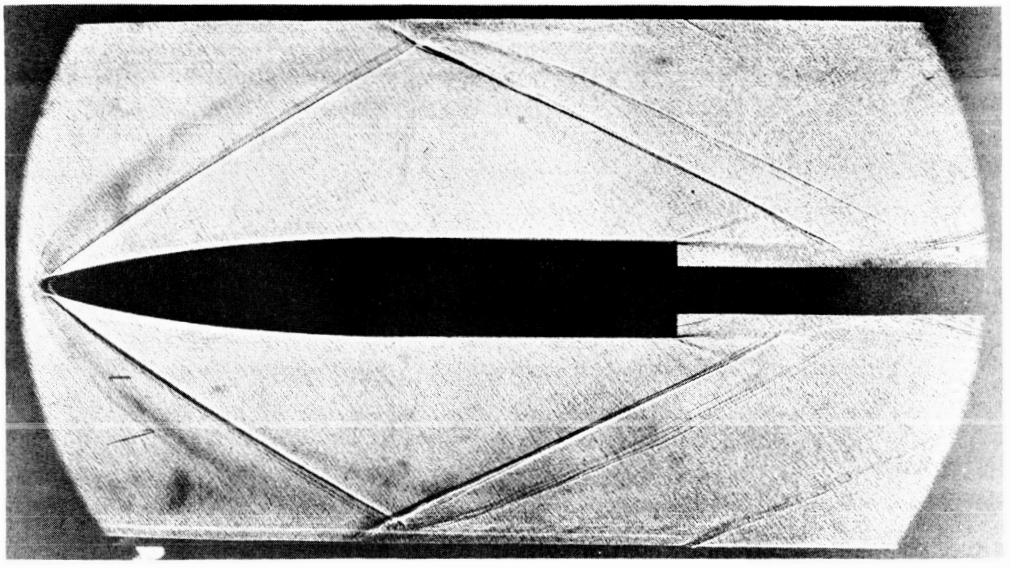

b) Shadowgraph Photograph

FIGURE 16. SCHLIEREN AND SHADOWGRAPH PHOTOGRAPHS SHOWING IMPROPER WAKE FLOW

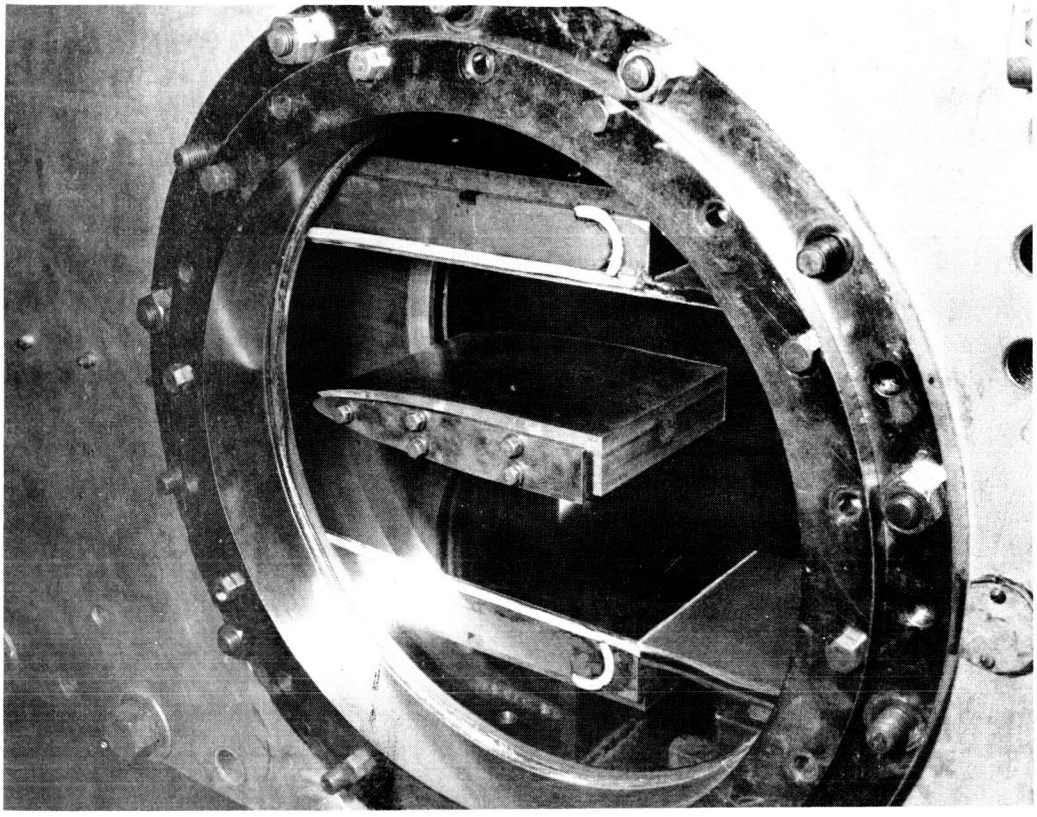

FIGURE 17. WINDOW INSTALLATION OF BLOCKAGE MODEL

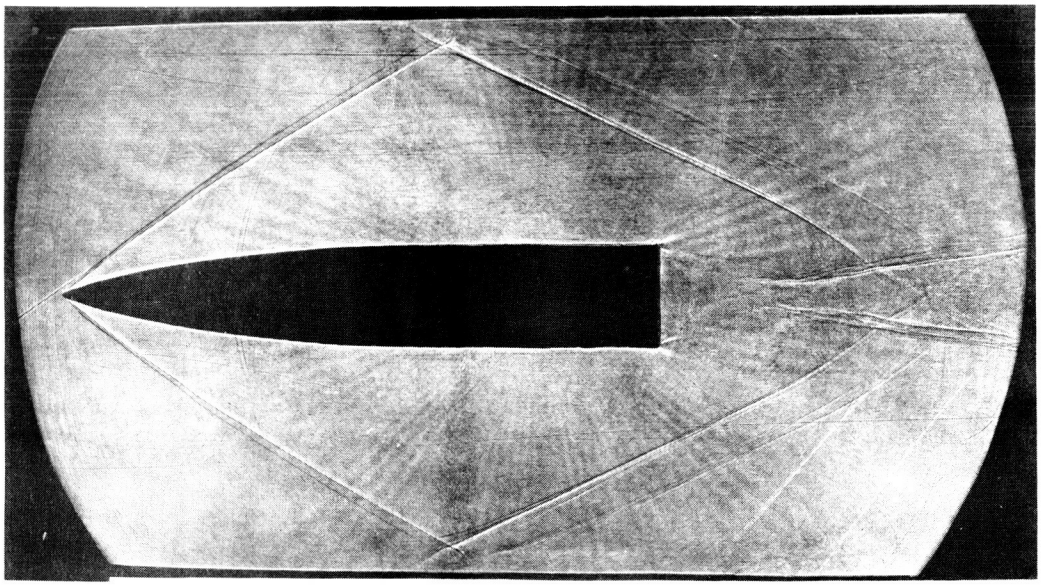

FIGURE 18. PROPER FLOW AROUND BLOCKAGE MODEL

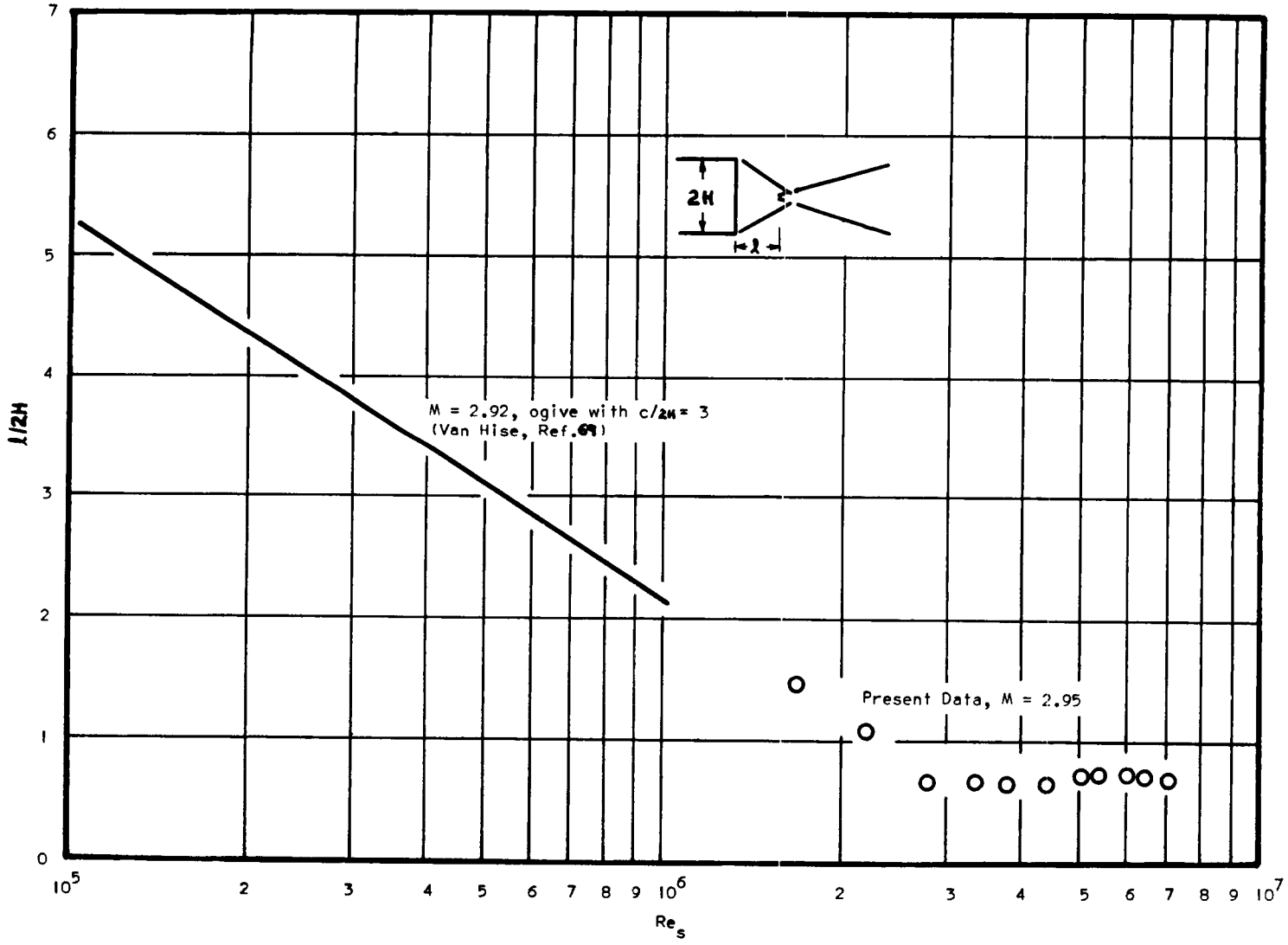

FIGURE 19. VARIATION OF MINIMUM DISTURBANCE LENGTH WITH REYNOLDS NUMBER

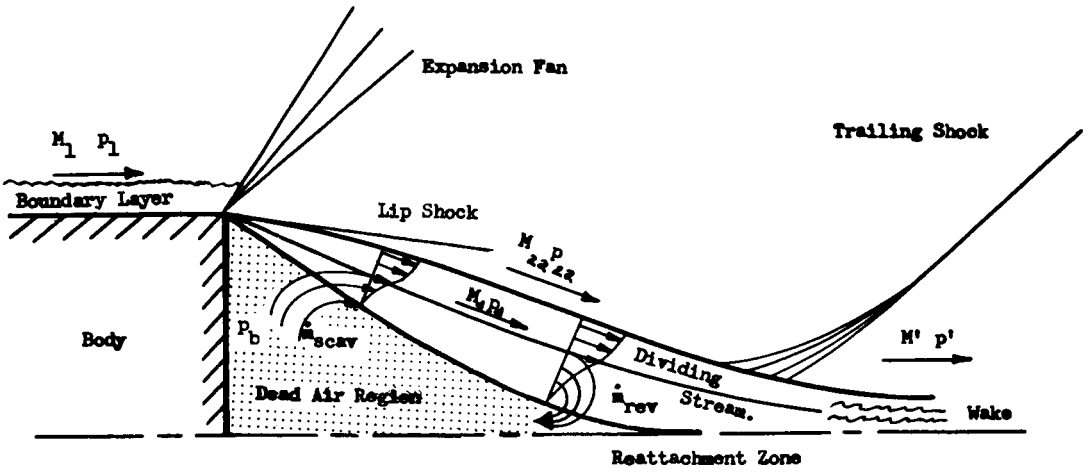

a) Scavenging and Reverse Flow Mechanism

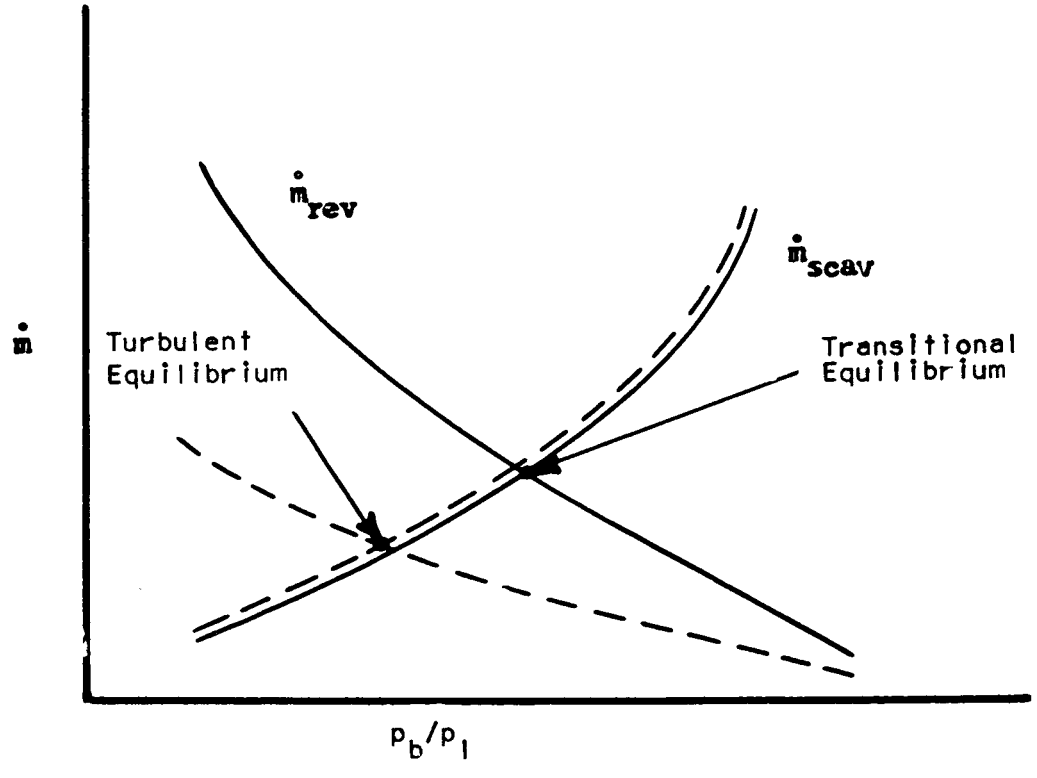

b) Balance of Scavenged and Reverse Flow

FIGURE 20. ESTABLISHMENT OF BASE PRESSURE

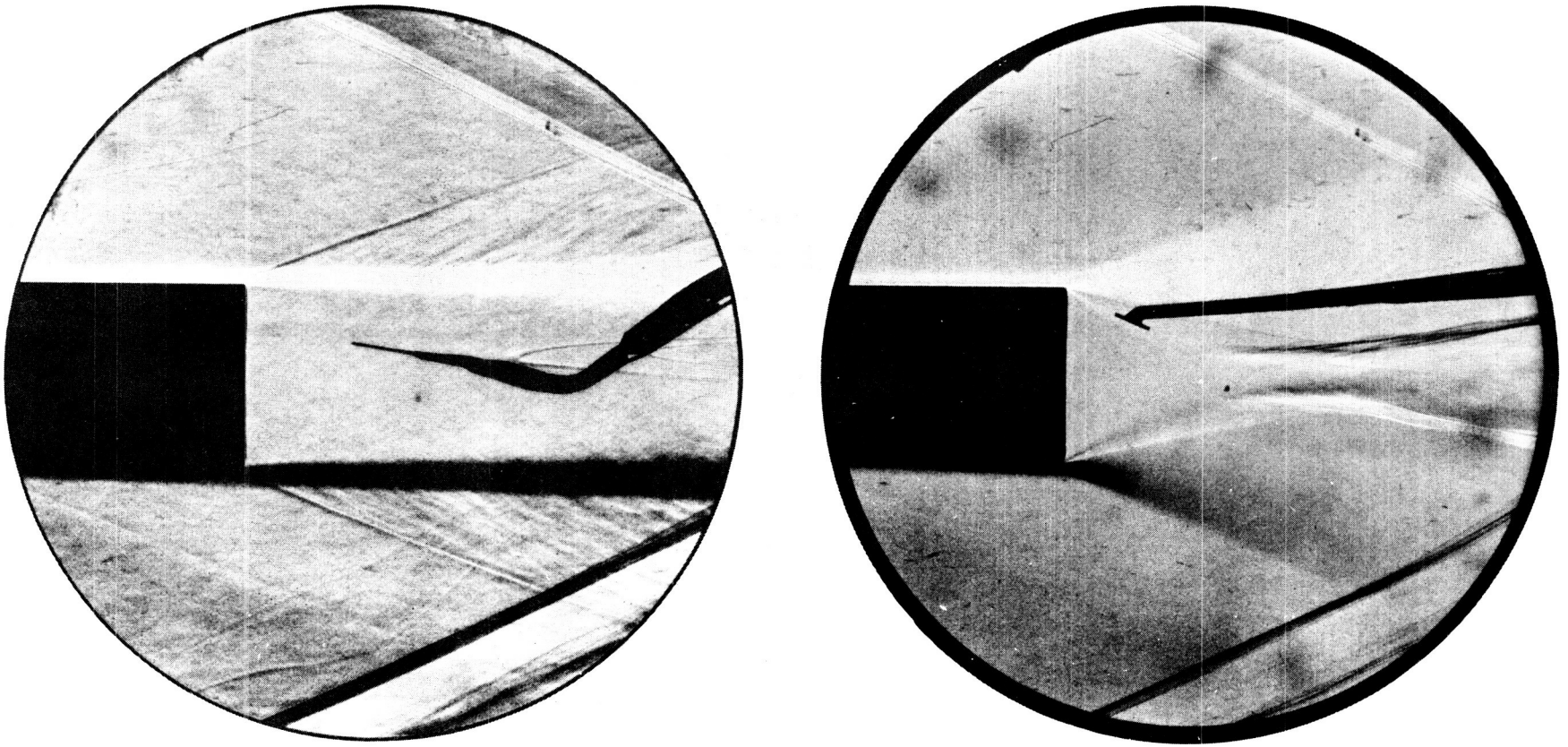

a) Flow not Established

b) Flow Established

FIGURE 21. THE INFLUENCE OF PROBING CONFIGURATION ON BASE FLOW

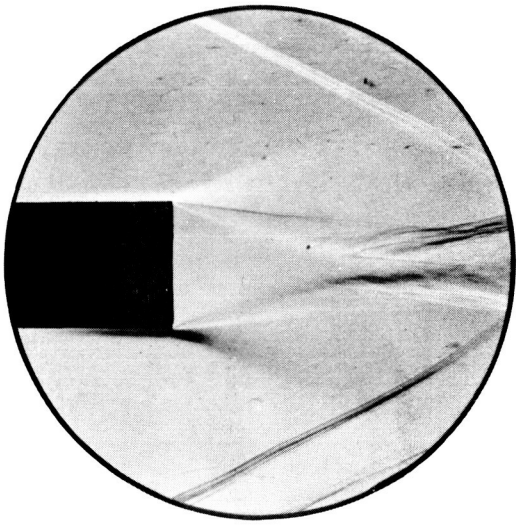

a) $Re_s = 1.67 \times 10^6$

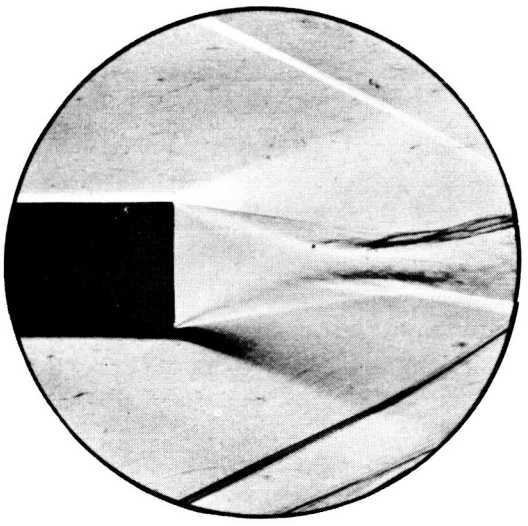

b) $Re_s = 2.19 \times 10^6$

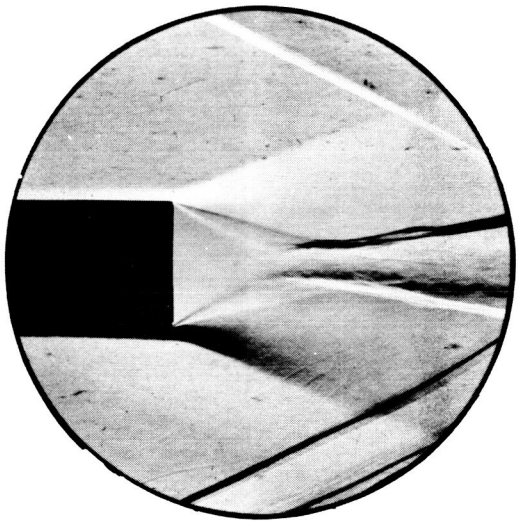

c) $Re_s = 2.78 \times 10^6$

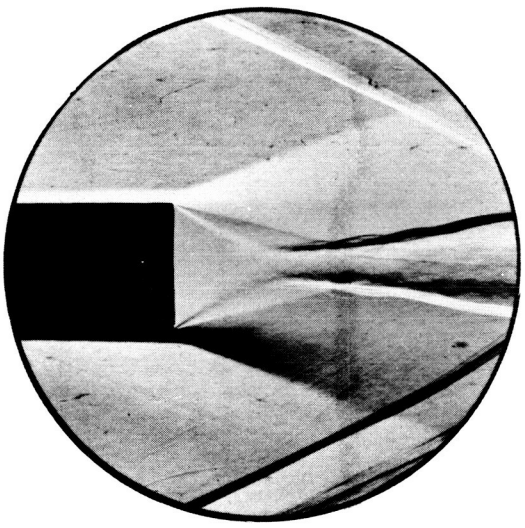

d) $Re_s = 3.35 \times 10^6$

FIGURE 22. SCHLIEREN PHOTOGRAPHS OF BASE FLOW OVER COMPLETE REYNOLDS NUMBER RANGE

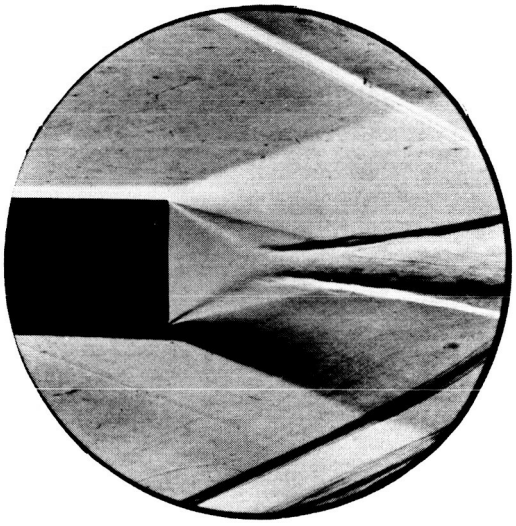

e) $Re_s = 3.78 \times 10^6$

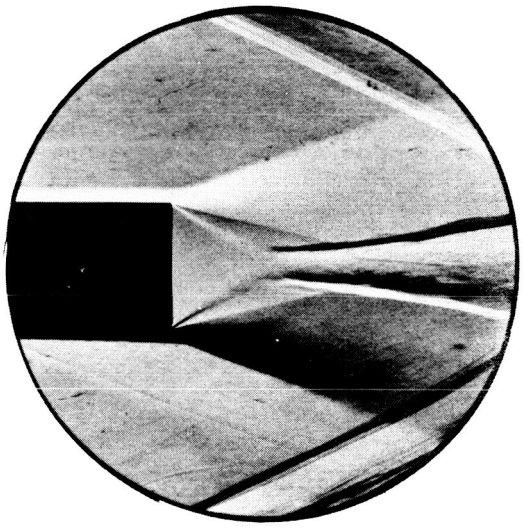

f) $Re_s = 4.40 \times 10^6$

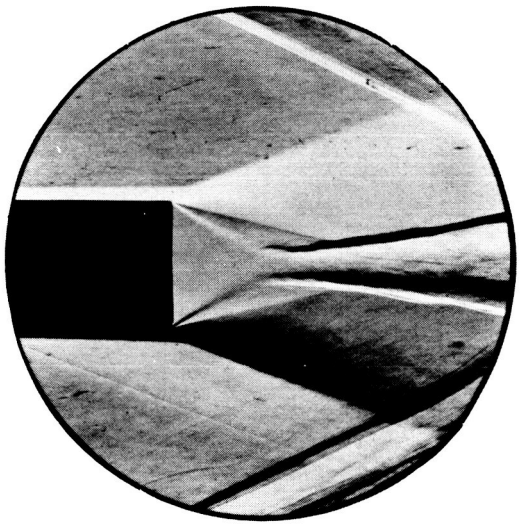

g) $Re_s = 5.02 \times 10^6$

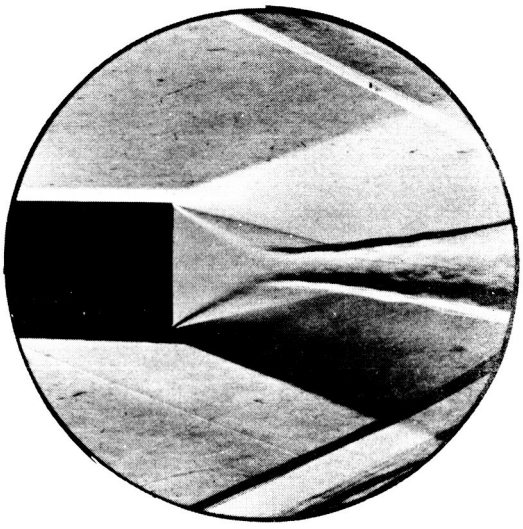

h) $Re_s = 5.40 \times 10^6$

FIGURE 22. (CONT'D)

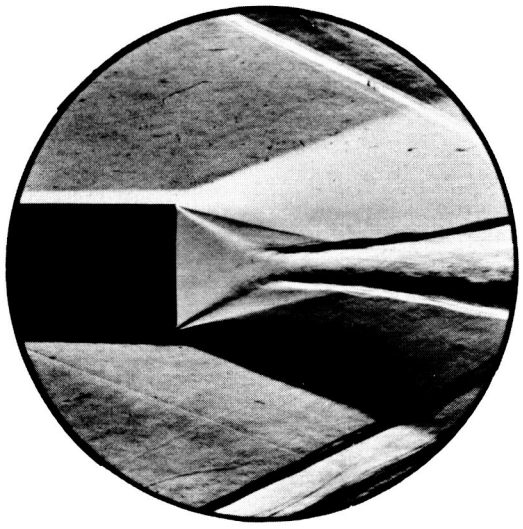

i) $Re_s = 6.02 \times 10^6$

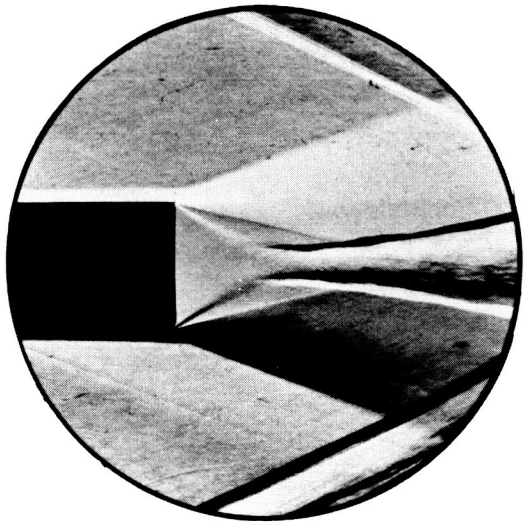

j) $Re_s = 6.43 \times 10^6$

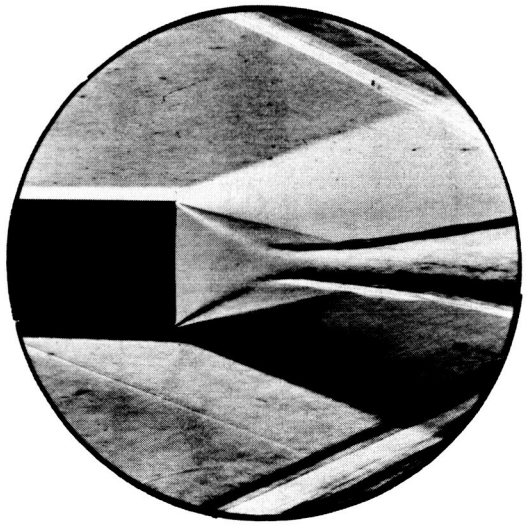

k) $Re_s = 7.02 \times 10^6$

FIGURE 22. (CONT'D)

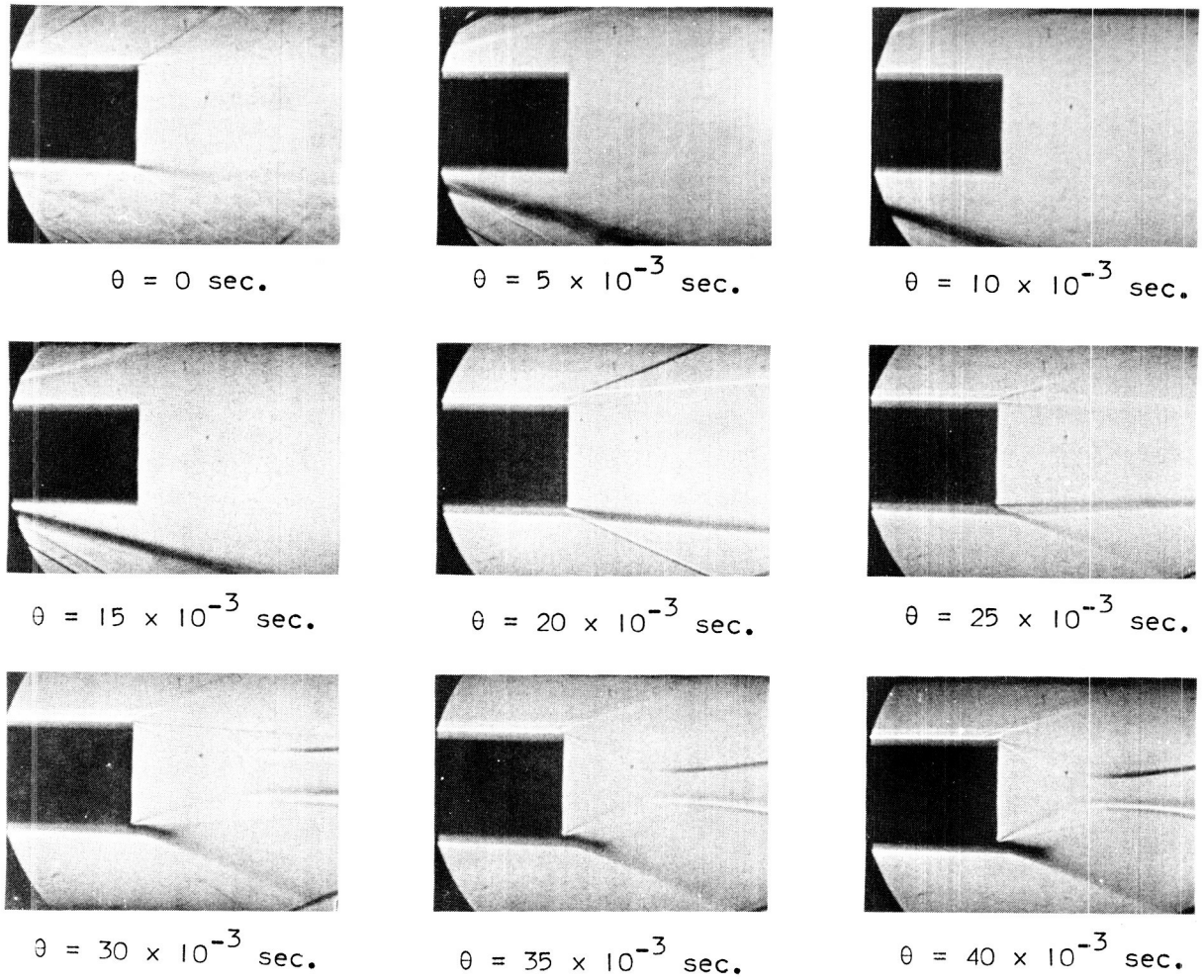

FIGURE 23. FASTAX SCHLIEREN PHOTOGRAPHS OF WAKE STARTING PROCESS

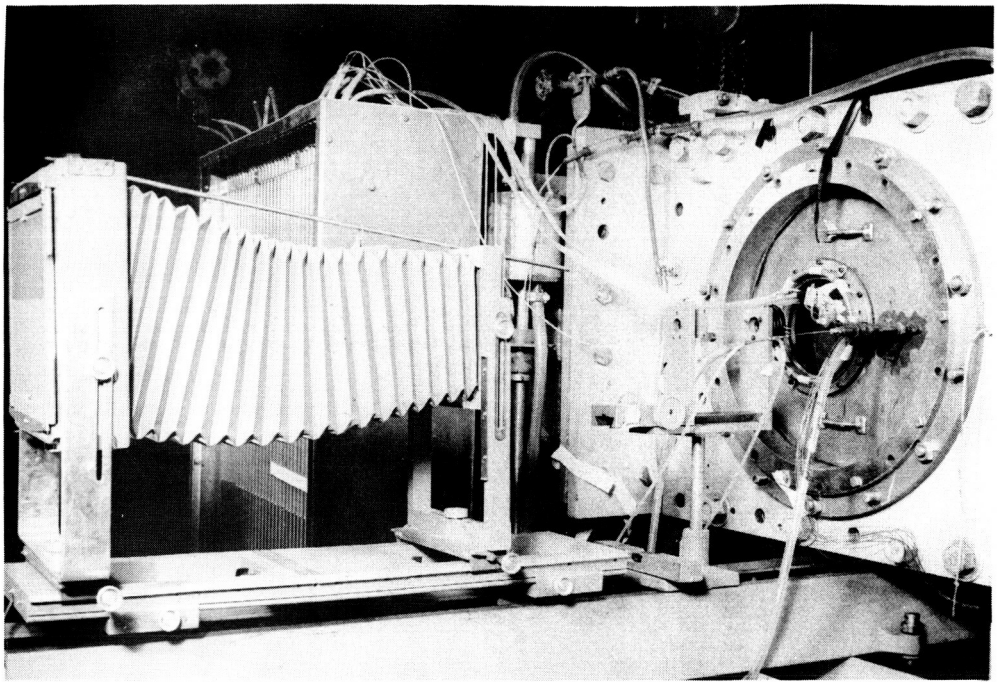

a) Microschlieren Equipment

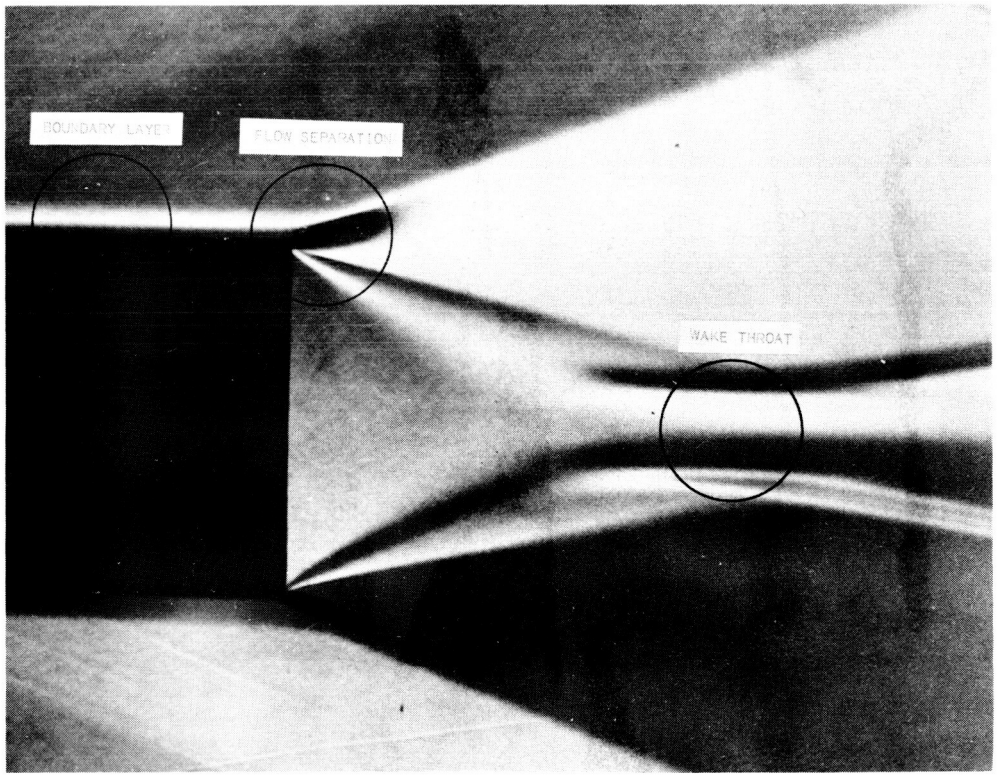

b) Locations of Photographs

FIGURE 24. MICROSCHLIEREN PHOTOGRAPHY (8 POWER MAGNIFICATION)

c) Flow Separating From Model

d) Wake Throat

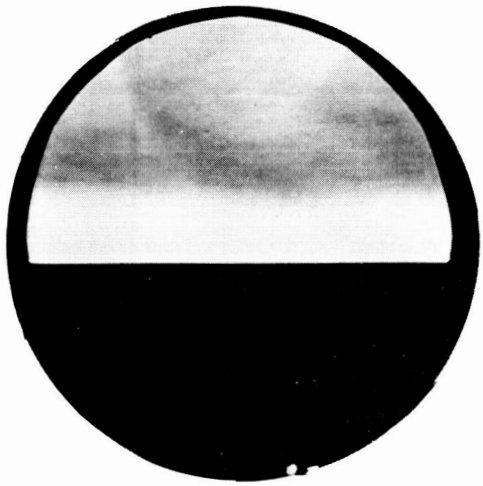

e) Model Boundary Layer

FIGURE 24. (CONT'D)

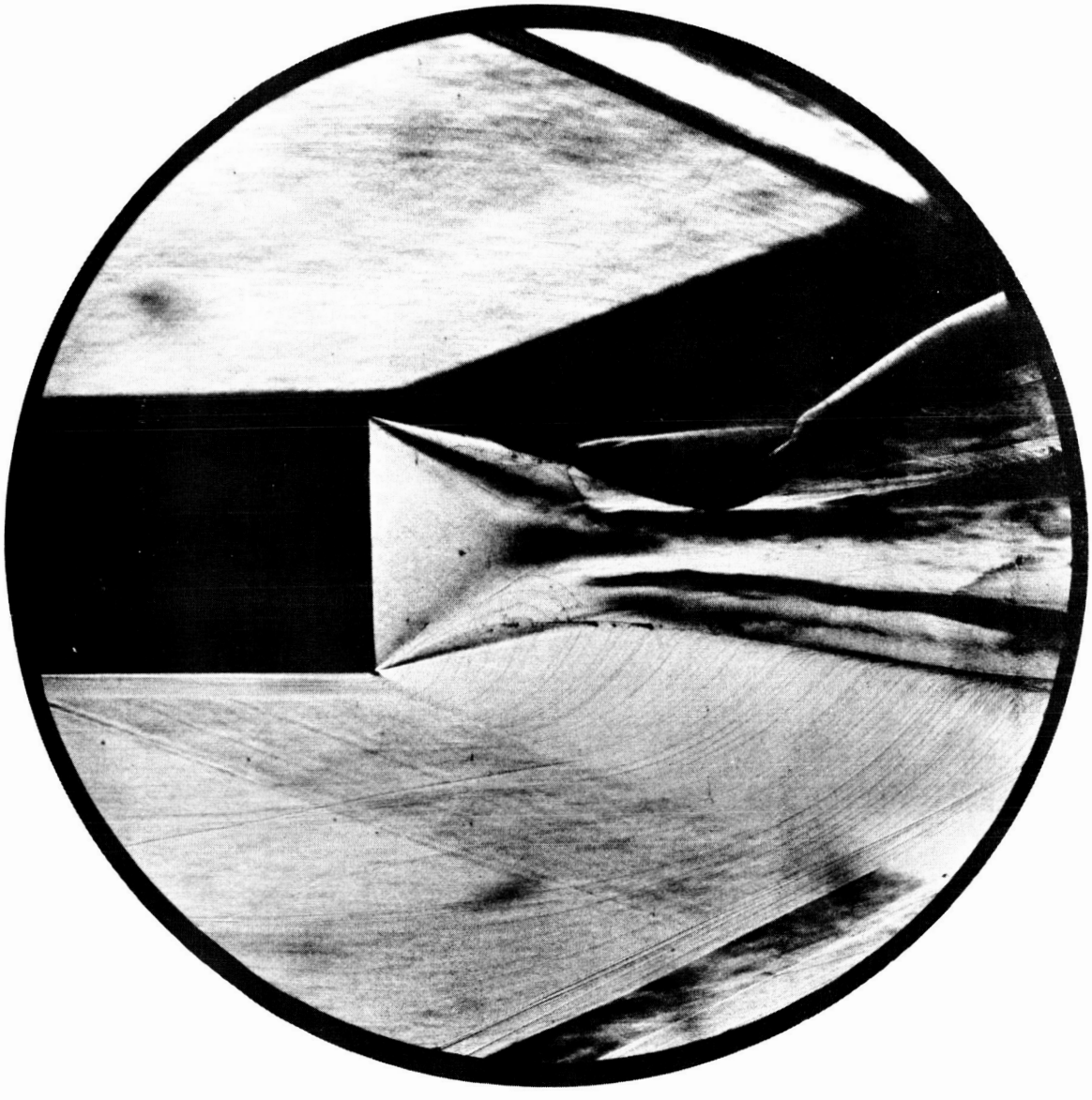

FIGURE 25. OIL STREAKLINE PHOTOGRAPHY

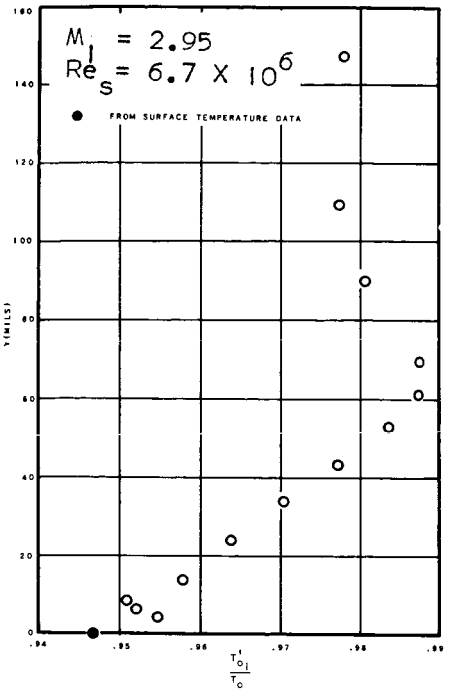

a) Uncorrected Temperature

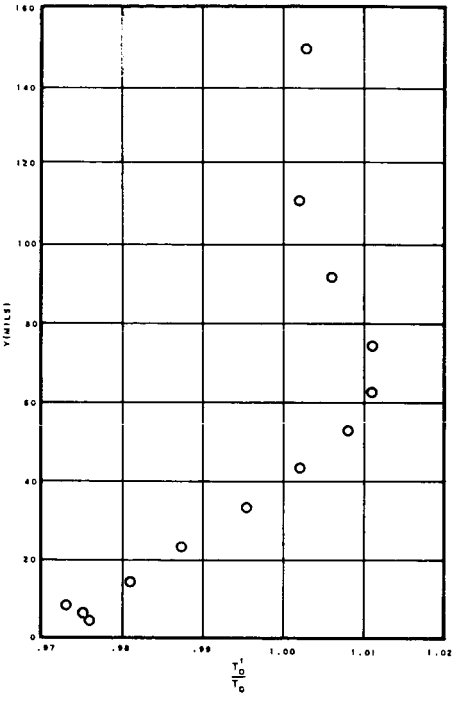

b) Corrected Temperature

FIGURE 26. TOTAL TEMPERATURE VARIATION THROUGH BOUNDARY LAYER

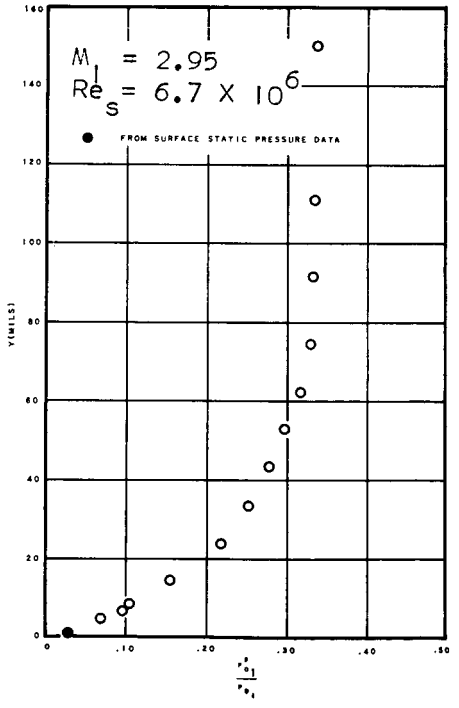

a) Impact Pressure

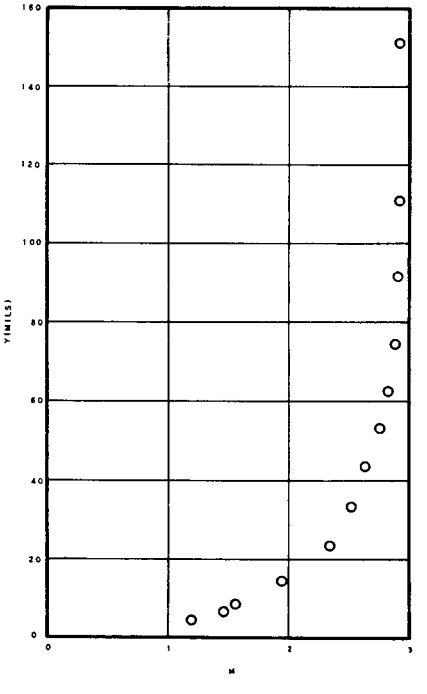

b) Mach Number

FIGURE 27. IMPACT PRESSURE AND MACH NUMBER VARIATION THROUGH BOUNDARY LAYER

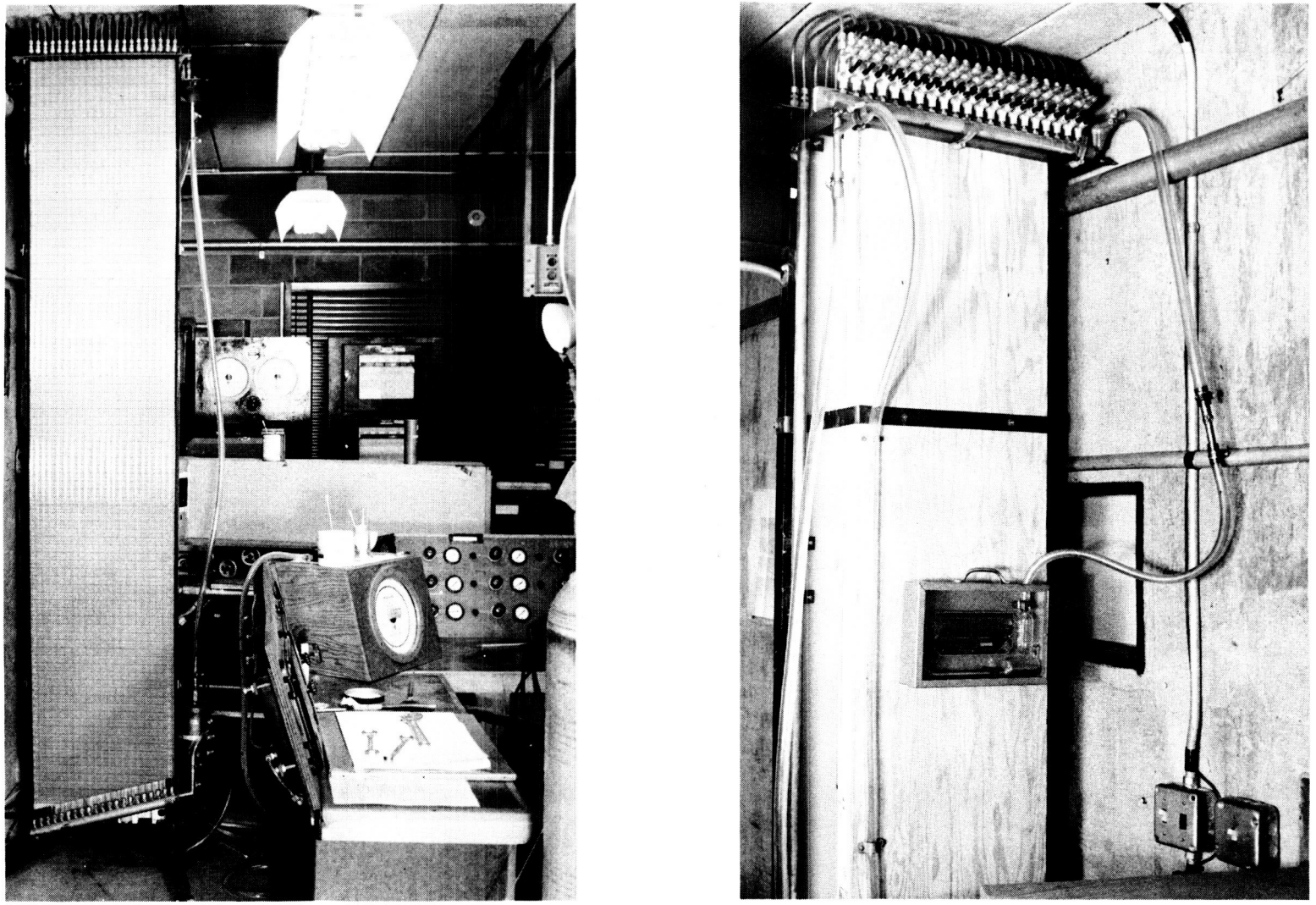

FIGURE 28. NINE FOOT PRECISION OIL MANOMETER BOARD

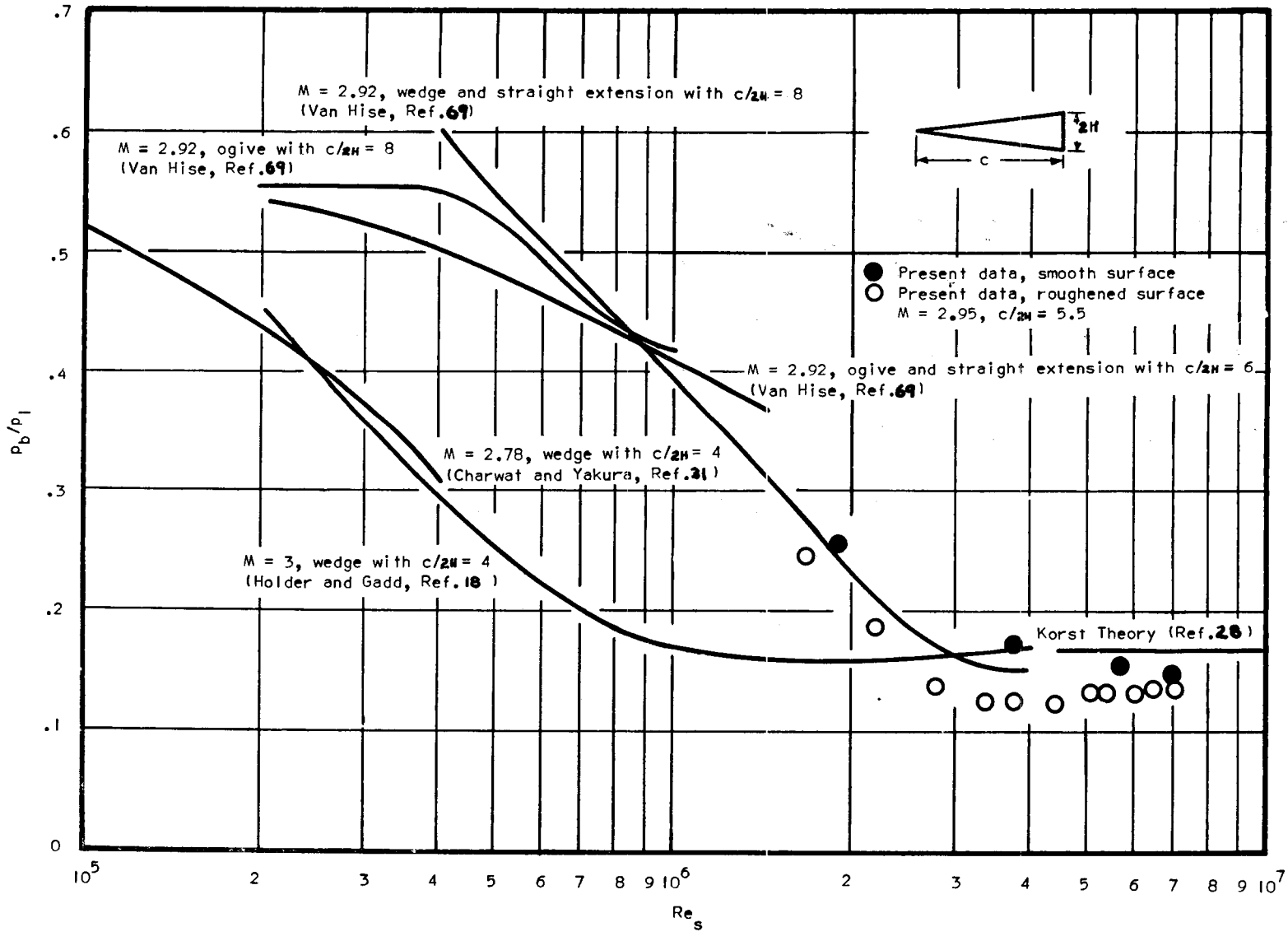

FIGURE 29. BASE PRESSURE VARIATION WITH REYNOLDS NUMBER

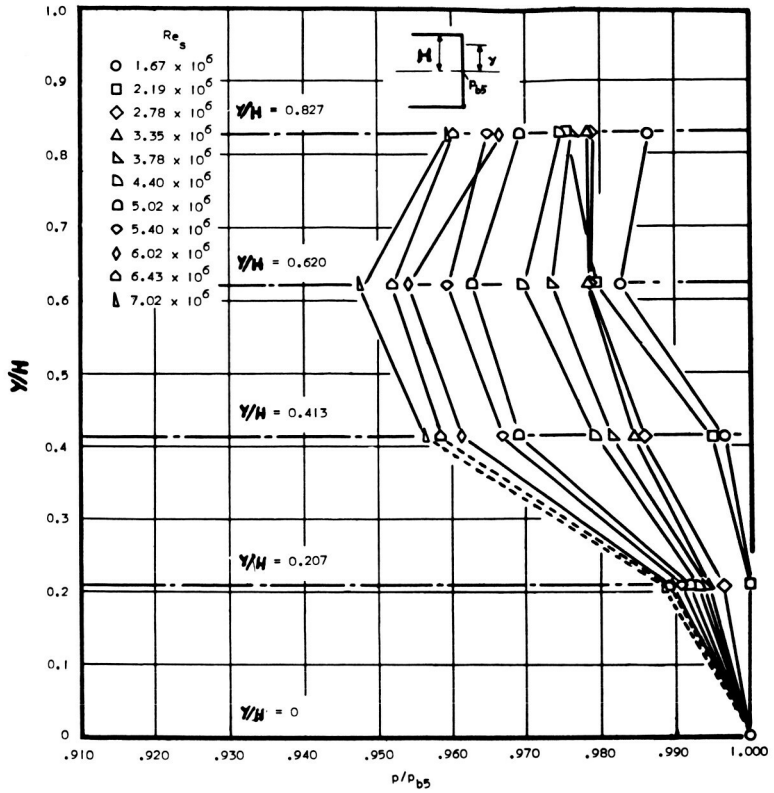

FIGURE 30. BASE PRESSURE VARIATION IN VERTICAL DIRECTION

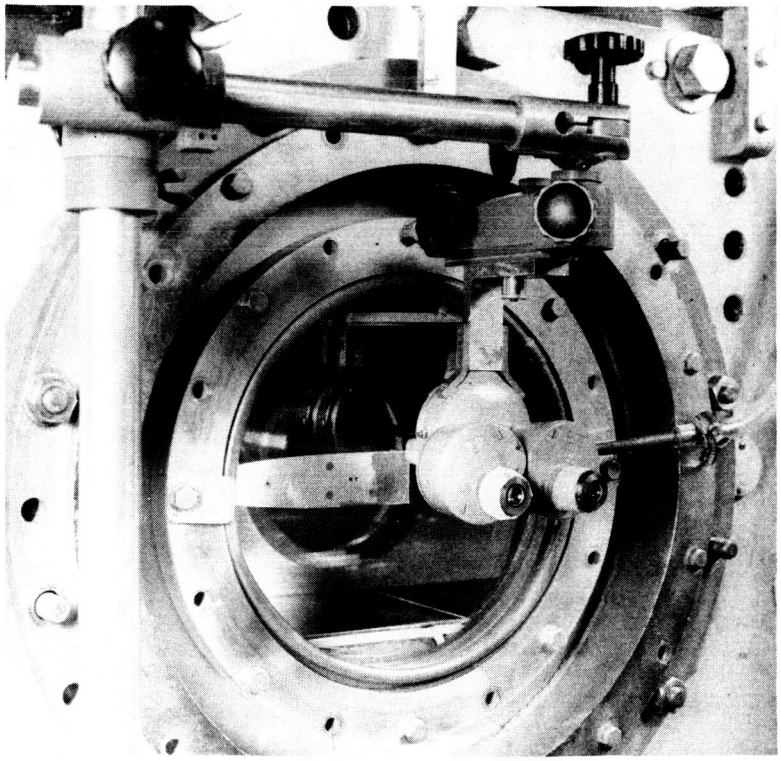

FIGURE 31. PROBE POSITIONING BINOCULAR MICROSCOPE

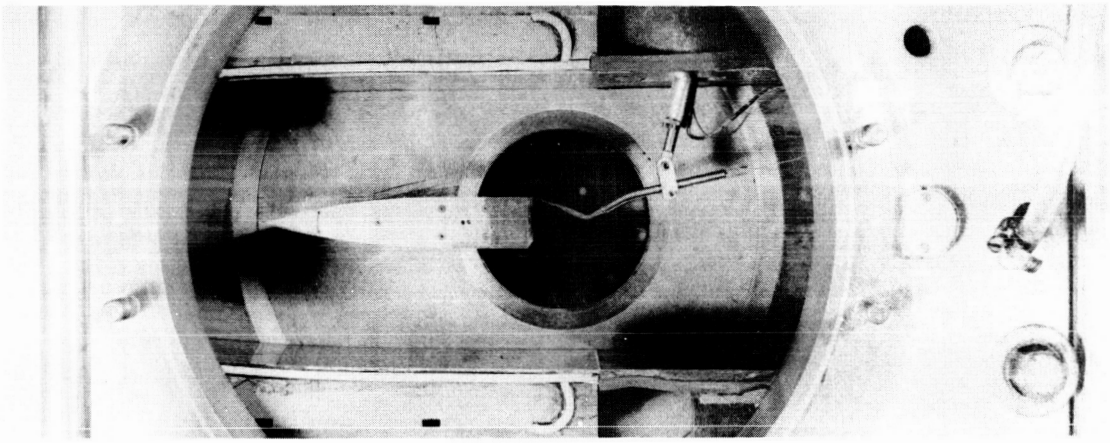

a) Installation in Tunnel

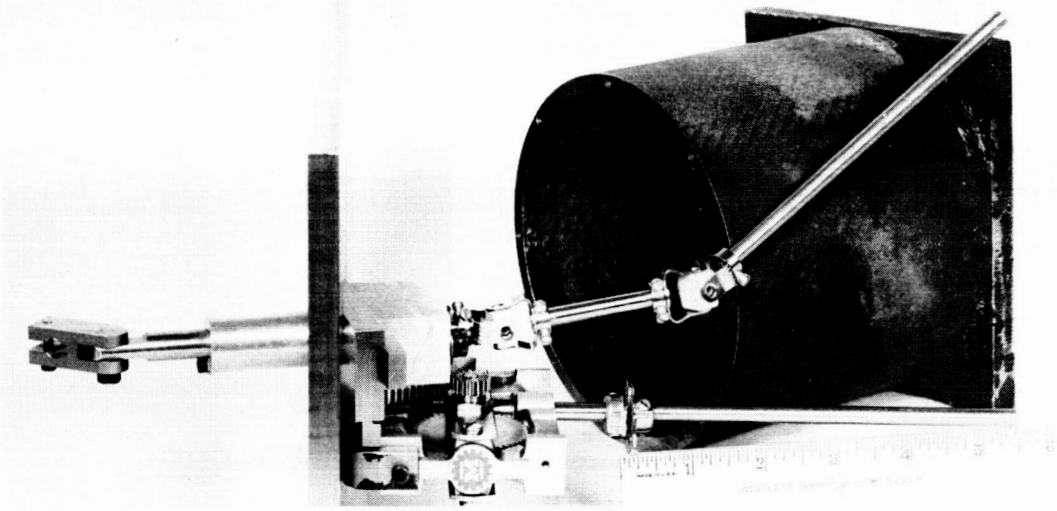

b) Details of Actuating Mechanism

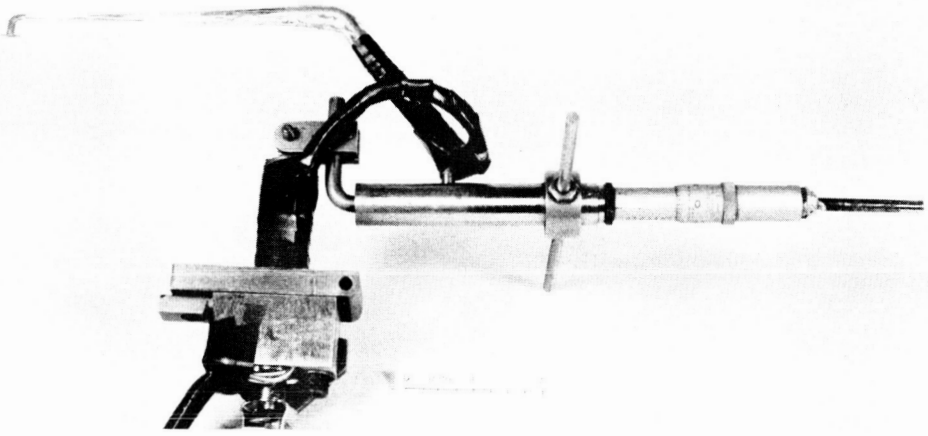

c) Longitudinal Traversing Component

FIGURE 32. PROBE POSITIONING DEVICE

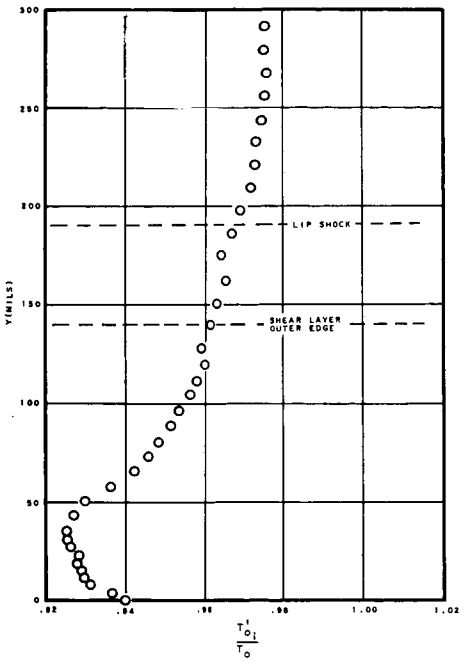

a) Uncorrected Temperature at Position 1

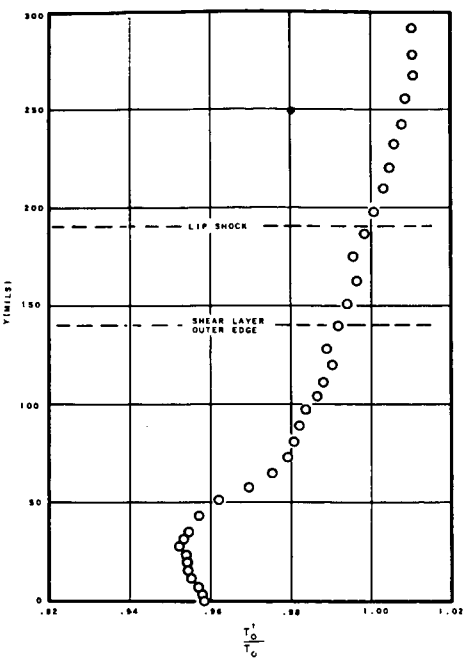

b) Corrected Temperature at Position 1

$M_1 = 2.95$
$Re_s = 6.7 \times 10^6$
$M_{2a} = 3.53$

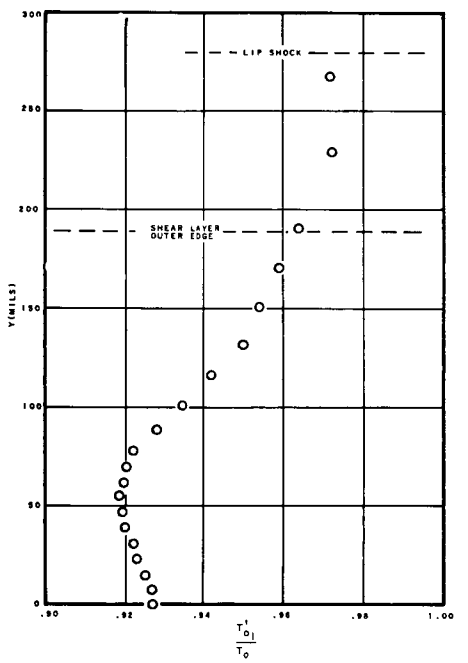

c) Uncorrected Temperature at Position 2

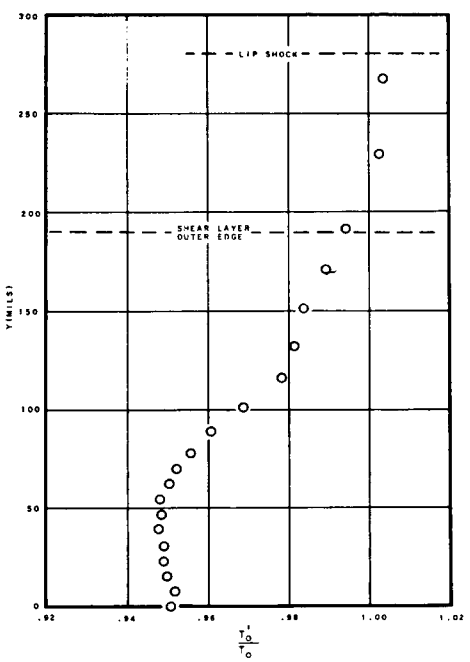

d) Corrected Temperature at Position 2

FIGURE 33. VARIATION OF TOTAL TEMPERATURE THROUGH SHEAR LAYER

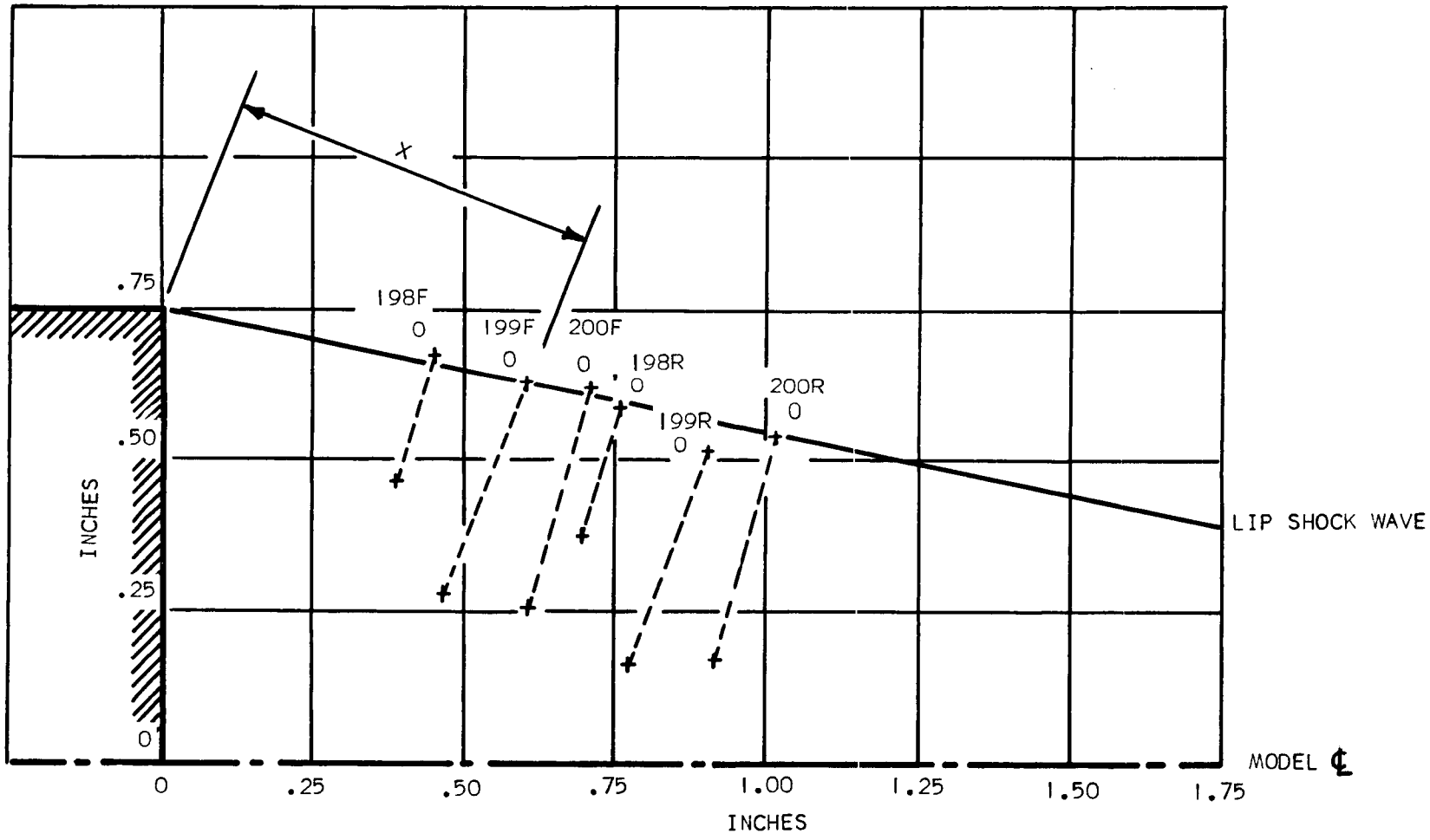

FIGURE 34. SHEAR LAYER PROBING LOCATIONS

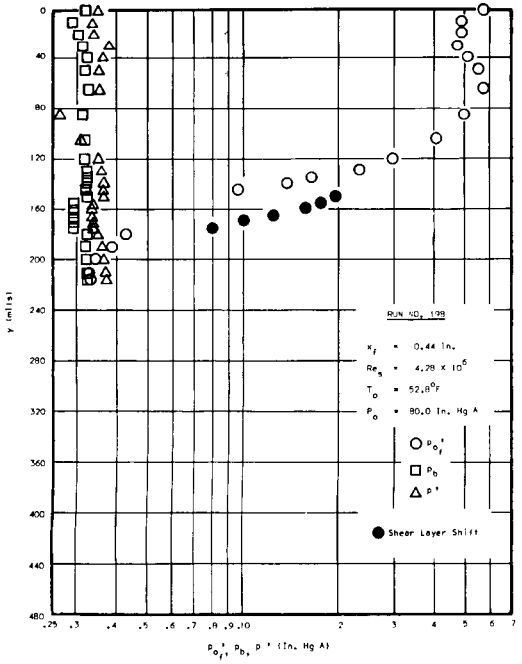

a) Forward Impact Pressure and Static Pressure (Run 198)

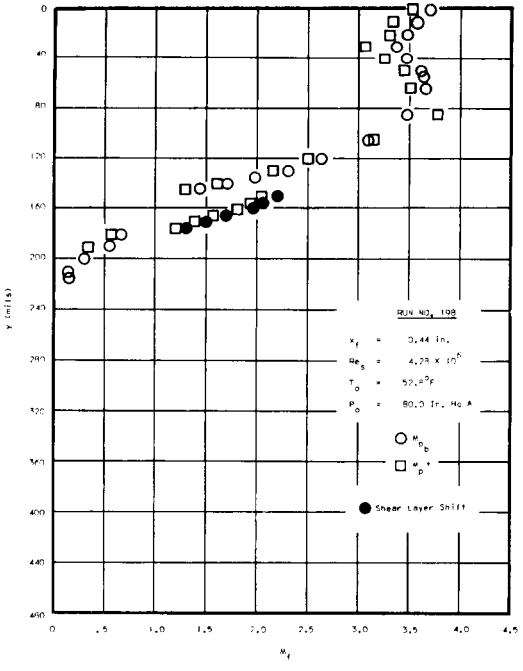

b) Forward Mach Number (Run 198)

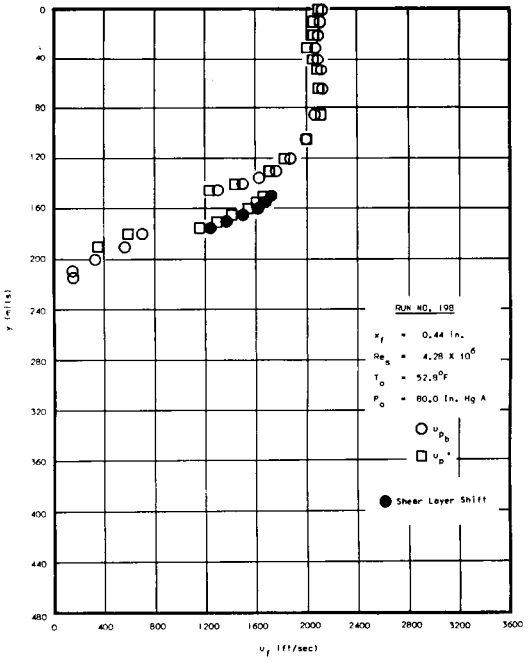

c) Forward Velocity (Run 198)

FIGURE 35. SHEAR LAYER PROBING DATA

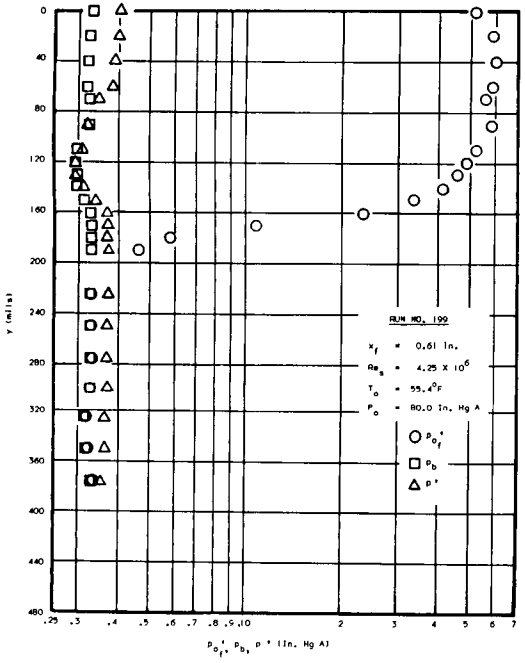

d) Forward Impact Pressure and Static Pressure (Run 199)

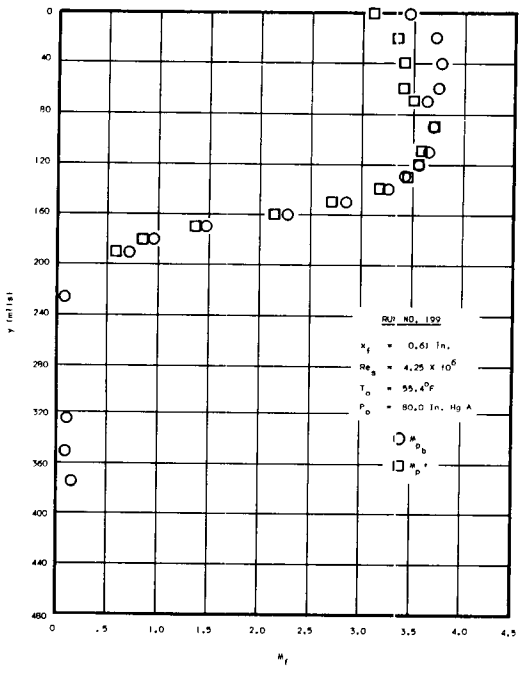

e) Forward Mach Number (Run 199)

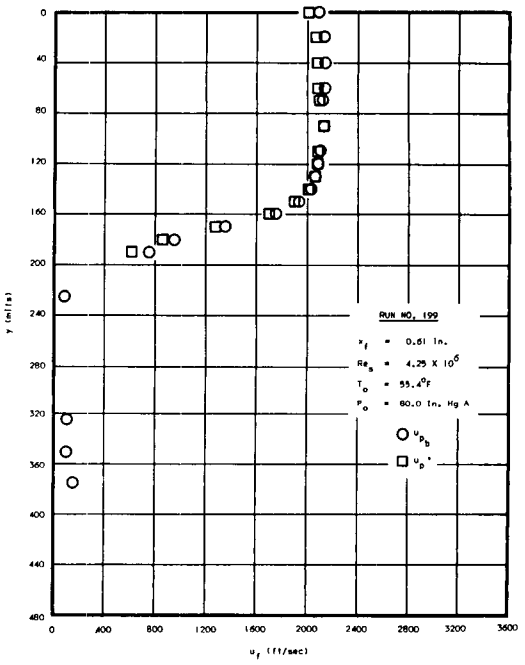

f) Forward Velocity (Run 199)

FIGURE 35. (CONT'D)

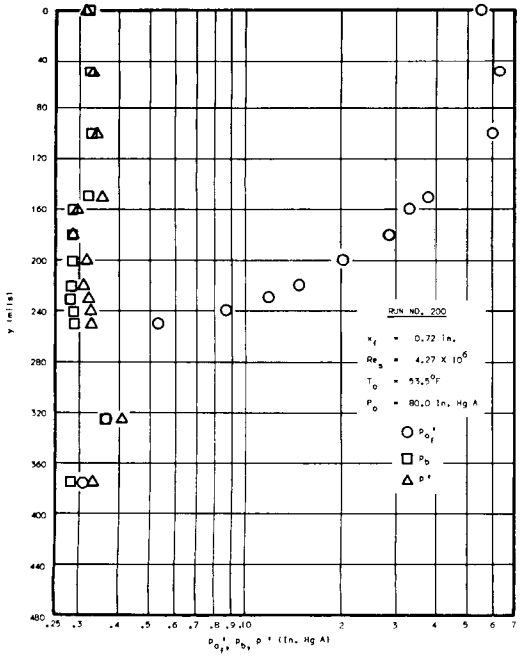

g) Forward Impact Pressure and Static Pressure (Run 200)

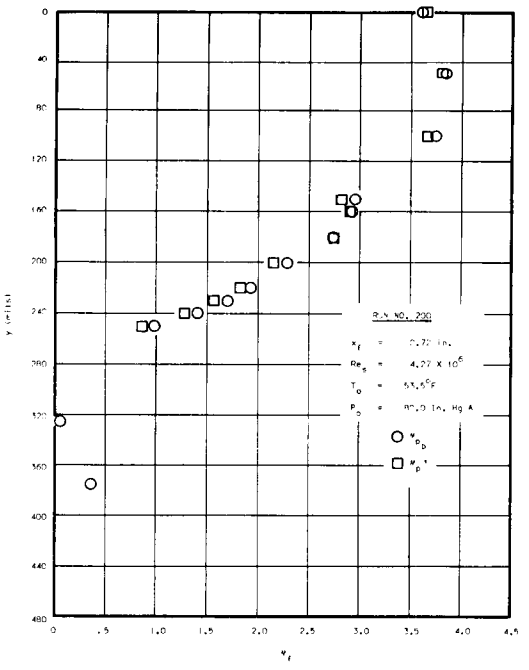

h) Forward Mach Number (Run 200)

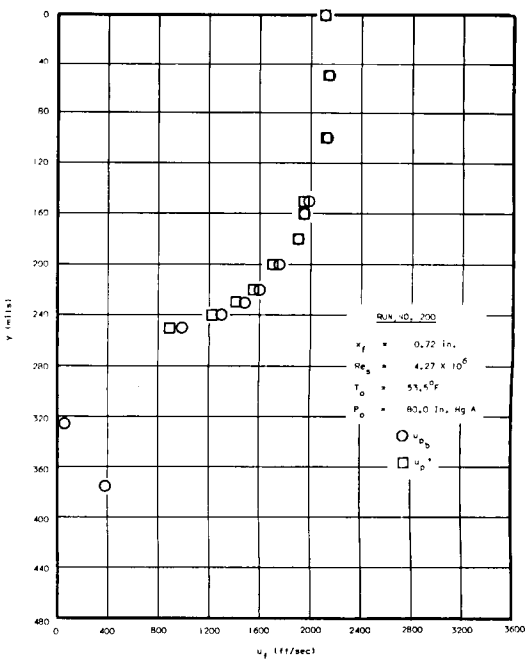

i) Forward Velocity (Run 200)

FIGURE 35. (CONT'D)

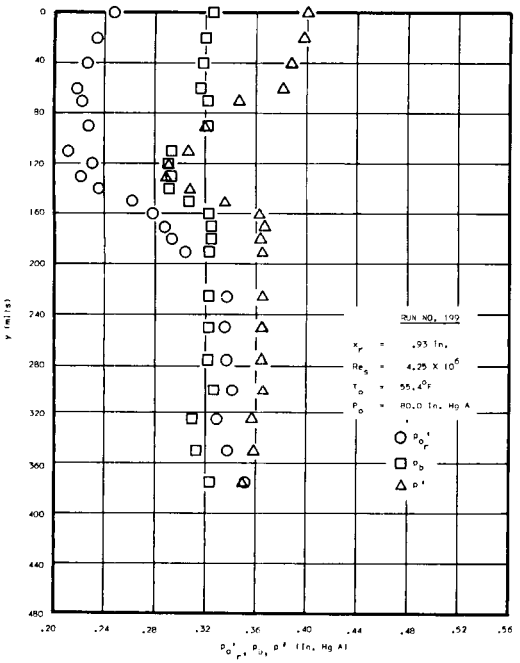

j) Rearward Impact Pressure and Static Pressure (Run 199)

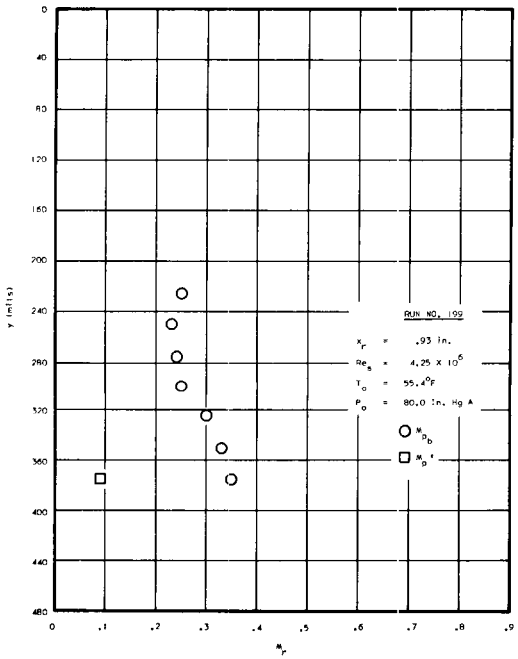

k) Rearward Mach Number (Run 199)

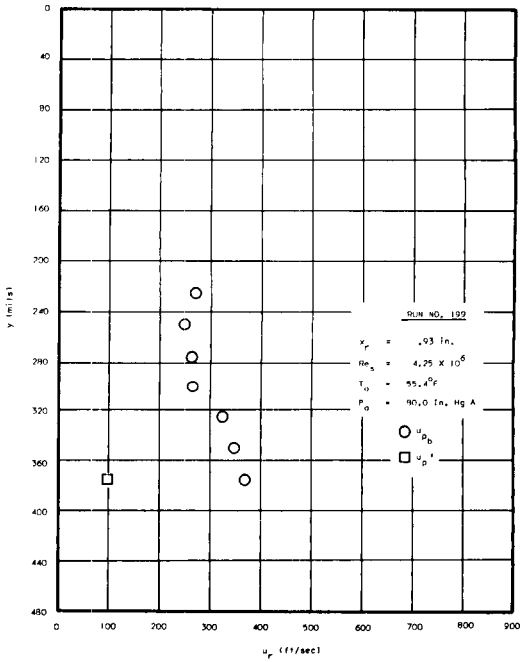

l) Rearward Velocity (Run 199)

FIGURE 35. (CONT'D)

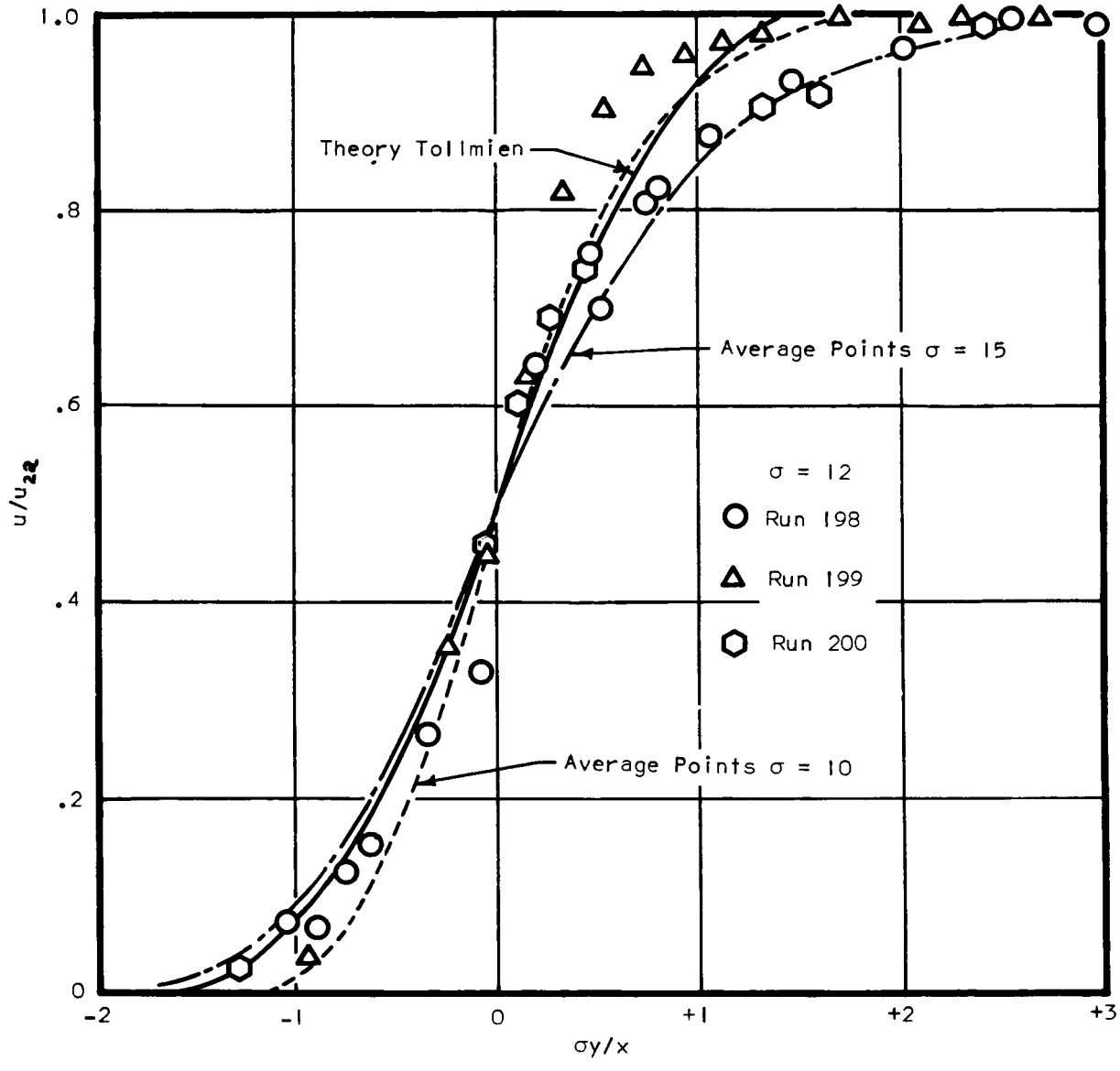

FIGURE 36. COMPARISON OF VELOCITY PROFILE DATA WITH THEORY

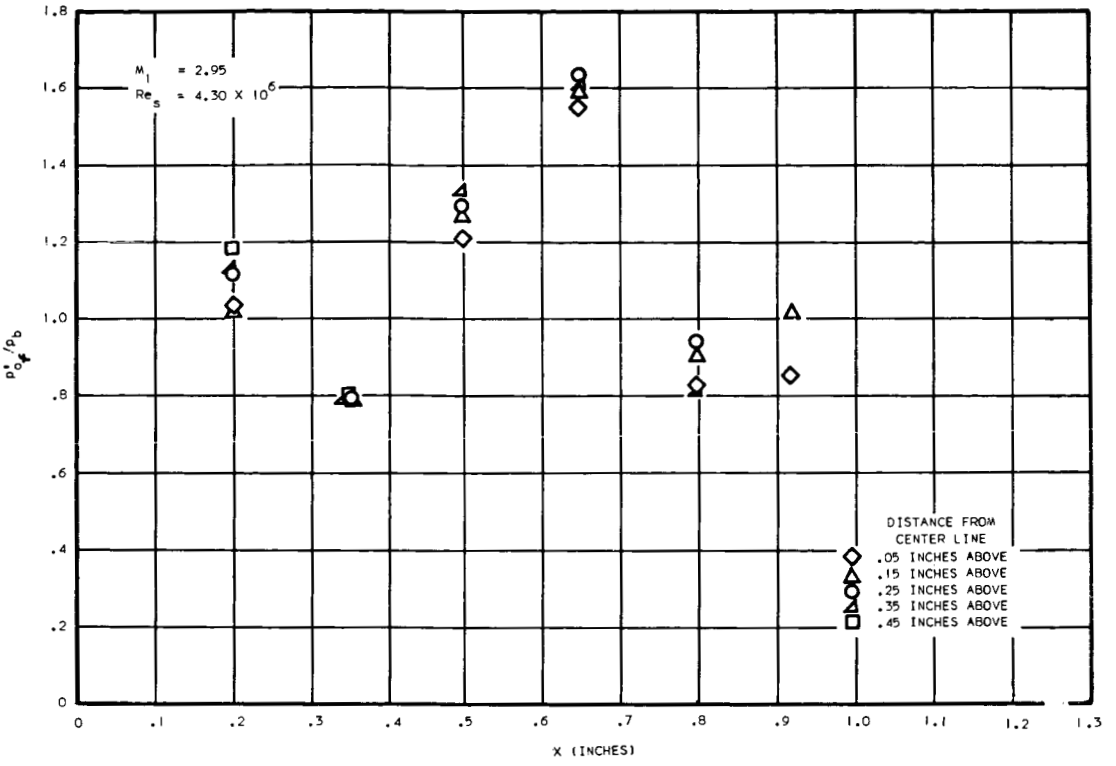

a) MEASURED WITH FORWARD-FACING PROBE

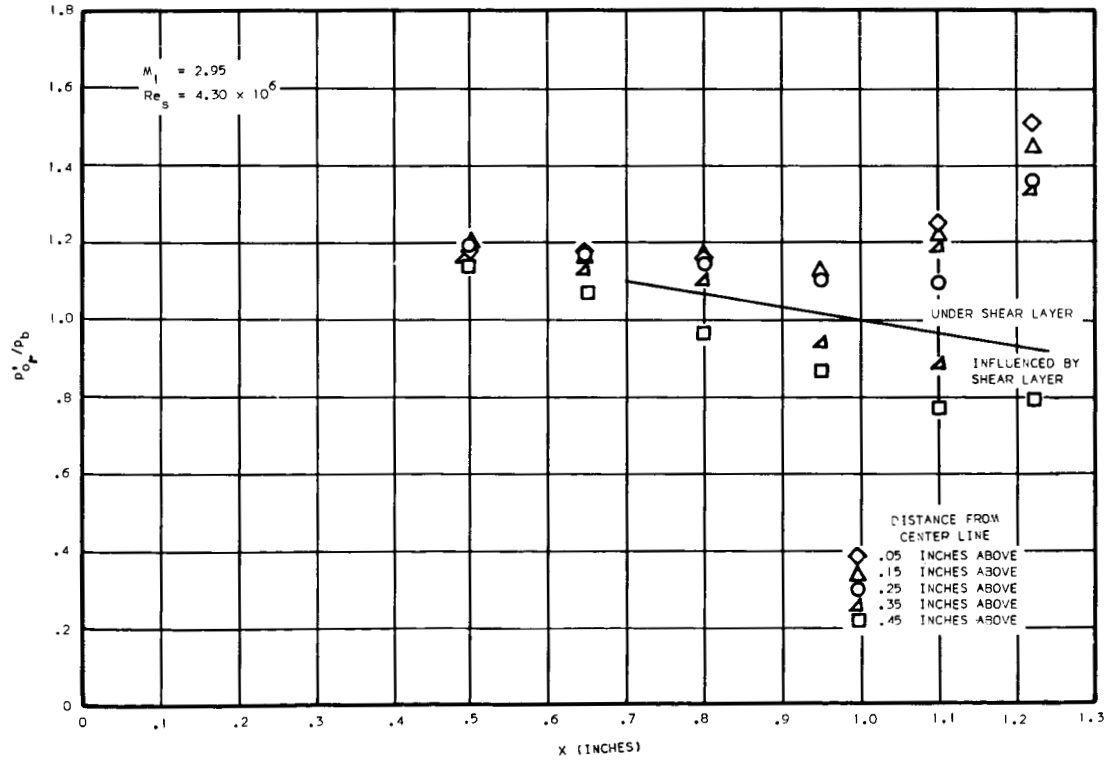

b) MEASURED WITH REARWARD-FACING PROBE

FIGURE 37. TOTAL PRESSURE VARIATION IN RECIRCULATION ZONE

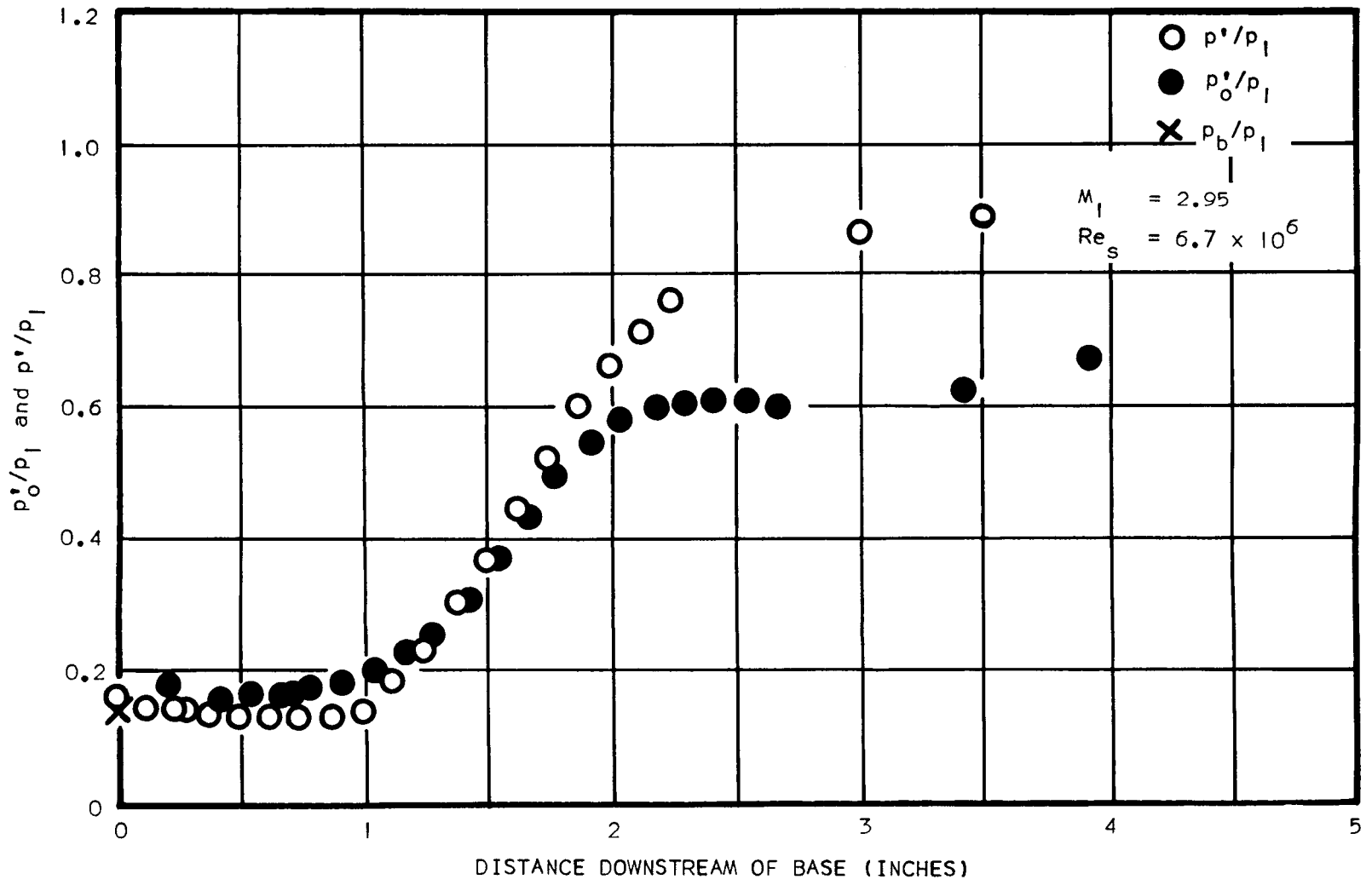

FIGURE 38. CENTERLINE STATIC AND TOTAL PRESSURE VARIATION

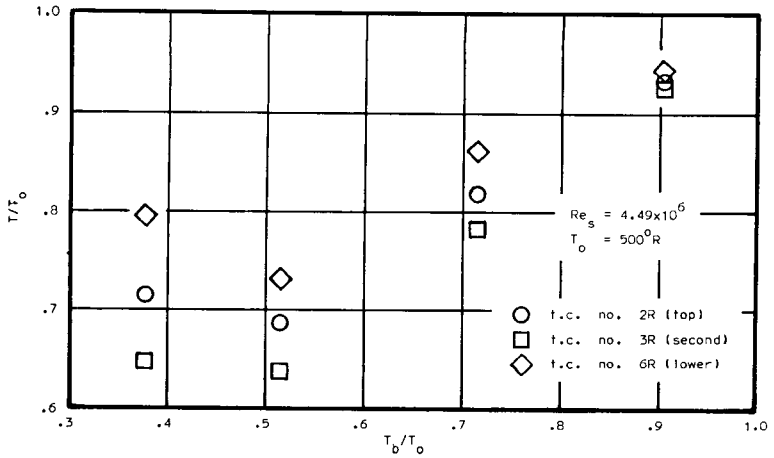

a. x = 0.010 in.

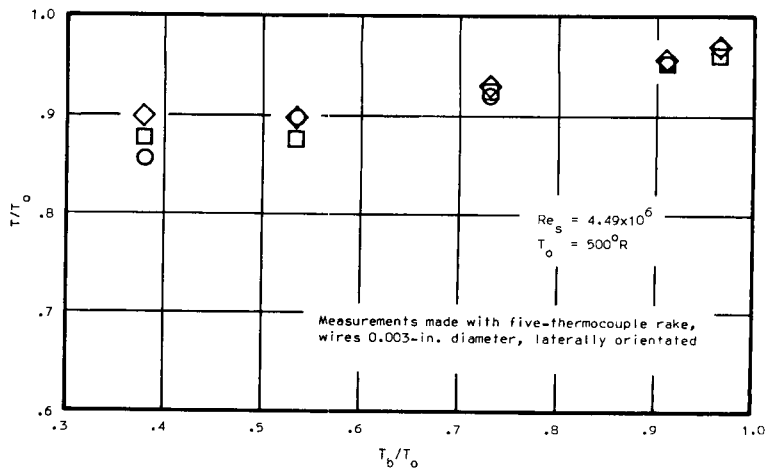

b. x = 0.250 in.

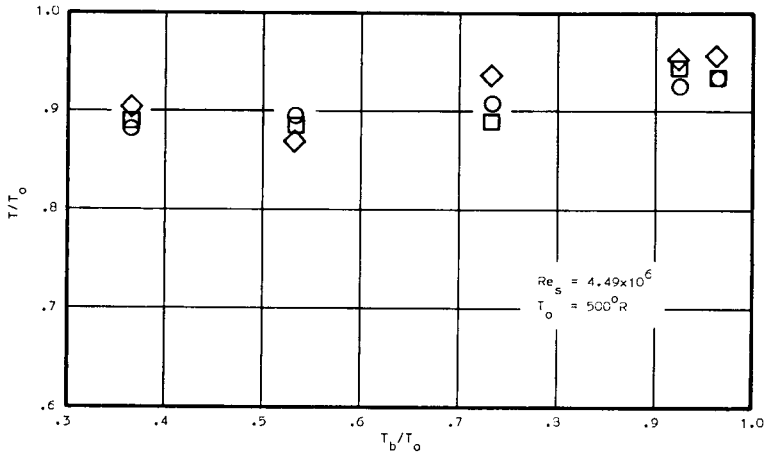

c. x = 0.500 in.

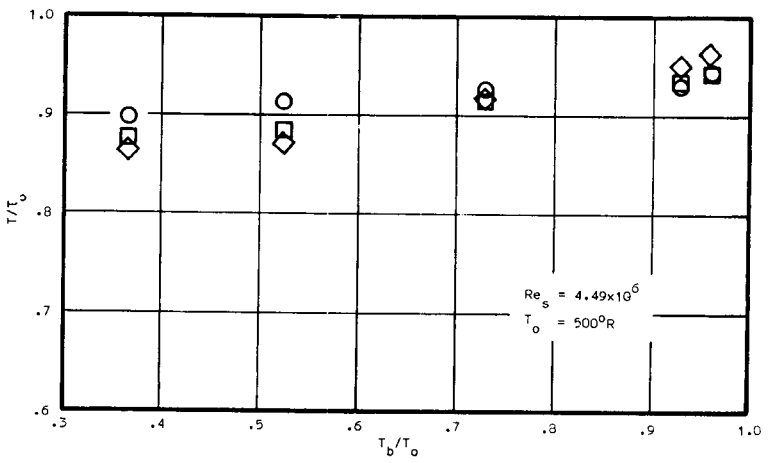

d. x = 0.750 in.

FIGURE 39. RECIRCULATION ZONE TOTAL TEMPERATURE VARIATION

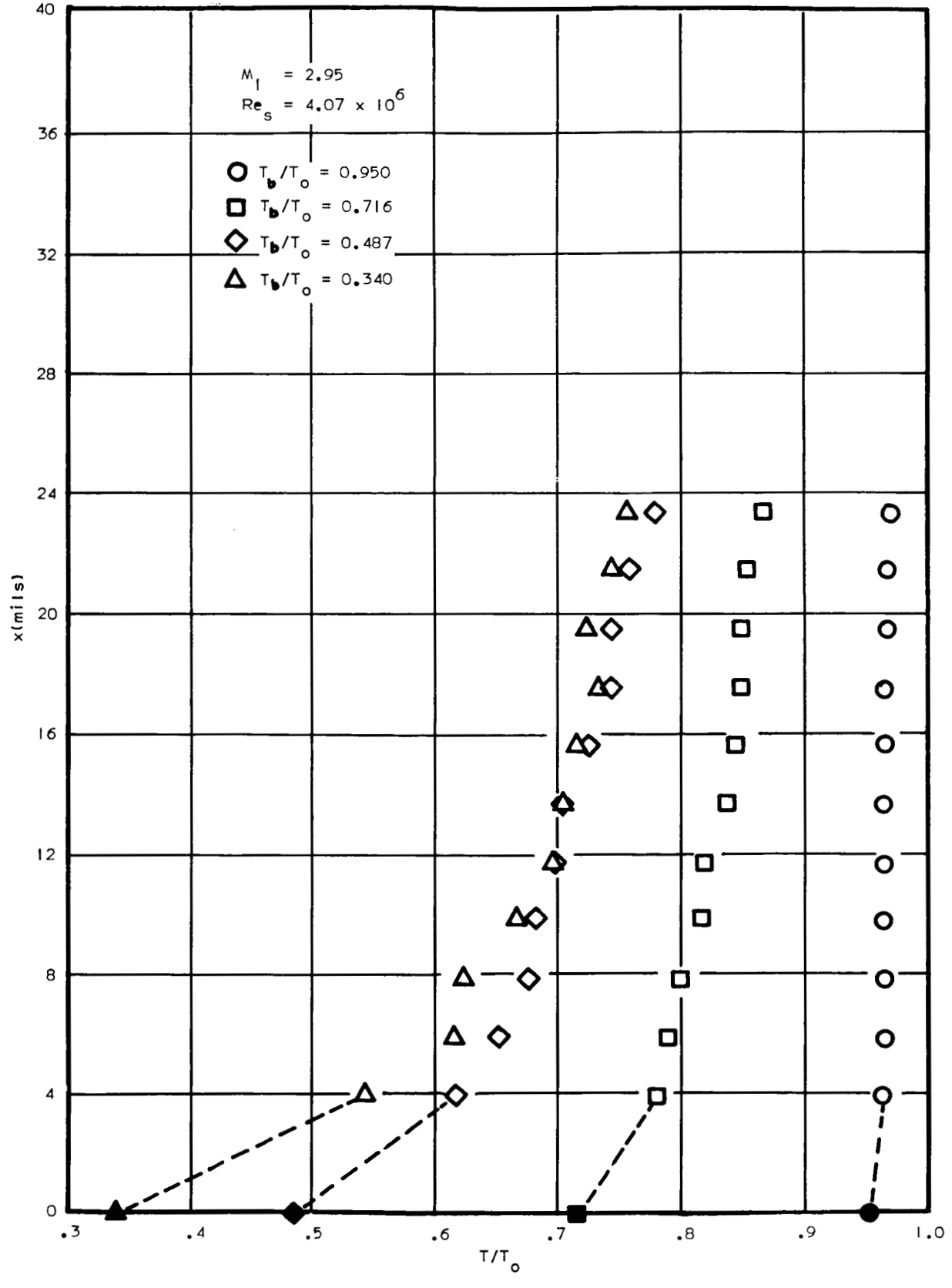

FIGURE 40. BASE THERMAL BOUNDARY LAYER DATA

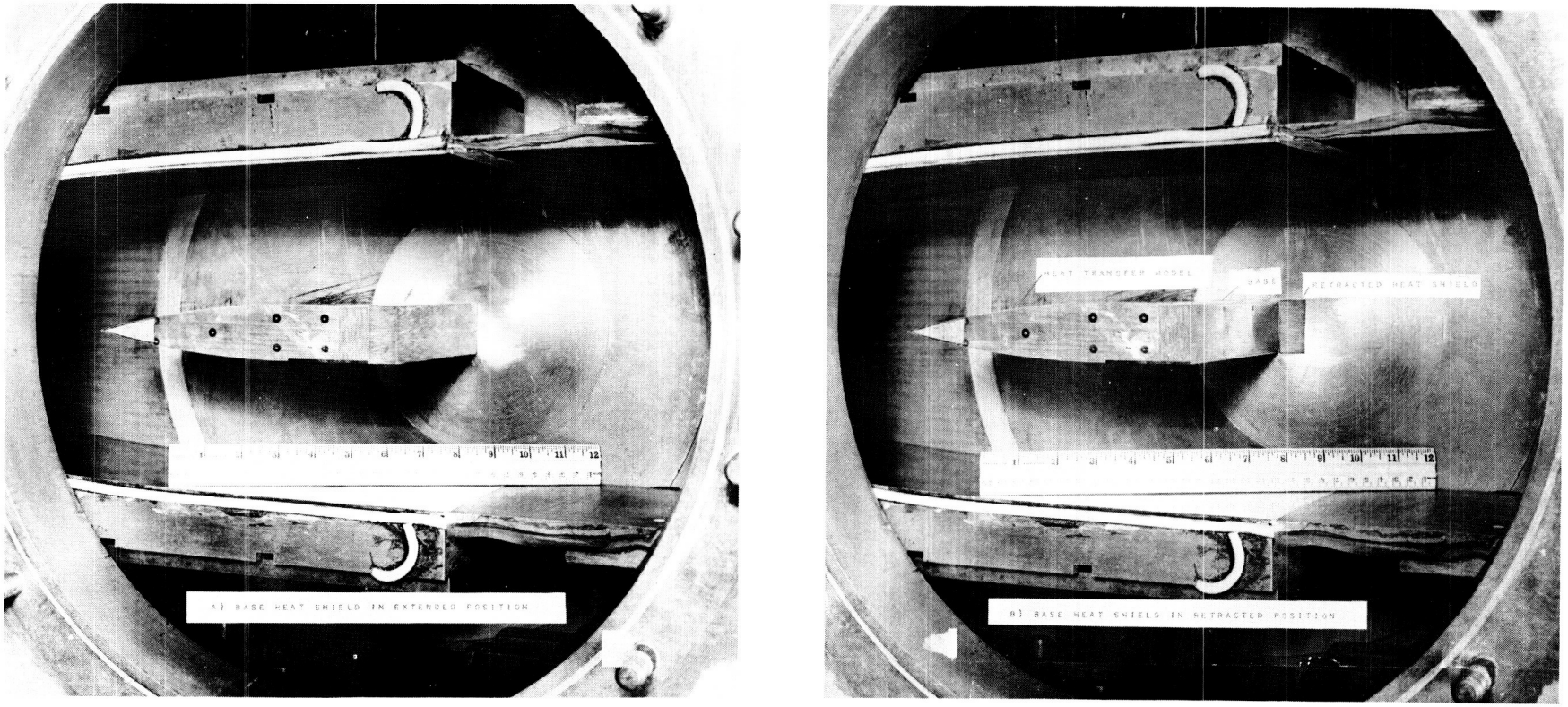

FIGURE 41. HEAT SHIELD MECHANISM

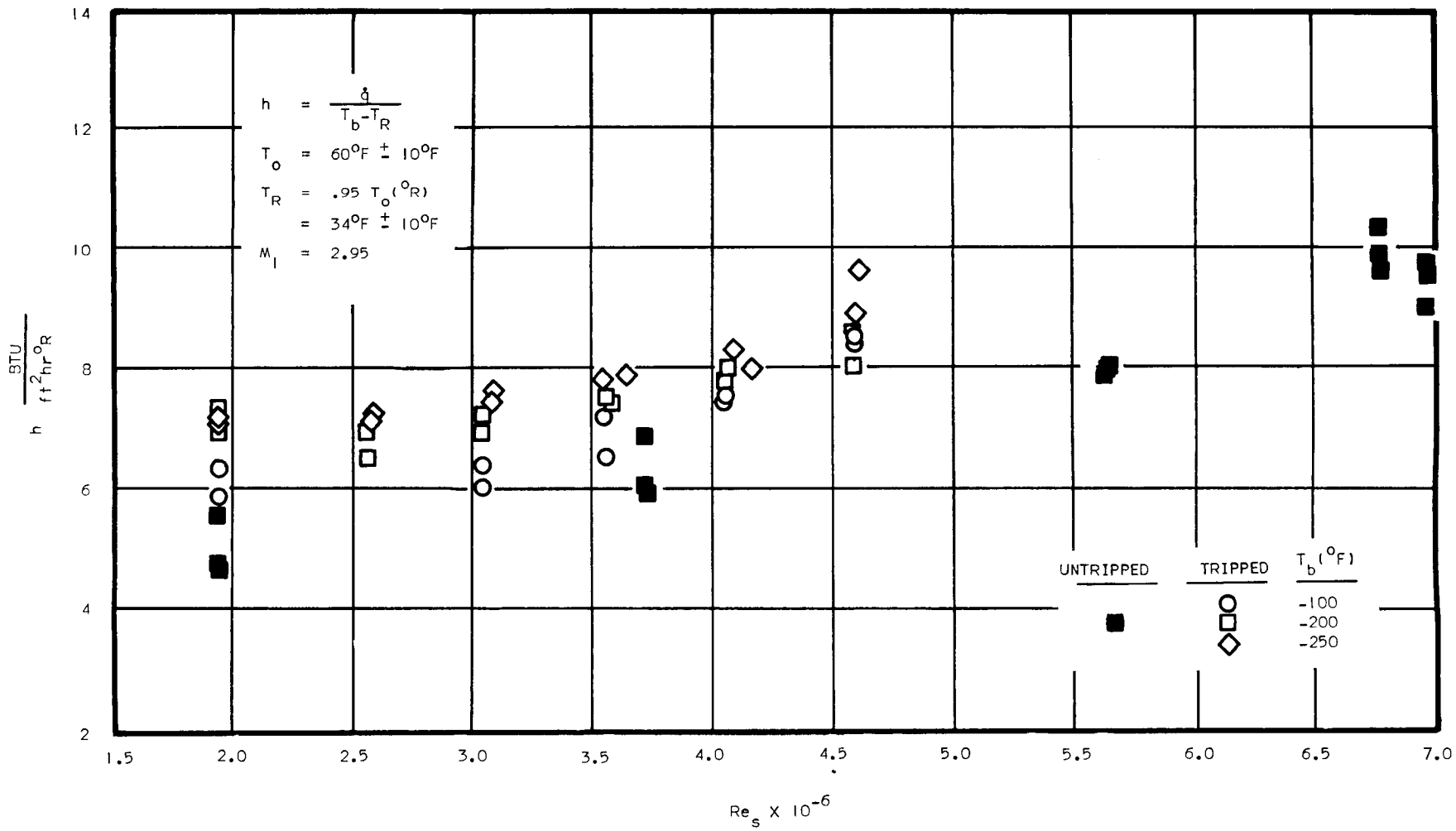

a) Base Heat Transfer Data

FIGURE 42. HEAT TRANSFER DATA

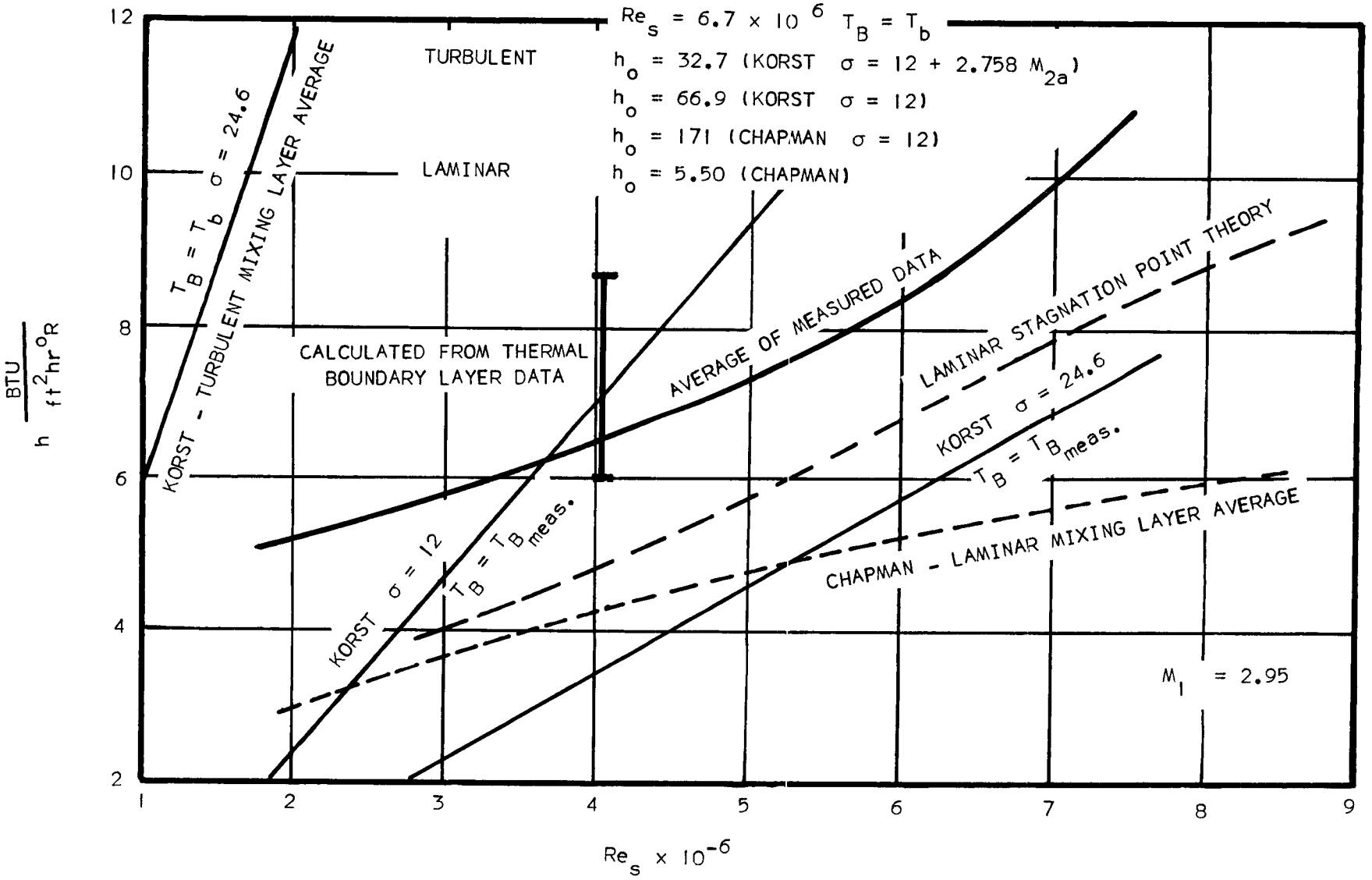

b) Comparison of All Heat Transfer Data With Theory

FIGURE 42 (CONT'D)

APPENDIX

BOUNDARY LAYER AND RECIRCULATION ZONE PROBING MEASUREMENTS

1. General Discussion of Probe Errors

In the experimental study of fluid flow phenomena it is possible to obtain information pertaining to the flow field generally by one of three methods. These methods are the following:

a. Visual observation of the flow field using optical techniques such as schlieren, shadowgraph, or interferometry.

b. Measurement of the effects experienced by a body immersed in the flow such as pressures, skin friction, or heat transfer.

c. Measurement of local flow properties using total temperature probes, total pressure probes, static probes, or hot-wire methods.

The first method does not interfere with the flow field or modify the overall flow pattern and the second will create only a minimum disturbance if proper precautions are observed. The second method supplies information which is a result of combined effects of the total flow field.

To obtain distributed information regarding the flow properties through the flow field it becomes necessary to insert probes or other measuring equipment into the flow pattern. Probing measurements, although extremely useful, are subject to more inherent errors and experimental difficulties than the first two methods. It is usually not too difficult to construct a probe which will sense any of the flow properties such as pressure, temperature, flow fluctuations, etc. To accurately interpret these measurements, however, is an entirely different matter.

For a probe to provide a meaningful measurement at any location in the flow field it is necessary that the presence of the probe does not interfere with the flow pattern. To obtain accurate profiles of flow properties through viscous layers it becomes necessary that the physical size of the probe be small compared to the layer thickness.

This is especially important when probing attached boundary layers on wind tunnel models where the thickness may be of the order of 30 mils or less.

Even if the flow is not disturbed because of small probe sizes, additional factors can influence the accuracy of the results. A very good discussion of probe errors is included in Reference 84. One large effect which can be encountered is the averaging effect which is created by the small size of the probe. The flow accelerates from zero velocity at the probe stagnation line to supersonic speeds in a small distance. This large velocity gradient creates correspondingly large gradients in pressure and temperature. It can be expected that the probe will then sense an average value due to the gradients across the probe face rather than the desired stagnation line value.

Another error encountered in probing of total pressure through viscous layers is called position error and is created by the strong gradients in flow parameters in the probe "freestream". Because of the finite size of the probe opening, it will sense not only the desired value of pressure at the stagnation line but will also be sensitive to the varying values above and below. The net result is that the indicated measurement will be an integrated value and will be a function of the pressure gradient and probe opening size.

Total temperature probes are subject to conduction errors which are created by the fact that the bottom, top, and sides of the probe are close to recovery temperature, which is a function of the local Mach number of the flow bathing the surfaces. The net result is a flow of heat away from the stagnation line, which theoretically would be at the local free stream total temperature. In addition, radiation errors can greatly influence the temperature reading, especially if the probe and environment as "seen" by the thermocouple have a large difference in temperature. In an analysis performed in Reference 84 regarding total temperature probe errors due to conduction it was found that the smaller the probe tip height the greater

would be the temperature error. It can also be reasoned that the probe structure itself should be made of a low heat conductivity material.

In summary, to present minimum disturbance to the flow it is necessary to utilize a small probe. In contrast, some of the probe errors are adversely affected by small probe size. It can be seen that some compromise has to be reached regarding probe size.

Viscosity can also play an important role in probe measurements. The usual simplifications made on the Navier-Stokes equations involve elimination of the viscous terms for many fluid flow calculations. In bluff body flow situations strong gradients exist in the flow parameters in the neighborhood of the stagnation point. For a real fluid, viscous effects are thus always present and their effect on the properties being measured must be considered. As the Reynolds number is a measure of the ratio of inertial forces to viscous forces, at low Reynolds numbers the viscous forces assume greater importance. At low Reynolds numbers (of the order of 1 to 10 based on probe half height) the effect of the viscous forces is to do work on the fluid particles moving along the stagnation streamline, which can result in measured local stagnation pressures and temperatures greater than actual reservoir conditions.

Although not investigated as thoroughly as viscous effect, Mach number could also influence probe readings. In incompressible flow, Reynolds number is the major governing similarity parameter. In compressible flow the Mach number must be considered as an additional similarity parameter. The results of several investigators including Bradfield (84) and Laufer and McClellan (85) give some insight into the magnitude of this effect for total temperature probes. In general, the effect is to lower the measured temperature as the Mach number increases. This possibly can be attributed to increase in the conduction of heat away from the junction. Using the usual definition of recovery factor and dividing the numerator and denominator

by T_o, it can be seen that as the Mach number increases, the wall recovery temperature decreases. This presents a larger temperature potential for possible heat flow from the junction to the colder probe surfaces.

2. Probe Calibration

The effects of viscosity and Mach number on impact temperature were investigated in the small free-jet wind tunnel described in Reference 84. Figure A1a is a photograph of the probe calibration set-up and Figure A1b is a scale drawing of the tunnel. Because of their small face height (approximately 7 mils) and because the probe Reynolds number reference length is usually taken as one half the probe height, it was necessary to calibrate the total temperature probes to determine their sensitivity to low Reynolds numbers. Another factor which necessitated their calibration was the influence of conduction and radiation of the probe recovery factor.

The probes were tested in two nozzles with nominal Mach numbers of 1.9 and 3.2. The unit Reynolds number was changed by varying the stagnation pressure from 0.4 cm Hga to approximately 250 cm Hga. At the extremely low pressures the nozzle boundary layer growths were sufficient to reduce the actual Mach number for each nozzle to about 1.4. To determine the variation in nozzle Mach number with stagnation pressure, i.e., Reynolds number, both nozzles were calibrated with a 1/16-in. diameter total pressure probe located at different positions with respect to the nozzle exit. This probe, because of its rather large diameter, is relatively insensitive to Reynolds number effects. The Mach number so calculated was then used to interpret the calibration data for the other Mach number sensitive probes. The Mach number 1.9 nozzle did not suffer an appreciable decrease in Mach number until a stagnation pressure of 15 cm Hga was reached. At this point the Mach number had dropped to 1.8. At lower stagnation pressures the Mach number dropped very rapidly, reaching a minimum of 1.4. The other nozzle reached a Mach number of 3.05 at the same stagnation pressure and then also suffered a decrease to 1.4 very rapidly.

The calibration data for the impact pressure and temperature probes are plotted versus the probe Reynolds number evaluated after the shock wave while the static probe calibration Reynolds number is evaluated at free stream conditions.

Data for the impact temperature probe are presented on Figure A2 along with results of Bradfield (84) for comparison. These results show that the largest error in temperature occurs at a Reynolds number of around 100 and as the Reynolds number is increased the impact temperature measured by the probe also increases. At high Reynolds numbers the increased convective heat transfer to the probe face overrides the conduction and radiation errors, resulting in an increasing total temperature ratio. As the Reynolds number is reduced below 100 the total temperature ratio again starts to rise. This happens because the effects of convection, conduction, and radiation are soon dominated by the viscous influence. As shown in Figure A2, as the Reynolds number decreases below 10 the impact temperature actually rises above the local total temperature.

In addition to viscous effects, other factors which influence the measured temperature such as Mach number, probe size, thermocouple material, and probe coating materials can be seen in Figure A2. The Mach number effect is easily discernible at $R^{r}_{h/2} > 10$ but for lower Reynolds numbers the two curves merge. This is because of viscous effects on the nozzles which lower the Mach numbers. The Reynolds numbers are evaluated at the existing Mach number so actually the two curves merge to become one. The effect of probe size is not proven by Figure A2 because the 4-mil, cemented, iron-constantan probe and the 7-mil, uncemented, copper-constantan probe calibrations of Bradfield both lie above the 7-mil, cemented, iron-constantan probe calibration. It appears that thermocouple materials and probe construction methods, due to their large influence on conduction errors, override the effect of probe size. The "bump" in the Mach 3.05 data was found to be reproducible but cannot be explained.

In general, it can be stated that coatings and high-conductivity thermocouple materials lower the probe recovery factor. In the Mach number range investigated, increasing Mach number also has this same effect. The exact effect of probe size is very difficult to isolate from the other factors because of small variances in probe construction, which can greatly influence the probe performance.

3. Probe Construction

3.1 Shear Layer and Boundary Layer Temperature Probes

The miniature total temperature probes used in this investigation were patterned after probes conceived in Reference 84, and were made of yellow birchwood toothpicks. Wood was selected because of its unique combination of insulating properties, strength, and machinability.

The front face dimensions of the turbulent boundary layer and shear layer probes were 7-mils x 50-mils while the base boundary layer probe had face dimensions of 10-mils x 90-mils. The width was increased to help reduce the wire conduction error.

A small groove was filed along the stagnation line of the face of the probe and a small pit formed at the center of the face. The probe used for the shear layer and forebody boundary layer surveys had a thermocouple constructed of 0.5-mil iron-constantan wire. The probe used for measurements on the model base had a 3-mil copper-constantan juction. The junction was placed in the small pit and the lead wires were placed in the slot on the stagnation line. The wires were then led off around the face of the probe along the sides and then soldered to larger diameter extension wire. Figure A3 shows a photograph and a scale drawing of the face of one of these probes.

A thin coating of radio cement was applied over the face, top, and sides of the probe. This was done to increase the structural strength and to help protect the fine thermocouple junction and lead wires. When a material such as radio cement is applied over the face of a probe the measured temperature decreases. This is due to the decrease in heat flow convected to the junction because of the insula-

ting barrier created by the cement. Because of the presence of small dust particles in the tunnel it was felt that this disadvantage would be counter-balanced by the expected increase in probe life. The actual probing runs made in the wind tunnel and the calibration runs made in the tiny tunnel proved this to be true, as not a single probe failure was experienced.

3.2 Recirculation Zone Temperature Rake

Measurements of total temperature in the recirculation zone were made using a rake having five bare wire iron-constantan thermocouples of 3-mil diameter. The rake was inserted from the sidewall using a special positioning mechanism and could be moved during operation of the tunnel. Figure A4 shows the rake in position behind the model.

3.3 Impact Pressure Probes

The impact pressure probes used were of two major configurations. The first shear layer probe was made of 1/32-in. diameter stainless steel tubing with the end flattened and finished to a face height of 4-mils and width of 25-mils.

The shear layer probe used later was double faced with both forward facing and rearward facing tubes with a static pressure orifice. It also was constructed of 1/32-in. diameter stainless steel tubing and the face dimensions were 15-mils by 20-mils. This probe is shown in Figure A6, which also shows temperature, static, and pressure probes on a common holder used for the first shear layer measurements (see also Figure 26). Shown also in Figure A6 is the combination temperature and pressure probe used for probing the forebody boundary layer. Figure A5 shows this probe in position and Figure A7 shows schlieren flow photographs with the various probes inserted in the flow field.

3.4 Recirculation Zone Impact Pressure Probe

For measuring impact pressures in the recirculation zone a forward-rearward facing total pressure probe similar to the second shear layer

probe was constructed. It also had a center static tap and was made of 1/32-in. diameter stainless steel tubing soldered to a 1/8-in. diameter steel extension (Figure A6). Shown also in this figure is an early version of this probe which created considerable flow disturbance. Schlieren flow photographs of both probes are shown in Figure A7.

3.5 Centerline Pressure Probe

Centerline data were obtained using a combination pitot-static tube. It was composed of 1/16-in. diameter steel tubing with a 1/32-in. diameter brass tube running along the inside. Four static orifices of 12-mil diameter were drilled through the 1/16-in. tubing at a distance of 7/16-in. from the nose of the probe. The small tube was inserted coaxially into the large one and the ends soldered together and finished to the usual pitot tube shape. In this manner the total pressure was measured by the 1/32-in. tubing and the static pressure was contained between the two tubings.

A hole was drilled into the base of the model on the centerline at a distance of 1 inch from the vertical center. The pitot-static probe extension tubing was then passed through the coolant line to the exterior of the tunnel. A special fitting was used to channel off the proper pressures. Figure A8 shows a photograph of the pitot-static probe installation on the model.

4. Summary of Probe Interference Effects

Evaluation of the probing data shows that various degrees of flow interference are created by the presentation of different probe configurations to the flow field.

The major methods of probe insertion were: insertion parallel to the shear layers from the external flow field, insertion longitudinal through the wake throat, vertical insertion from the external flow field, longitudinal insertion from the base, and insertion from the side wall.

A summary of the errors in base pressure and associated disruption of the flow field created by the various probing configurations is presented in Figure A9. Figure A10 shows some of the probing locations.

In general, it was found that probings of the boundary layer and longitudinal insertions from the base or through the wake throat resulted in negligible errors in base pressure and minimum disturbance of the base flow field. The largest error occurred when inserting the probe from the side wall.

Figure A7 shows schlieren photographs of the various probes inserted into the flow field.

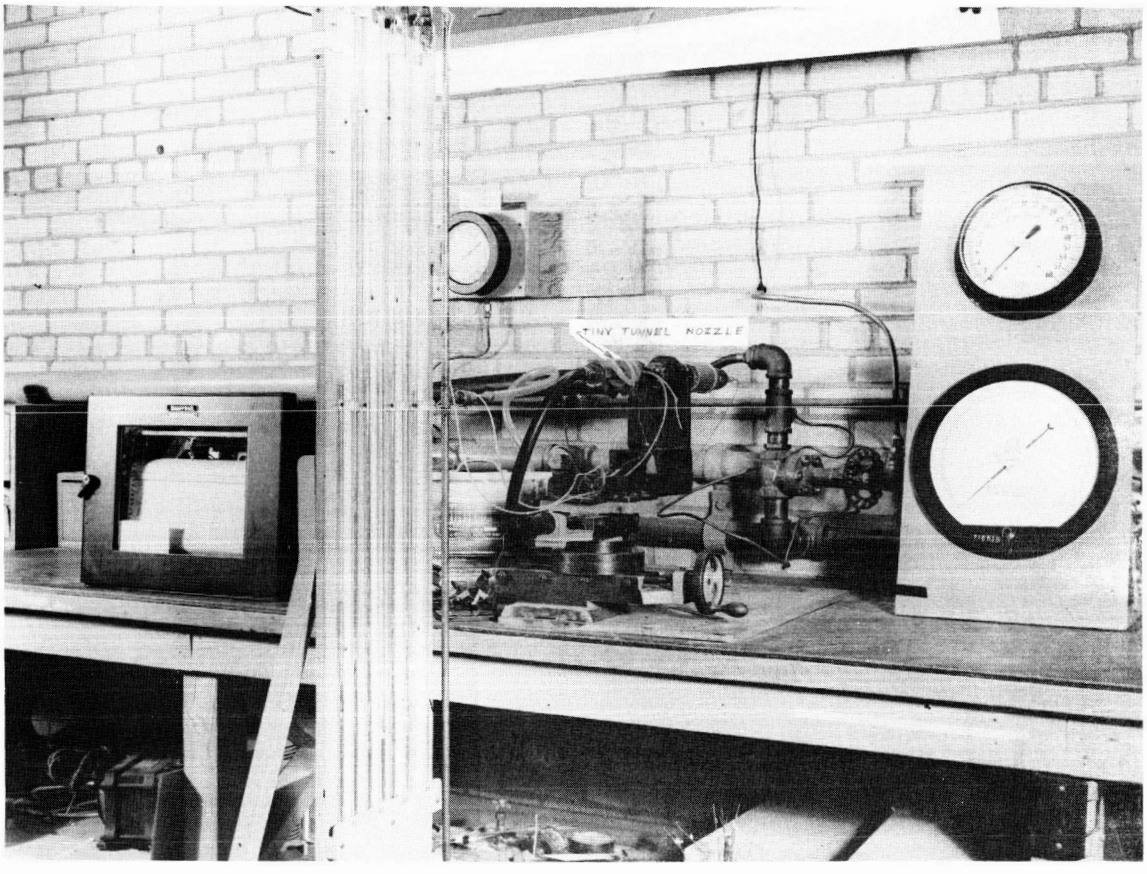

a) Calibration Set up

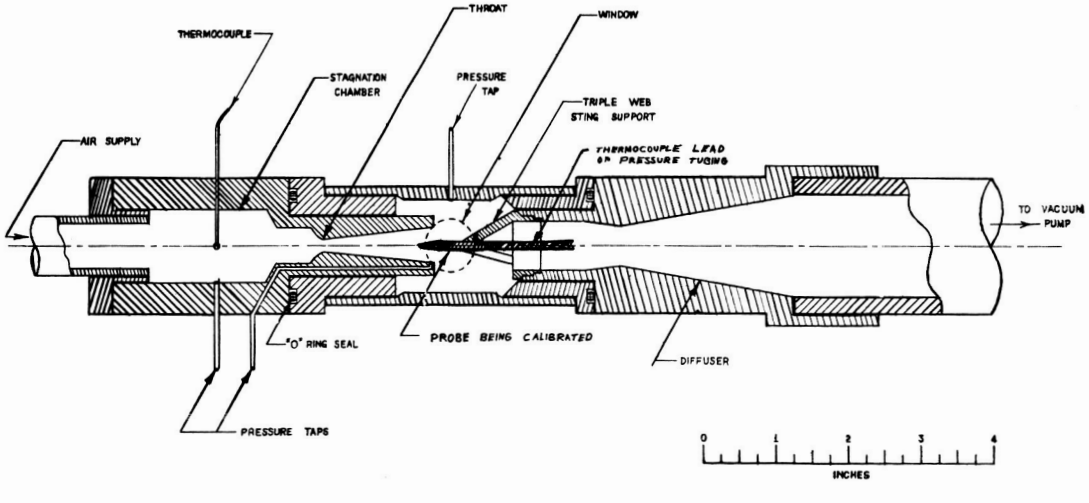

b) Drawing of Tunnel

FIGURE A1. PROBE CALIBRATION EQUIPMENT

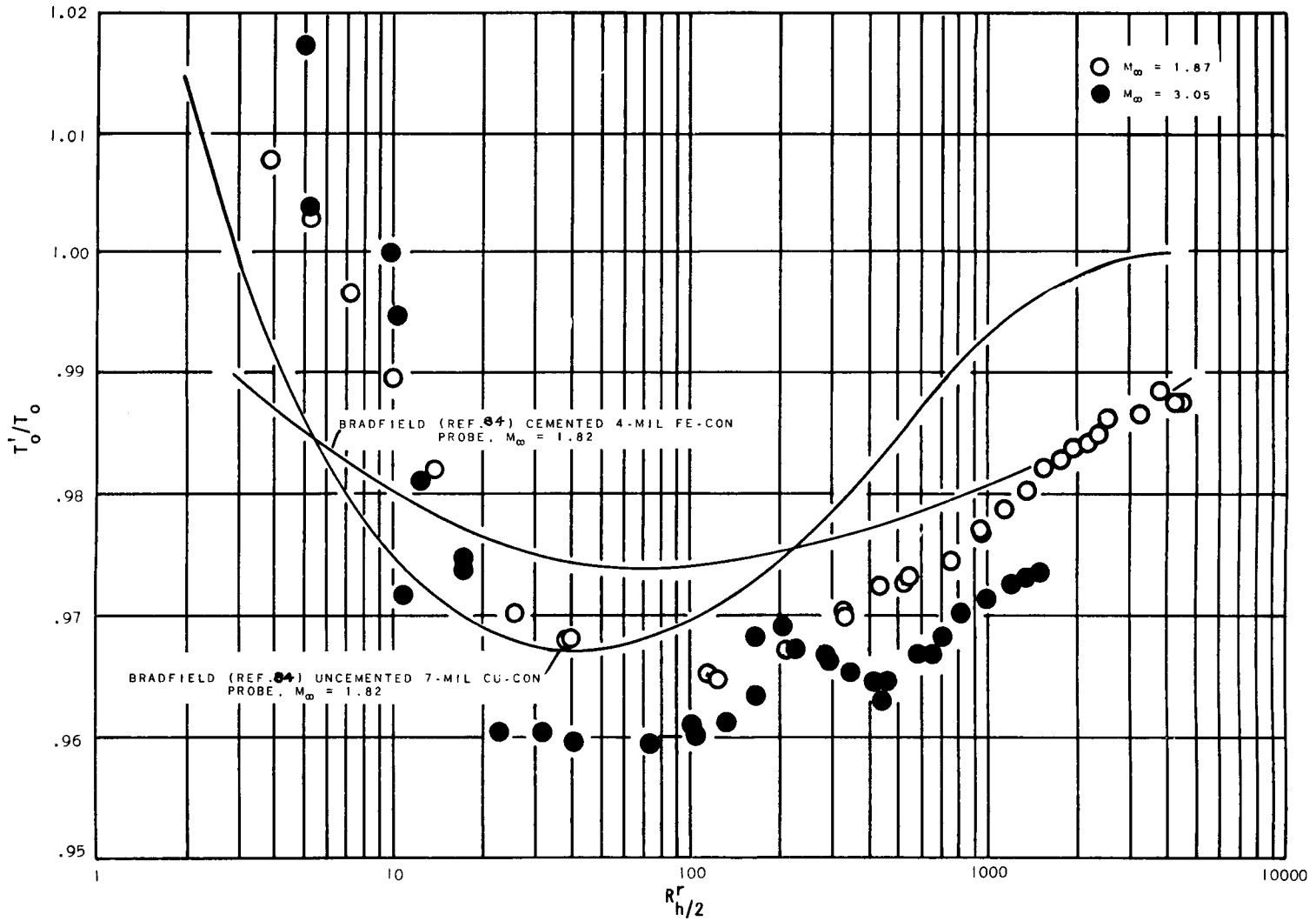

FIGURE A2. TOTAL TEMPERATURE PROBE CALIBRATION DATA

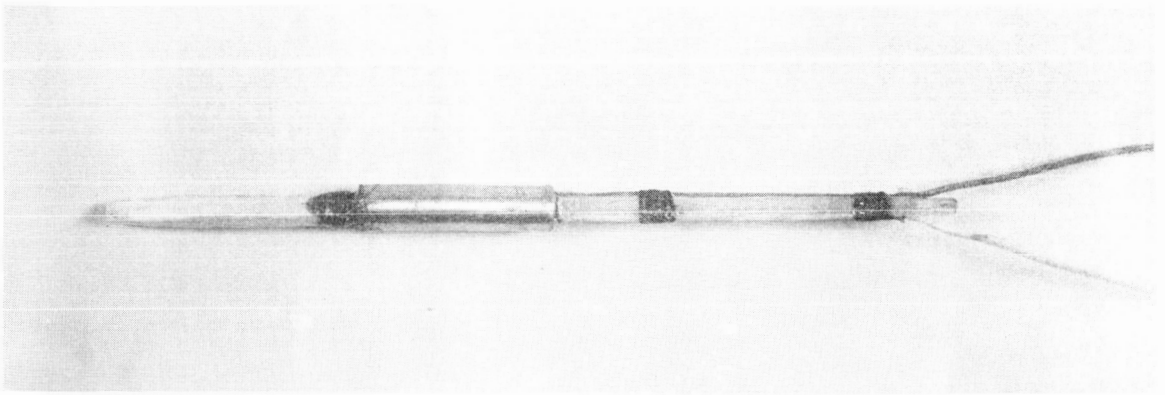

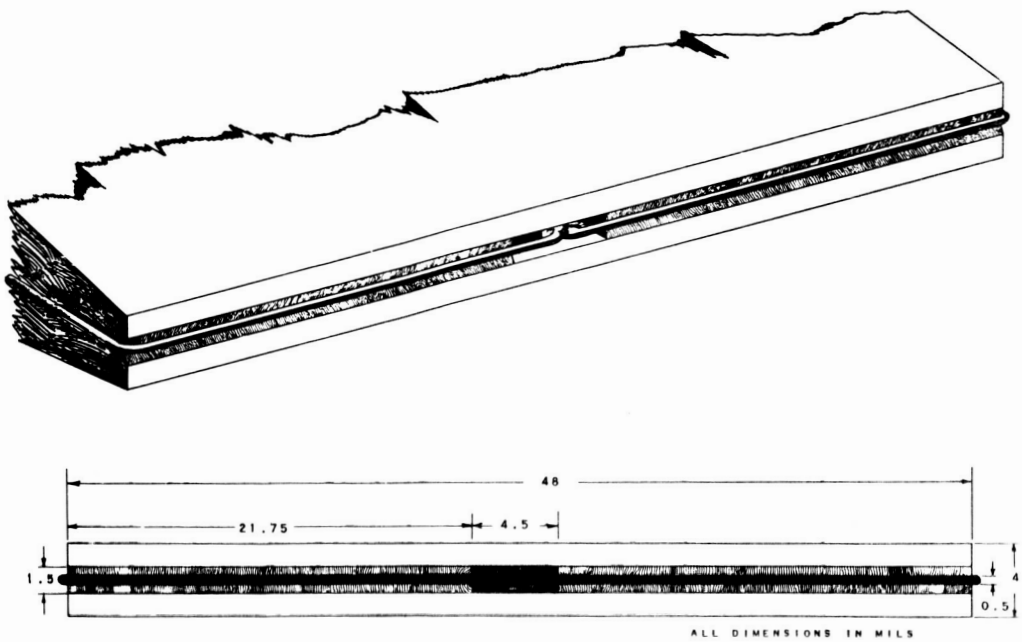

FIGURE A3. TOTAL TEMPERATURE PROBE

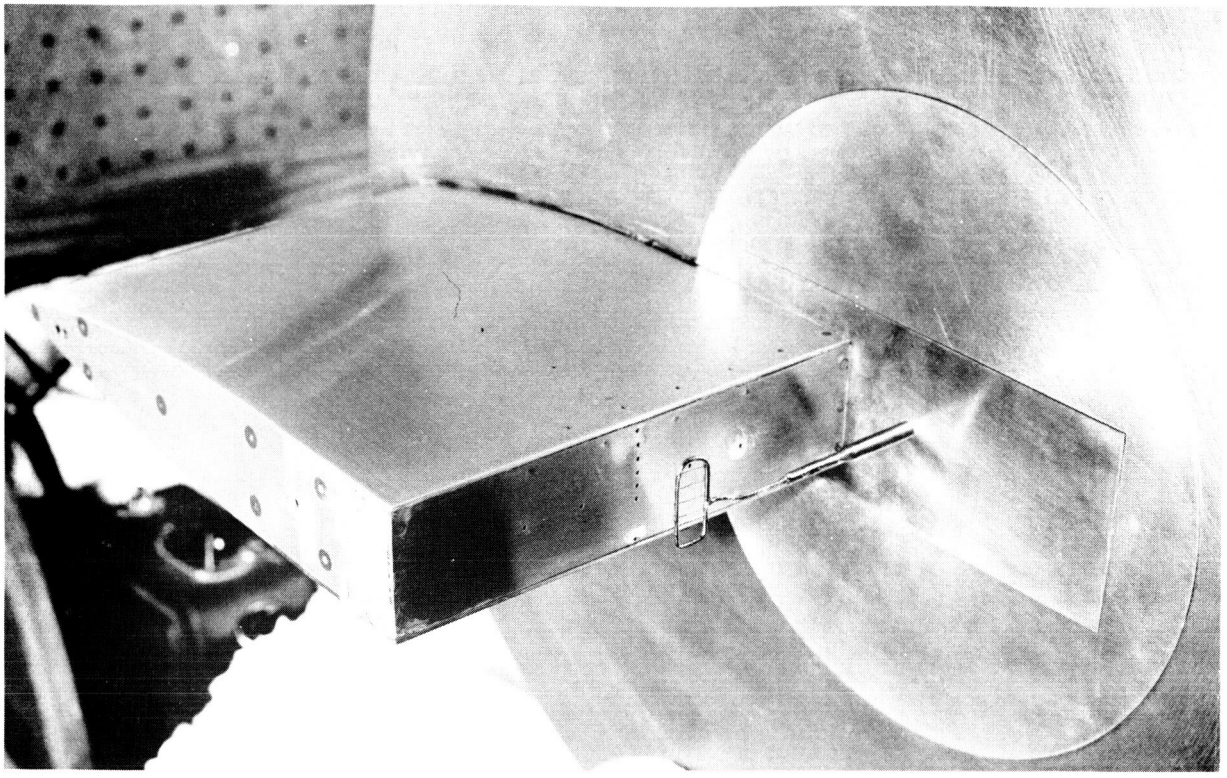

FIGURE A4. RECIRCULATION ZONE TEMPERATURE RAKE

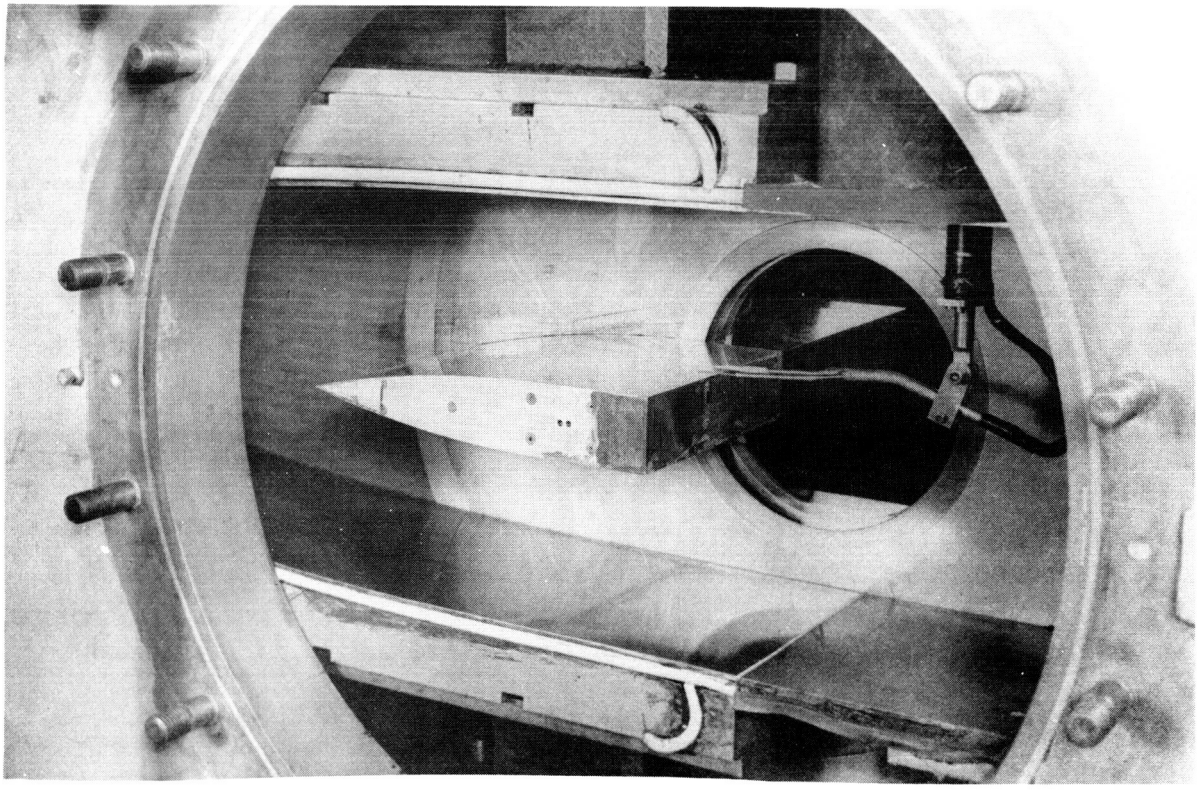

FIGURE A5. FOREBODY BOUNDARY LAYER PROBE IN POSITION

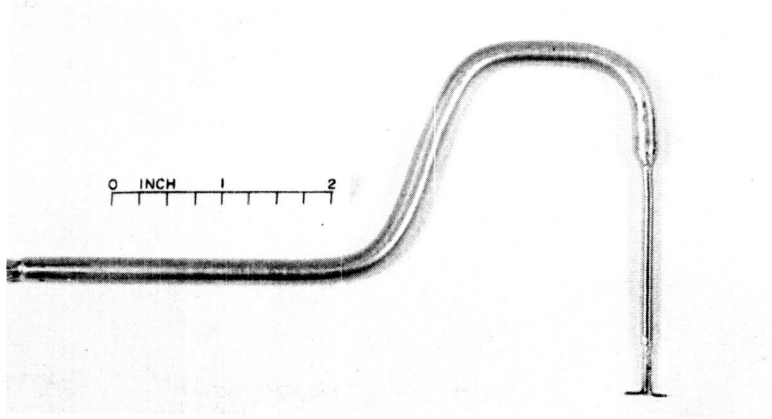

a) Early Recirculation Zone Probe

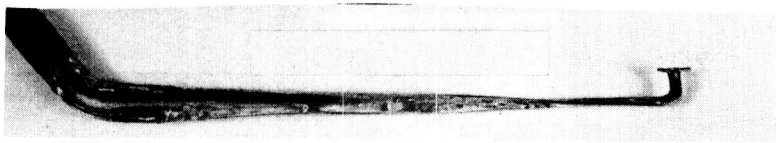

b) Improved Recirculation Zone Probe

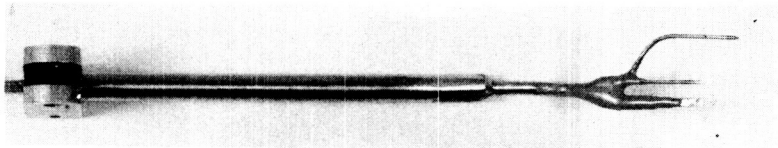

c) Early Shear Layer Probe

d) Later Shear Layer Probe

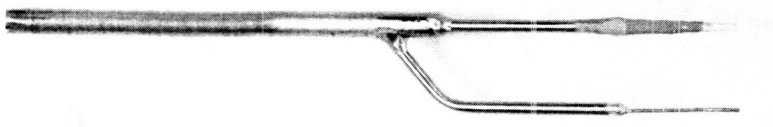

e) Forebody Boundary Layer Probe

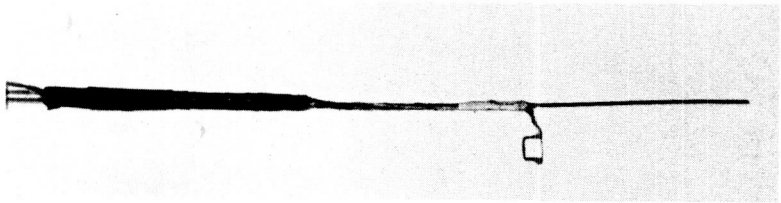

f) Early Base Thermal Boundary Layer Probe

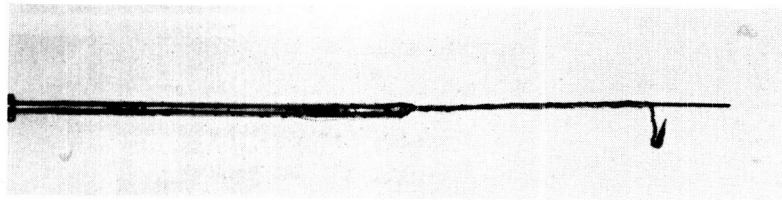

g) Improved Base Thermal Boundary Layer Probe

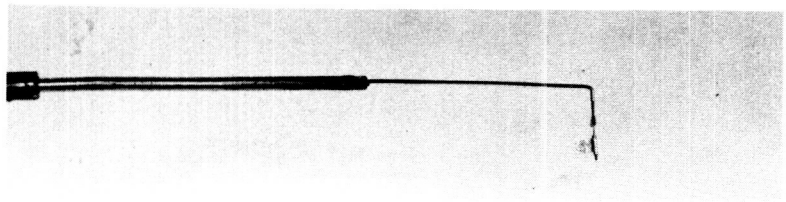

h) Recirculation Zone Wind Vane

FIGURE A6. RECIRCULATION ZONE AND BOUNDARY LAYER PROBES

a) Early Recirculation Zone Probe

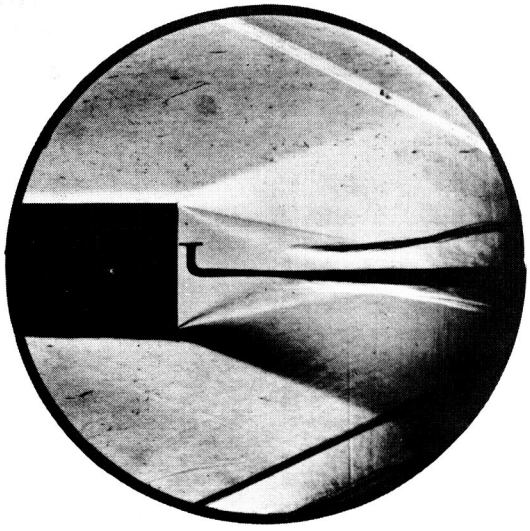

b) Improved Recirculation Zone Probe

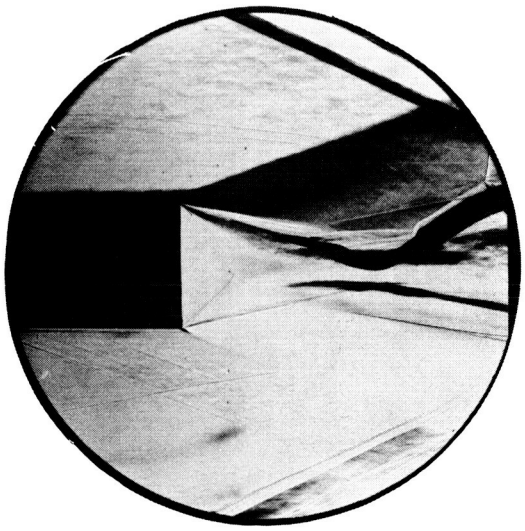

c) Early Shear Layer Probe

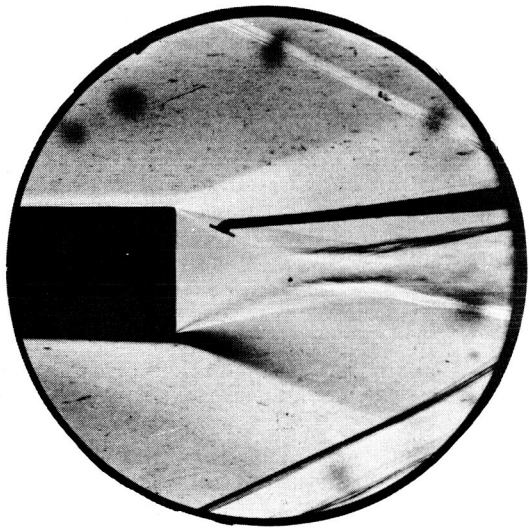

d) Later Shear Layer Probe

FIGURE A7. SCHLIEREN FLOW PHOTOGRAPHS WITH VARIOUS PROBES INSERTED IN FLOW FIELD

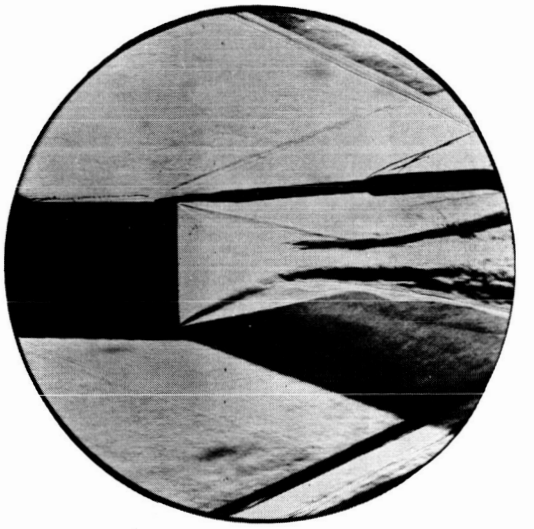

e) Forebody Boundary Layer Probe

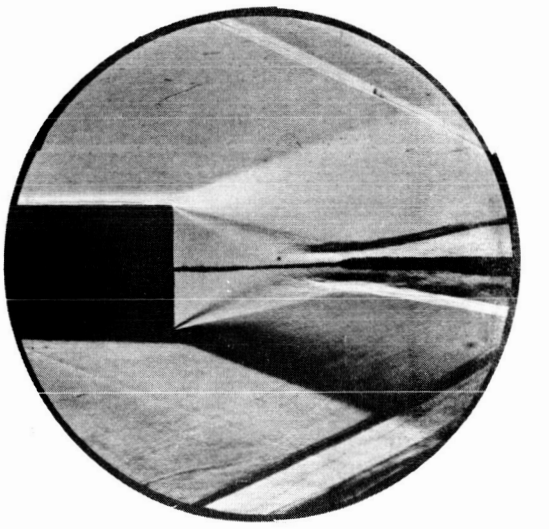

f) Early Base Thermal Boundary Layer Probe

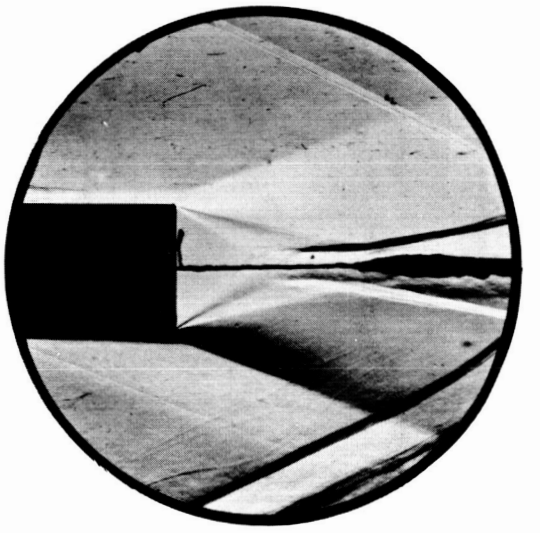

g) Improved Base Thermal Boundary Layer Probe

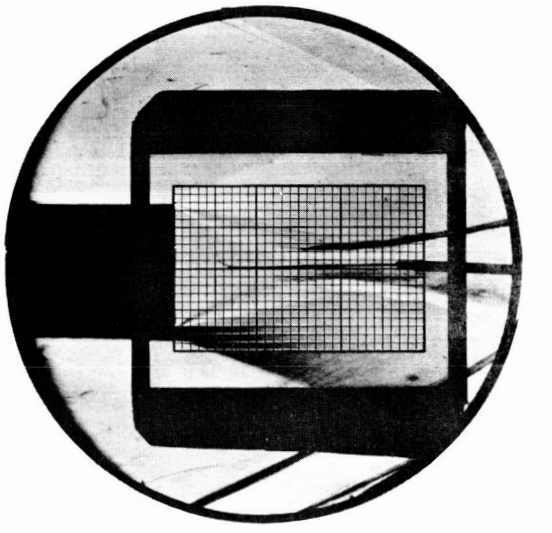

h) Recirculation Zone Wind Vane

FIGURE A7. (CONT'D)

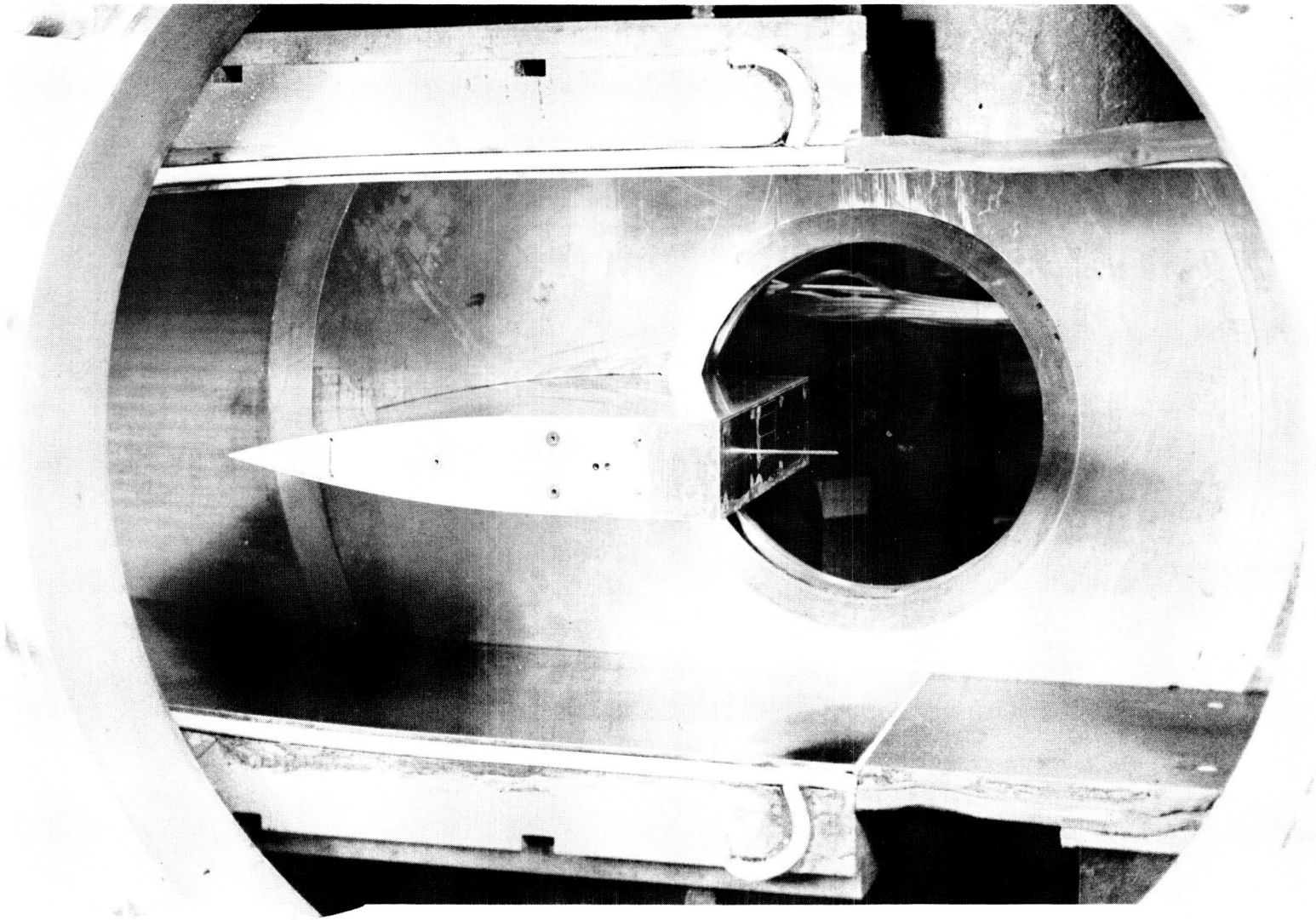

FIGURE A8. CENTERLINE PROBE INSTALLATION

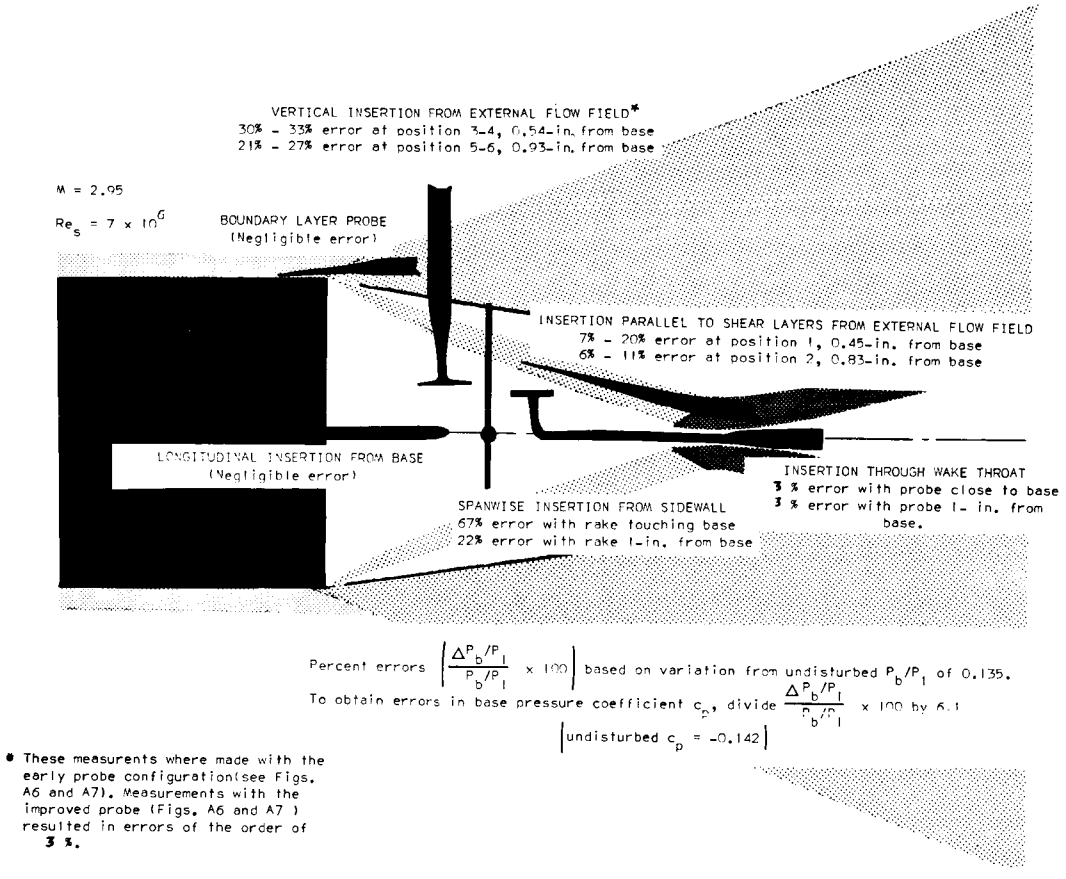

* These measurents where made with the early probe configuration(see Figs. A6 and A7). Measurements with the improved probe (Figs. A6 and A7) resulted in errors of the order of 3 %.

FIGURE A9. SUMMARY OF PROBE INTERFERENCE EFFECTS

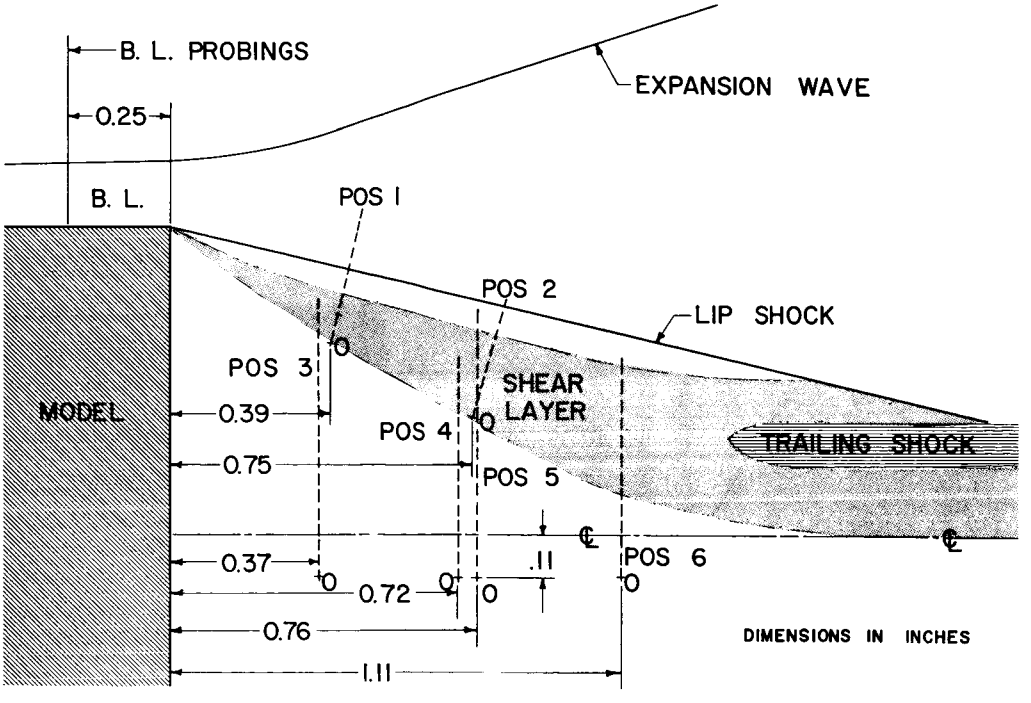

FIGURE A10. PROBING LOCATIONS OF EARLY MEASUREMENTS